HYDROGEOLOGICAL CHARACTERIZATION

OF THE MABOU GROUP IN THE PICADILLY REGION, NEW BRUNSWICK

A Thesis Submitted to the College of

Graduate Studies and Research

in Partial Fulfillment of the Requirements

for the Degree of Master of Science

in the Department of Civil and

Geological Engineering

University of Saskatchewan

Saskatoon

By

Craig K. Hamilton

Permission to Use

In presenting this thesis in partial fulfilment of the requirements for a Postgraduate degree from the University of Saskatchewan, I agree that the libraries of this University may make it freely available for inspection. I further agree that permission for copying of this thesis, in whole or in part, for scholarly purposes may be granted by the professor or professors who supervised my thesis work or, in their absence, by the Head of the Department or the Dean of the College in which my thesis work was done. It is understood that any copying or publication or use of this thesis or parts thereof for financial gain shall not be allowed without my written permission. It is also understood that due recognition shall be given to me and to the University of Saskatchewan in any scholarly use which may be made of any materials in my thesis.

Request for permission to copy or to make other use of material in this thesis in whole or in part should be addressed to:

Head of the Department of Civil and Geological Engineering

University of Saskatchewan

Saskatoon, Saskatchewan

S7N 5A9

ABSTRACT

The Mabou Group in the Picadilly region of New Brunswick consists predominantly of red siltstones with interbeds of sandstone and conglomerate. The Mabou is of importance in this region as it overlies evaporite deposits of economic value. Given that the Mabou is several hundred meters thick, yet possesses no significant marker beds, it has remained stratigraphically undifferentiated in the Picadilly region over the course of previous regional mapping efforts in the area. Given the lack of a stratigraphic framework, coupled with insufficient hydrogeological sampling and test data to delineate any laterally extensive flow zones, the hydro-stratigraphy of this sedimentary package has not been established.

Based on experience gained at other operations, Potash Corporation of Saskatchewan Inc. (PCS) recognized the need to take a proactive approach towards understanding the hydrogeology of the Picadilly mine development site. PCS has used a specialized technique in characterizing boreholes to measure depth-profiles of hydrophysical properties by logging the electrical conductivity of the borehole fluids over a period of time. Through the interpretation of these logging results, with the context provided by conventional geophysical logging data and nearby exploration drill core, this research seeks to identify zones of flow and assess whether or not any major units with lateral connectivity can be identified.

The results highlight four zones of interest within the Mabou: the Upper Mabou; vuggy porosity directly above gypsum-infilled fractures; vugs and fractures within the Medium Sandstone subdivision; and the lower Mabou Siltstone at the base of the Mabou Group (within ~15m of base). Three of these zones are of interest as they tend to have relatively high permeabilities, with permeabilities over 10 000 md measured within the Upper Mabou, as high as 1800 md in the vuggy porosity zone directly above gypsum-filled fractures and as high as 1900 md within the Medium Sandstone subdivision . The fourth zone, found at the base of the Mabou Group, is of interest because the modest to low

permeability recorded (as high as 38 md) is higher than the surrounding rocks and is in close proximity to the caprock of future mining activity.

The permeabilities of the rocks studied in this research are believed to be dominantly controlled by secondary porosity. In the case of the permeable zone identified above the zone of gypsum-infilled fractures, relatively high porosities (9 to 15%) were interpreted from geophysical logs. These elevated porosities are due to the presence of vuggy porosity in this zone. However, no clear correlation between log-derived porosity and permeability was observed for the other permeable zones. This is believed to be due to the fact that fractures were the dominant control on porosity in these zones, and that the incremental contribution of fracture porosity to total porosity was too small to be readily identified.

ACKNOWLEDGEMENTS

I would like to thank the Department of Civil and Geological Engineering for their support financially, academically and administratively during my years spent at the University of Saskatchewan. Thank you to my advisors Chris Hawkes and Doug Milne for their insight and inspiration throughout the process of writing this thesis. Thank you to my committee members Jitendra Sharma, and Malcom Reeves for their constructive criticism, helpful discussions, and review of the research. Thank you to Don Gendzwill for externally examining this thesis and providing important feedback.

Special thanks to Potash Corporation of Saskatchewan Inc. for financially supporting this research and to all the employees from Potash Corporation of Saskatchewan Inc. who directly influenced this research: Anastasia Vandermost; Terry Danyluk; Craig Funk; Arnfinn Prugger; Brian Roulston; and Robert McVeigh to name a few.

Thank you to Zig Szczepanik for all your pleasantries and help during laboratory testing of rock samples at the University of Saskatchewan Rock Mechanics Laboratory.

Finally I would like to thank all my family and friends who have been there for me over the years. Especially to my parents, without their love and support growing up I would not be lucky enough to have made it to where I am today.

TABLE OF CONTENTS

LIST OF TABLES

LIST OF FIGURES

NOMENCLATURE

atm – Atmospheres, unit of measurement relative to atmospheric pressure

b – aquifer thickness (Thiem solution)

cm - centimetre

cm/s – centimetres per second

C - constant

C_o - the initial salinity of the wellbore water

C_i - fluid salinity for interval i

Cgl – Conglomerate

DGI – a down hole geophysical survey company (DGI Geosciences Inc.)

DST – Drill stem test

FEC - fluid electrical conductivity

GR_{CLEAN} - Log response from gamma-ray tool in a clean sandstone (i.e., free of shale)

GR_{LOG} - Log response from gamma-ray tool

GR_{SHALE} - Log response from gamma-ray tool in a shale formation

HPL – Hydrophysical logging

KB – Kelly Bushing

k - permeability

$k \cdot h$ - permeability-thickness cross-product

km - kilometre

kPa – kiloPascal

K - hydraulic conductivity (cm/s)

l/s – litre per second

L - length of tested interval

m- metre

m - the slope of Horner Plot trendline

m^2/day – metre squared per day

m^3/day – cubic metre per day

masl – Metres above sea level

md – millidarcies

med – Medium

NE – Northeast

Pa·s – milliPascal seconds

P_0 – an initial pressure read off Horner Plot (kPa)

P_{10}- pressure at one log time cycle greater than P_0 on the Horner Plot (kPa)

PCS – Potash Corporation of Saskatchewan Inc.

q_i - inflow rate for interval i

Q - flow rate prior to shut-in (in standard cubic metres per day or Sm^3/D)

$Ø_D$ - density porosity

$Ø_{EFF\_ND}$ - effective neutron and density porosity

$Ø_N$ - neutron porosity

$Ø_{ND}$ - averaged neutron and density porosity

$Ø_{sonic}$ - sonic porosity

r_1 - radial distances of first observation well (m)

r_2 - radial distances of second observation well (m)

r_e - effective radius of influence of DST test (m)

r_w - radius of the well or tested interval (m)

RAS – a groundwater flow evaluation company (RAS Inc.)

Rm^3 -"reservoir" or in-situ cubic metre

RQD – Rock Quality Designation

s_1 - drawdown of first observation well

s_2 - drawdown of second observation well

SiltS - Siltstone

Sm^3 - standard cubic metre

Sm^3/D - standard cubic metre per day

SS - Sandstone

t_p - total flowing time of a drill stem test prior to shut-in (minutes)

t_{LOG} - log transit time (µs/m)

t_{ma} - matrix mineral transit time (µs/m)

t_{SH} - shale transit time (µs/m)

t_{SS} - Sandstone transit time (µs/m)

T – transmissivity (m^2/day)

USGPM – United States Gallons per Minute

V_{SH} - Volume fraction of shale

w - borehole flow rate from below the surveyed section

X - shale content (fraction)

β_0 - formation volume factor (Rm^3/ Sm^3).

Δh_w - drawdown from ambient flow conditions and pumping conditions

ΔQ_i - the change in flow rates from ambient flow conditions and pumping conditions

Δt - shut-in time of a drill stem test

μ - viscosity of the flowing phase (mPa·s)

1 INTRODUCTION

1.1 Background

Potash Corporation of Saskatchewan Inc. (PCS) currently operates an underground potash mine in New Brunswick, Canada at a site located 8 km east of the town of Sussex (Figure 1.1). The company is mining a salt diapir which is within an antiformal structure that trends 50-70 degrees NE. The antiform is the result of tectonic stresses acting on the Maritimes Basin sediments during the evolution of the basin. The northwest side of the antiform, where mining operations currently occur, has been named the Penobsquis area. The southeast side of the antiform is the location of the future mine, which is referred to as the Picadilly area (see Figure 1.2).

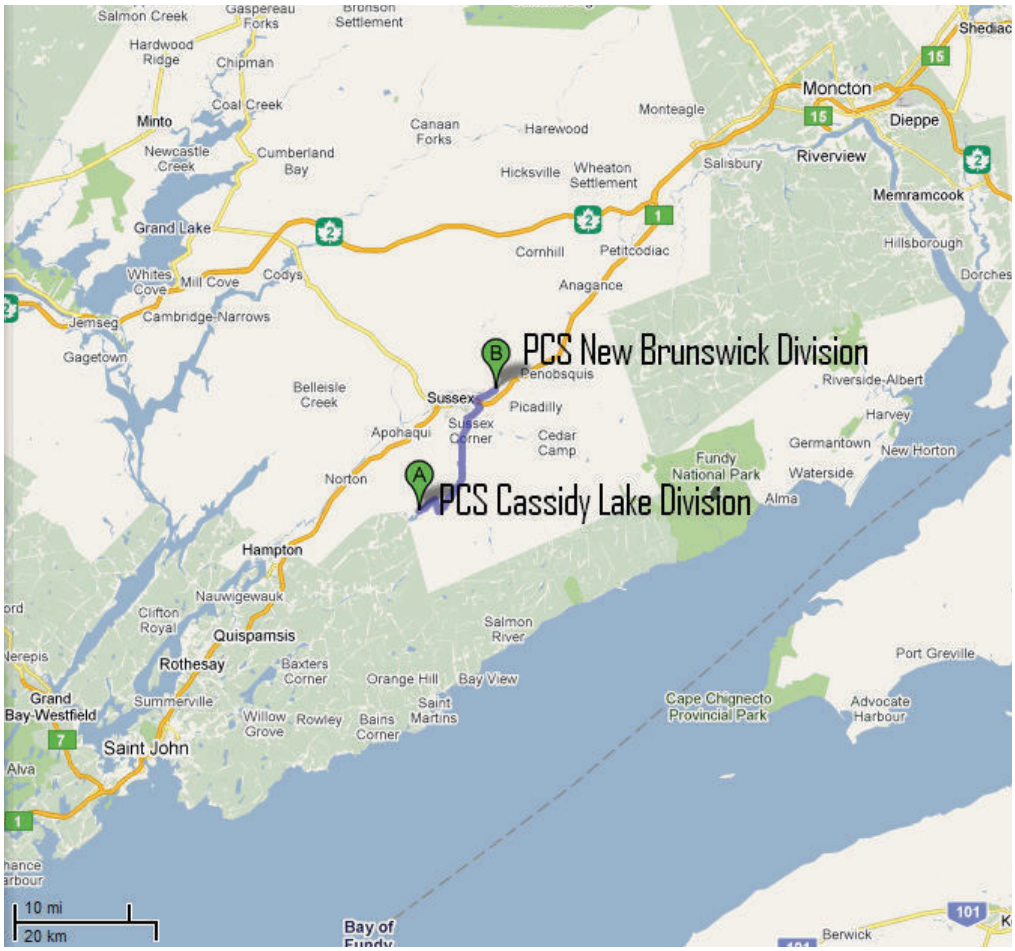

Figure 1.1 – Area map of PCS Properties in New Brunswick (after Google, 2010)

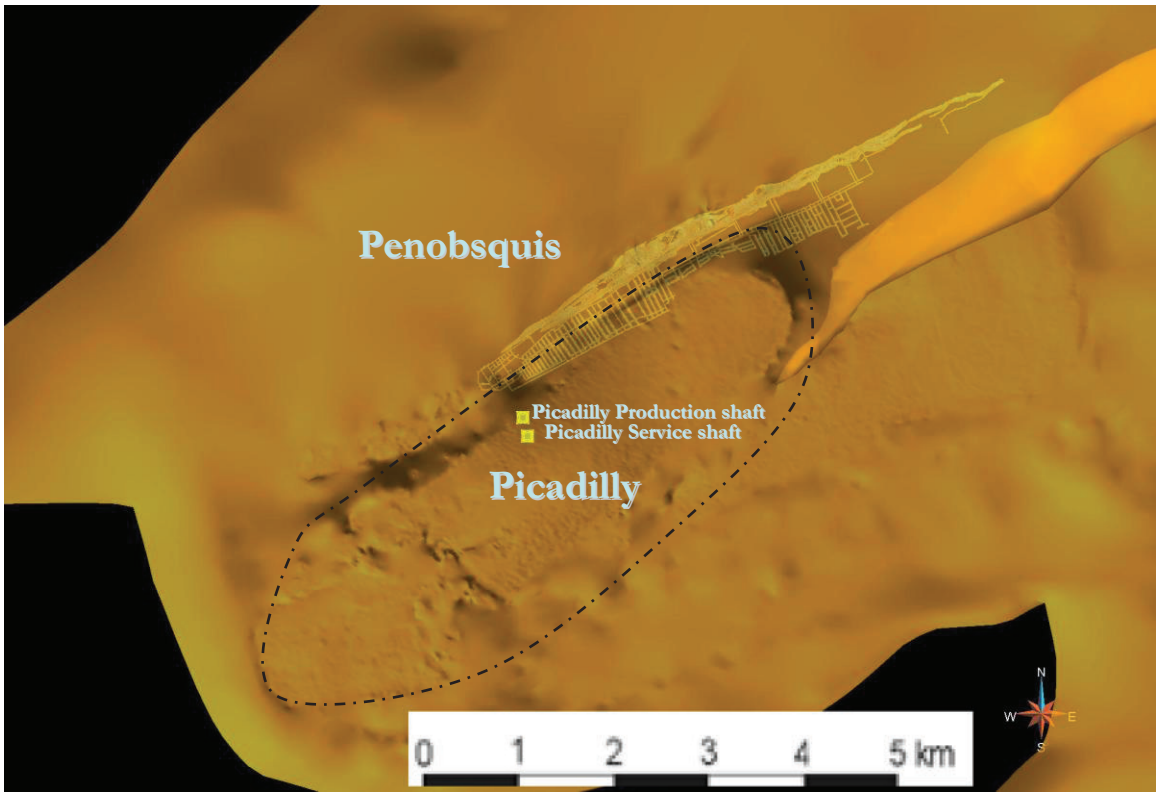

Figure 1.2 - Study area outline. The orange-gold surface shown is the current PCS interpretation of the base of the Mabou Group interpreted from seismic reflection profiles and surface geology

In 1998, the Penobsquis operation developed an inflow of brine into underground workings. To a certain degree, mitigation efforts have controlled the amount of brine entering the mine from the Mabou Group, but the problem has yet to be eliminated. At the present time, the brine inflow is considered to be chronic, but manageable at significant cost.

Historically, the incidences of inflows into potash mines sites have forced the abandonment of operations and/or have added costs to maintain operations at the mine sites. Costs are incurred as the inflow must be pumped to the surface and disposed of appropriately. A continual inflow of water, not completely saturated with salts, requires the implementation of grouting operations in order to seal or slow the leak and filling of void spaces created by any salt dissolution that may have occurred.

Early (1961) efforts at potash mining resulted in the inundation of water into the Continental Potash Corporation shaft near Unity Saskatchewan from a 106 m thick sand zone at 558 m depth (Fuzesy, 1982). By 1968 the shaft had been rehabilitated but the site was sealed and abandoned. Potash Corporation of America (now the Patience Lake Division of PCS) also ran into water problems early in its mine life. In 1959, only one year after shaft completion, shaft seepage through the concrete liner forced production to be suspended. Seepage was the consequence of a fire in the freeze plant, which allowed freeze holes to thaw. Seepage was not curtailed to manageable limits until 1965 (Prugger 1991).

The Cominco mine, (now Agrium Inc.) 40 km southwest of Saskatoon, was the second operational potash mine to become flooded in Canada. During routine grouting of the concrete lining in May 1970, an abandoned freeze hole was intersected. Days later, high pressure water had flooded the mine workings and the two shafts. After two years of rehabilitation after the flood occurred, production at the mine started again (Prugger, 1979).

The third Canadian incidence of a potash mine becoming flooded as inflow exceeded manageable limits occurred in 1987 in Saskatchewan (Prugger 1991). At the time of flooding, the mine was owned by Potash Corporation of America (now the Patience Lake Division of PCS). After attempts to rehabilitate the conventional mine failed, the operation was transformed into a solution mine.

Another potash mine that was flooded was in New Brunswick. Southwest of Sussex, the Clover Hill potash mine, owned by Denison Potacan Co., could not keep up to a rising inflow rate into the mine and shut down in 1997. The Clover Hill mine has since been acquired by PCS (now Cassidy Lake Division).

Two operational potash mines in Canada currently manage ongoing inflows. The first is the Esterhazy K2 mine, operated by the Mosaic Company in southern Saskatchewan, which must continually pump water from its operation. The second is PCS's

aforementioned Penobsquis operation in New Brunswick, which requires ongoing inflow management.

To reduce the risk of mine flooding in the New Brunswick Division, PCS has taken a proactive approach and is working on interpreting the hydrogeology of the rocks surrounding the Picadilly area, and is continually monitoring inflow at their current (Penobsquis) operation.

The evaporites, which are the target of the Penobsquis and Picadilly projects, are contained within the Windsor Group. Stratigraphically overlying the Windsor Group are the clastic sedimentary rocks of the Mabou Group. The hydrogeological data collected for the Mabou Group has never been systematically analyzed. For example, no three-dimensional interpretation of the distribution of hydrogeological properties has been undertaken. Without such an effort, the locations of water-bearing permeable zones (i.e., aquifers) are challenging to delineate. This is of concern, as aquifers in the Mabou Group have the potential to contribute to inflows while mining the potash and halite of the Cassidy Lake Formation in the Windsor Group.

1.2 Objectives

The overall objective of this research project is to analyze existing data and cores in order to characterize the hydrogeological attributes of the Mabou Group within the Picadilly area (see Figure 1.2 on page 2).

The specific sub objectives are to establish the following:

- The identities of lithological units and/or structural features which govern flow;
- The spatial distributions of these lithological units and/or structural features; and
- The hydrogeological properties of these units / features.

1.3 Scope

The mandate for this research project was to integrate and interpret existing data. The research made use of field testing results collected by PCS employees and service companies contracted by PCS. A limited amount of laboratory testing was included in the scope of this project, in order to assess the permeability of selected cores.

A field excursion was undertaken October 13 to 17, 2009, in order to view Mabou Group outcrops and gain a better general understanding of its stratigraphy. In conjunction with the outcrop observation, core boxes from PCS 0502 were viewed during the field excursion.

Detailed lithological analysis of the Mabou was beyond the scope of the project, even though Mabou outcrops were visited and drill core photographs were studied. The excursion to the outcrops and observation of drill core photographs were conducted to obtain high-level observations of the lithology and the continuity of sedimentary strata. Detailed lithological and geochemical analysis of drill cores from the study area is being conducted by a PhD student at the University of New Brunswick, but his results were not available soon enough to serve as a reference for the hydrogeological research presented in this thesis.

2 BACKGROUND OF GEOLOGY AND CHARACTERIZATION OF TOOLS

This chapter provides a summary of the geological setting for the study area, , and the general principles of hydrogeology in rock masses. This knowledge is important for understanding the challenges encountered during the research, and the relationships between geology and hydrogeology presented in this study. The analysis of geological and hydrogeological features presented in this research involved the interpretation of down hole geophysical logs, seismic reflection survey results and downhole hydraulic tests. As such, the principals of these methods are also presented in this chapter.

2.1 Geological and tectonic setting

2.1.1 Geological setting

The Moncton Subbasin (Figure 2.1) is one of several subbasins within the Eastern Canada Maritimes Basin that was formed at equatorial latitudes during the Carboniferous Era (i.e., during the time of the super-continent Pangea through to the opening of the Atlantic Ocean approx. 340 million years ago). Three depositional sequences (allocycles) were originally interpreted to have occurred in the Moncton Subbasin. The oldest allocycle or depositional sequence has since been split into two depositional sequences (Keighley, 2009). As such, the Moncton Subbasin is currently interpreted to have four allocycles of sediment, each being interrupted by an unconformity or disconformity. The four allocycles, shown in Figure 2.2 are the Horton allocycle; the Sussex allocycle; the Windsor/Mabou allocycle; and the Cumberland/Pictou allocycle.

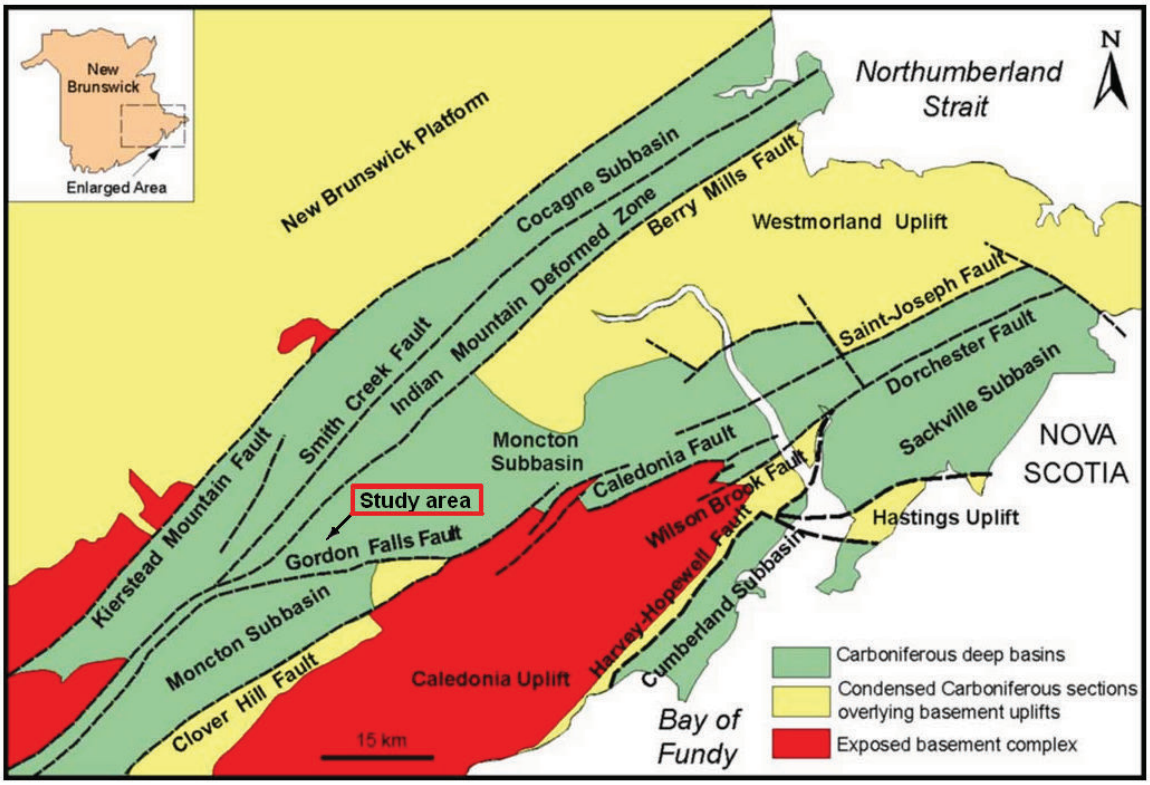

Figure 2.1 – General location of study area within Moncton Subbasin (after DNR, 2011)

	STAGE	GROUP	FORMATION
PENNSYLVANIAN	MOSCOVIAN	PICTOU	
			SALISBURY
	BASHKIRIAN		
		CUMBERLAND	BOSS POINT
MISSISSIPPIAN	SERPUKHOVIAN		
		MABOU	UNDIVIDED UNITS
	VISEAN	WINDSOR	CLOVER HILL
			CASSIDY LAKE
			UPPERTON
			MACUMBER
			HILLSBOROUGH
		SUSSEX	WELDON
			ROUND HILL
	TOURNAISIAN		
		HORTON	BLOOMFIELD
			ALBERT
			MEMRAMCOOK
FAMMENIAN			
PRE-MID DEVONIAN		BASEMENT COMPLEX	

Figure 2.2 - Formations for the western Moncton Subbasin (after Wilson et al., 2006)

Stratigraphically, the Mabou, Cumberland and Pictou Groups all overlie the Windsor Group. The surficial geological map (Figure 2.3) created by St. Peter (2002) has been modified by this author to include the surface locations of boreholes in the Picadilly area. The strata of the Cumberland and Pictou Groups have been eroded away immediately above the PCS Penobsquis mining region and the study area in Picadilly, leaving only the Mabou Group as a potential source for inflow into underground mines located in the Cassidy Lake Formation evaporites of the Windsor Group.

There are currently no formal subdivisions of the Mabou Group in the Penobsquis or Picadilly areas. Subdivision of the Mabou Group by Anderle et al. (1979) (also known as the Hopewell Group in Nova Scotia and areas of New Brunswick; Figure 2.4) was performed at the Cassidy Lake Division (formerly Denison Potacan Co) in the Marchbank syncline, part of a nearby subbasin roughly 15 km southwest of the Picadilly study area. The subdivisions of the Mabou clastic sediments by Anderle et al. (1979) were based on broad lithological categories, as they found the stratigraphy to be too complex (e.g., rapid and numerous facies changes and pinchouts; scarcity of marker fossils) to enable correlation of each facies change. The subdivisions made by Anderle et al. (1979) have yet to be correlated to Carboniferous sediments within the Fundy Basin or associated subbasins.

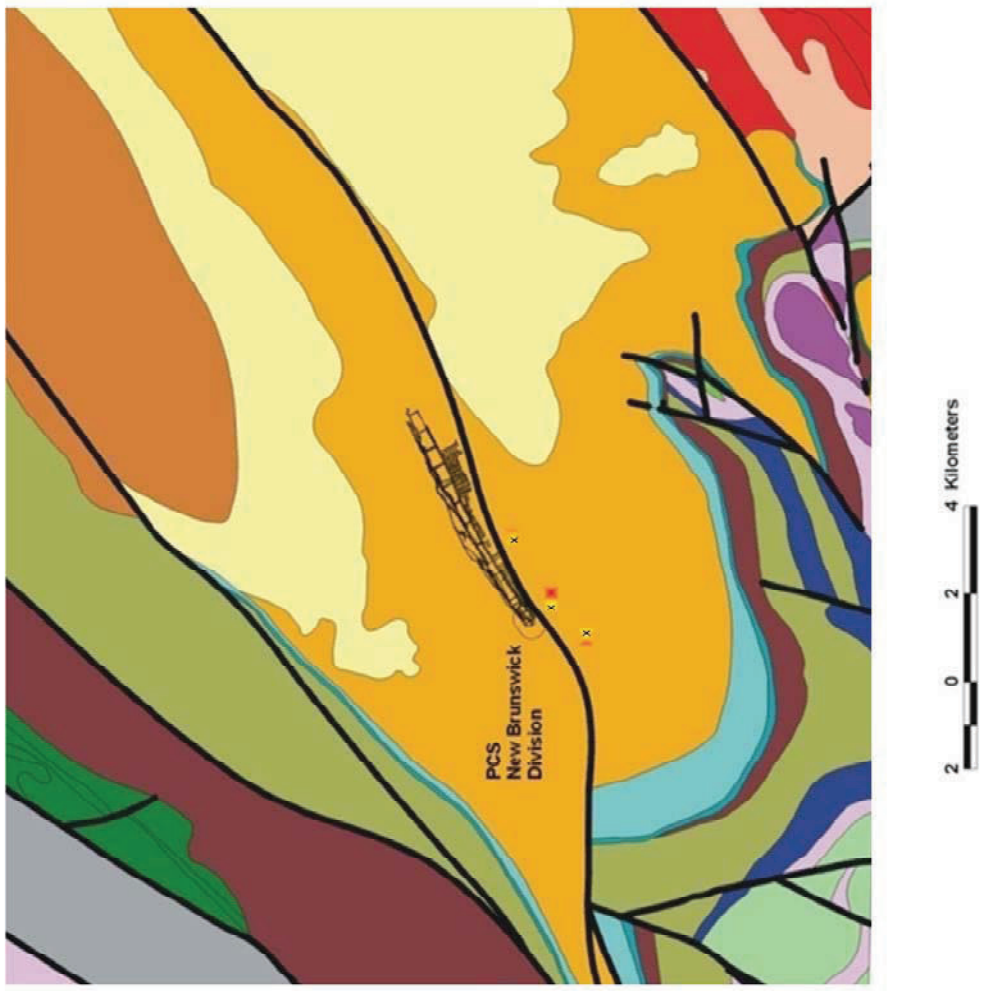

Figure 2.3 – Surficial Geological Map of the Sussex Area (after St. Peter, 2002).

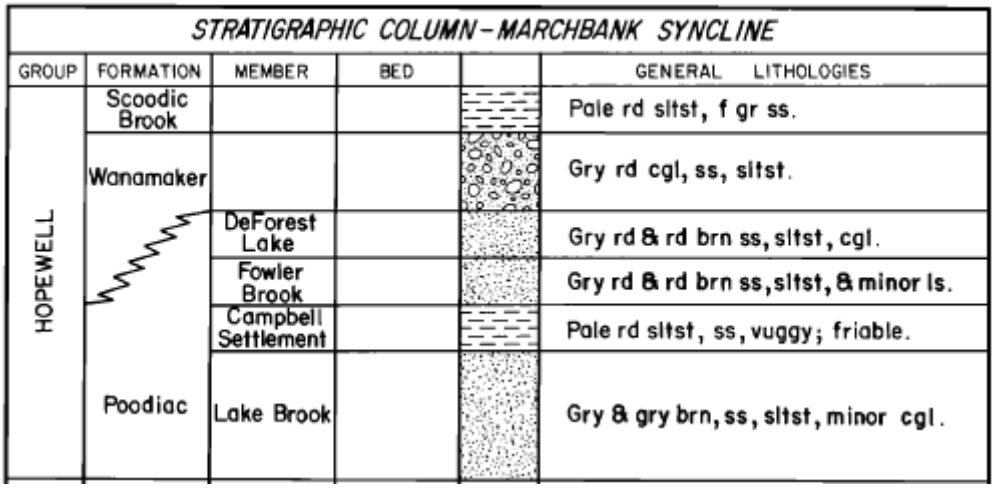

Figure 2.4 - Stratigraphic column of the Marchbank syncline (after Anderle et al., 1979). [Note that Hopewell Group is an alternate name used for the Mabou in Nova Scotia and parts of New Brunswick.]

Gypsum is known to have infilled fractures within the study area. Precipitation of gypsum within fractures has two possible origins. The dominant theory for the area posits that gypsum in the fractures is a product of the upper anhydrite of the Windsor Group. This theory is based on the knowledge that gypsum is the hydrated form of anhydrite; gypsum is deposited and during burial and diagenesis turns into anhydrite. If the reverse reaction occurs and anhydrite is returned closer to the surface, hydration replaces anhydrite with gypsum (Murray, 1964). In the case of the study area, it has been postulated that as the Penobsquis thrust fault brought the anhydrite closer to surface, hydration of the anhydrite occurred and gypsum was dissolved by water, which then redistributed the hydrated gypsum, by precipitating out gypsum crystals into open fractures and vugs.

A second theory this author brings forth stems from studies conducted in Spain, and pertains to the mixing of salt water and fresh water during the inland advancement of seawater. Specifically, Gomis-Yagues et al. (2000) suggest that gypsum precipitation can occur as a result of cation exchange processes taking place as salt water invades an aquifer containing fresh water that is at equilibrium with its clays and carbonates.

Further studies are required to determine which theory, if either, offers the most plausible explanation for the presence of gypsum-filled fractures and vugs. In any case, knowledge of the presence of gypsum in the Mabou is more important than understanding its origins, and will be demonstrated in Chapter 4.

2.1.2 Tectonic setting

Researchers have attempted to analyze the timing and the displacement events that created the regional faults within the study area's rock mass. Wilson and White (2006) concluded that the timing of some of the displacements near the study area occurred syn-depositional to the Mabou. The justification for syn-depositional tectonism was based on the interpretation of a two-dimensional seismic survey taken along the line labelled X-X' on Figure 2.5. The seismic reflection survey data showed the geometry of a structural triangle seen in the cross-section (Figure 2.6), located southeast of the Berry Mills fault. The triangle has been interpreted to be Sussex Group and pre-Horton basement rock, overlain and underlain by Windsor Group rocks. This structure and stratigraphic sequence infers that thrusting occurred towards the southeast, as older sedimentary rocks overlay younger sedimentary rocks. This thrusting was interpreted by Wilson and White (2006) to have occurred during Mabou deposition. The interpretation was based on the change in dip of Mabou Group reflectors overtop the structural triangle, where relatively steeply dipping reflectors are overlain by more shallowly dipping reflectors.

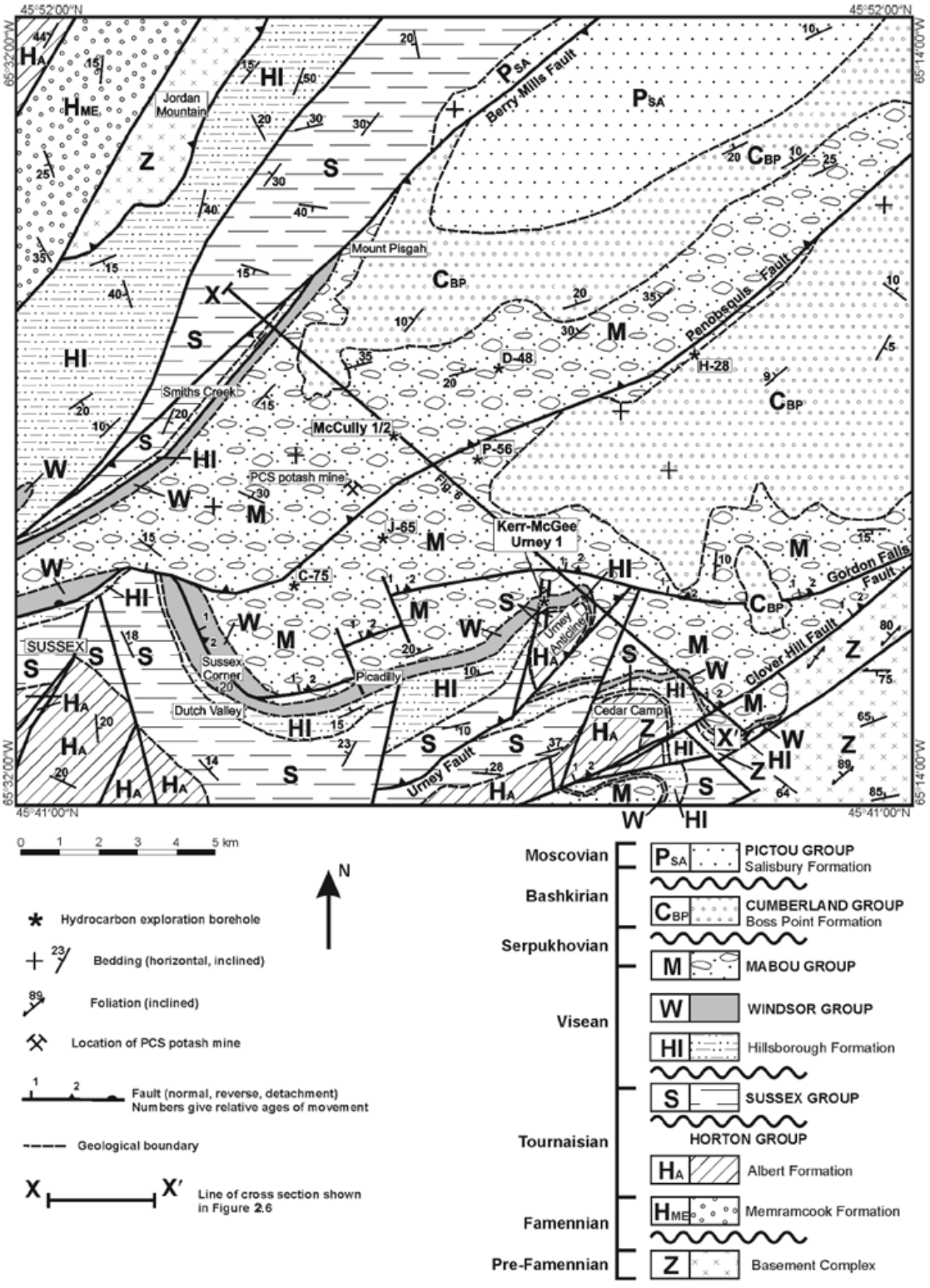

Figure 2.5 - Simplified geological map of the McCully area (after Wilson and White, 2006)

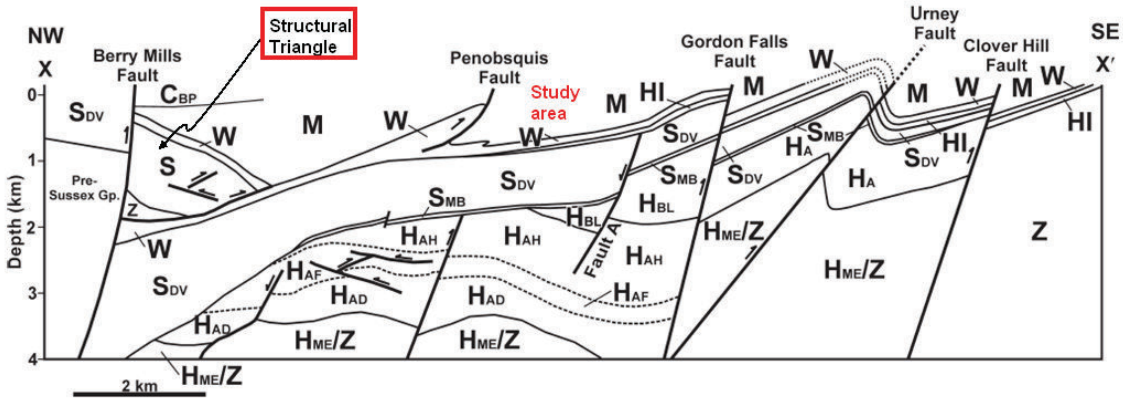

Rock units:

CBP – Boss Point Formation;

M – Mabou Group;

W – Windsor Group;

S – Sussex Group (undifferentiated);

HI – Hillsborough Formation;

S_{DV} – Dutch Valley Formation;

S_{MB} – Mill Brook Formation;

H_{BL} Bloomfield formation;

H_A – Albert Formation (undifferentiated);

H_{AH} – Albert Formation (Hiram Brook Member);

H_{AF} – Albert Formation (Frederick Brook Member);

H_{AD} – Albert Formation (Dawson Settlement Member);

H_{ME} – Memramcook Formation;

Z – pre-Horton basement.

Figure 2.6 – Composite cross section (X-X' on Fig. 2.5) constructed using information from seismic reflection profiles, borehole intersections and field mapping in the McCully area (after Wilson and White, 2006)

The end of Mabou Group deposition is interpreted to have been due to a compressional, or possibly transpressional, basin event (St. Peter, 1993). The basin event is one of several "successive phases of basin subsidence and inversion, reactivation of tectonic lineaments, halokinesis, and erosion of earlier strata" (Gibling et al., 2008) that formed the Maritimes Basin.

2.2 Rock Mass Characterization methods

To characterize a rock mass one may use a surface characterization method such as surface mapping, and/or down-hole characterization methods such as core logging or geophysical logging.

2.2.1 Surface characterization methods

Surface mapping is a common approach used to characterize rock masses, when large continuous outcrops of rock exist. This approach is useful for measuring the orientation of joint sets, and observing the presence and continuity of alterations and facies changes. However, if there is a scarcity of outcropping rock, as is the case in the study area, there is limited applicability of this method for characterizing a rock mass.

2.2.2 Down-hole characterization methods

2.2.2.1 Core logging for formation characterization

Core logging is a method of characterizing the lithology and the presence of features in a rock mass by using cores from a drill hole, and can all be done at the drilling site. The cores can also be transported to a laboratory and tested for permeability and porosity.

Strip logs are series of depth-indexed lithological descriptions made by a geologist from analyzing drill core (or drill cuttings, if core is not acquired). Strip logs are subjective in nature, since they are based on the interpretation of the geologist. As a result, geologists logging the same drill core, (or drill cores from nearby wells) may label identical features or lithologies differently. This subjectivity must be considered when using multiple boreholes logged by multiple geologists to characterize an area.

Secondary features observable in cores include: iron reduction staining, the presence of secondary porosity in the form of joints, fractures and vugs, and the infilling of joints, fractures and vugs due to mineral precipitation.

Iron reduction staining is present in the Mabou Group and is caused by dissolution of iron minerals. It is readily visible as localized green-coloured features within the predominantly red beds of the Mabou.

A manner of expressing the presence and degree of jointing and fracturing in a rock mass is the Rock Quality Designation (RQD) (Deere, 1964). RQD is calculated by measuring the length of core pieces greater than 10 cm over the length of a core run. Strong competent rock will result in a high RQD, up to 100%, whereas heavily jointed and fractured rocks will present itself with a low RQD. Zones of low RQD with a large number of joints are indicators of potential for secondary permeability within a rock mass.

2.2.2.2 Geophysical tools for formation characterization

Geophysical measurements are useful tools to aid in rock mass and hydrogeological characterizations of the Mabou Group, as the measurements provide information on the in-situ properties of the rock and/or formation fluids. The downhole or wireline logging tools make use of geophysical principles to infer subsurface geology. The wireline logs relevant to this study include: the gamma-ray log; the lithology-density log; the neutron log; the sonic log; the induction/resistivity log; and the fullbore formation micro-imager.

The standard gamma-ray tool aids in the interpretation of shale content in sandy-shaley sequences. The determination is based on the principle that radioactive elements such as uranium, potassium and thorium tend to concentrate in clays and shales. By using a scintillation detector, the natural radioactivity of formations is logged (Schlumberger, 1991).

The lithology-density tool provides a measure of the bulk density of the formations and an indication of the minerals present. The tool uses a gamma source, commonly Cesium 137, to bombard the nearby formation with gamma-rays. The gamma rays collide with electrons within the formation and lose part of their energy. The gamma rays that reach

the detector at a known distance from the source are counted, and serve as an indication of the formation's density (Schlumberger, 1991). As discussed in the following section, an important use of this tool is for calculating porosity. Since washouts and the borehole diameter affect the density calculation, caliper logs are almost always run in conjunction with the lithology-density tool.

The neutron log provides a measure of the presence of hydrogen in the formations. The thermal neutron tool uses a neutron source, commonly Americum251/Berillium to bombard the nearby formation with neutrons. The neutrons collide with the molecules present in the formation and either bounce off larger molecules or transfer their energy to molecules of similar size (hydrogen). The neutrons that reach the detectors at a known distance from the source are counted and serve as an indication of the formation's hydrogen content. Older tools and smaller wireline companies present the number of neutrons that reached the detector. While, larger wireline companies derive a porosity value using the detector's count numbers.

Calipers log the size and rugosity (i.e., roughness) of the borehole wall. Calipers may be run as independent tools; however, they are often run in conjunction with the lithology-density tool.

The borehole compensated sonic tool measures the velocity of compressional sonic waves in the formation, which can be converted to porosity if the matrix material transit time is known. Another key reason for running a sonic tool in association with the other standard logging tools presented here is to correlate the properties of the other logging tools to processed seismic data (Schlumberger, 1991). Correlation with seismic data is possible as the compensated sonic tool provides an acoustic profile of the near well conditions (approximately 0.1 metre radius). The results are usually presented as interval travel time or "slowness", which is the reciprocal of velocity.

The phasor induction log provides an indication of whether or not the drilling mud is invading the formations by simultaneously logging the electrical conductivity at different

depths of investigation. The different depths of investigation are recorded as the tool is set up with varying receiver coil spacings, to record current generated in the formation by a transmitter coil. The transmitter coil uses an alternating current passing through it, to set up an alternating magnetic field, which in turn creates a current in the formation. The voltage measured by the receiver coils are proportional to the formation's electrical conductivity, which is then converted to a resistivity (Schlumberger, 1991). Each receiver coil creates a curve for its intended investigation depth, which when investigation depths are overlaid, allows one to infer invasion of drilling fluid. Impermeable formations result in a stacking of all the curves as no drilling fluid is able to invade the formation and alter the conductivity profile. Permeable formations allow drilling fluid to enter the formation, resulting in a change in the conductivity near the well bore. The induction log responds to porosity and pore fluid but also reacts to conductive minerals present in a formation (e.g., the presence of pyrite in sedimentary rocks).

The fullbore formation micro-imager (FMI) uses an array of 192 button electrodes to measure electrical variations from an upper electrode source and create a high-resolution 360 degree image of electrical resistivity variations on the borehole wall. The spacing and size of the button electrodes allows features larger than 5.1 mm (0.2 inch) to be identified from the FMI image (Schlumberger, 2002). The technology applied by the FMI allows identification and orientation of bedding planes, electrically conductive and non-conductive (i.e. resistive) fractures, cross-bedding, drilling-induced breakouts, and the presence of vuggy porosity. Such features are displayed using a tadpole plot. The dip of a feature on a tadpole plot is presented as a dot on a depth-dip graph. The tail extending from the dot corresponds to the dip direction of the feature with the upwards direction on the page representing north.

2.2.2.3 Porosity estimation using geophysical tools

Three of the logging tools described in the preceding section are commonly used to estimate formation porosity; i.e., the density log; the neutron log; and the sonic log.

Porosity is calculated from bulk density measured by a litho-density tool using assumed densities for the pore fluid and of the dominant matrix mineral present. Standard matrix minerals used for porosity calculations are quartz for sandstone, calcite for limestone, and dolomite for dolostone. As such, the calculated porosity is most accurate for "clean" lithologies (e.g., sandstone, in a setting predominated by clastic sedimentary rocks). Similarly, logging companies generally interpreted porosity from neutron logs using algorithms that are calibrated for "clean" lithologies such as sandstone (comprised solely of quartz) limestone (calcite) or dolostone (dolomite). The neutron and density logging tools are calibrated such that, in a "clean" lithology, the two porosity curves stack on top of each other. If the curves are not stacked on top of each other, which occurs for lithologies that are not "clean", the neutron and density porosity logs can be averaged as follows to attempt to remove some of the lithological effects (Doveton, 1999):

$$\emptyset_{ND} = \frac{\emptyset_N + \emptyset_D}{2} \tag{2.1}$$

Where:

$Ø_{ND}$ = averaged neutron and density porosity
$Ø_N$ = neutron porosity
$Ø_D$ = density porosity

Porosities derived from sonic logs are not commonly presented, as there is more than one equation for calculating sonic porosity. One such equation is the Raymer-Hunt equation, which is presented in Schlumberger (1991) as follows:

$$\emptyset_{sonic} = C\,\frac{t_{LOG} - t_{ma}}{t_{LOG}} \tag{2.2}$$

Where:

$\emptyset_{sonic}$ = sonic porosity

C = constant

t_{LOG} = log transit time (μs/m)

t_{ma} = matrix transit time (μs/m).

Porosity values measured by geophysical logs in sandstone often overestimate the porosity measured on cores. The cause is typically the shale content present in the rock. To correct for the shale content and determine the effective porosity, the porosity where pores are interconnected, the gamma ray logging tool results are used. The effective porosity is important as rocks may possess significant porosity and have no fluid permeability, because the pore spaces are all isolated and are not interconnected. The shale content and volume fraction of shale present are calculated using the log responses of the gamma ray, as follows:

$$X = \frac{GR_{LOG} - GR_{CLEAN}}{GR_{SHALE} - GR_{CLEAN}} \tag{2.3}$$

Where:

X = shale content

GR_{LOG} = log response from gamma ray tool

GR_{CLEAN} = log response from gamma ray tool in a clean sandstone (i.e., free of shale)

GR_{SHALE} = log response from gamma ray tool in a shale formation

$$V_{SH} = \frac{0.5*X}{1.5-X} \quad (2.4)$$

Where:

V_{SH} = volume fraction of shale
X = shale content

If clean sandstone and shale are present in the succession that has been logged, the gamma ray readings obtained in these lithologies are used for GR_{CLEAN} and GR_{SHALE}, respectively. Otherwise, estimations of clean sand and shale values must be used.

The calculated volume fraction of shale is used to correct the averaged neutron-density porosity and the sonic porosity values described above. The effective neutron-density porosity (Equation 2.5):

$$\emptyset_{EFF\_ND} = \emptyset_{ND} * (1 - V_{SH}) \quad (2.5)$$

Where:

$\emptyset_{EFF\_ND}$ = effective neutron and density porosity
$\emptyset_{ND}$ = averaged neutron and density porosity
V_{SH} = volume fraction of shale

The corrected sonic porosity is still calculated using Equation 2.2, but the matrix transit time is modified to account for shale volume fraction as follows:

$$t_{ma} = t_{SH} * V_{SH} + (1 - V_{SH}) * t_{SS} \quad (2.6)$$

Where:

t_{ma} = matrix mineral transit time (μs/m)
t_{SH} = shale transit time (μs/m)
t_{SS} = sandstone transit time (μs/m)
V_{SH} = Volume fraction of shale

2.3 Hydrogeology of rock masses

The hydrogeological properties of rock masses are a result of their geological and tectonic histories. In a sedimentary basin, the permeability is initially a function of the size and interconnectivity of pore spaces, reflecting the lithology and depositional environment. Subsequent alteration of the deposited sediment, resulting from changes in the geological and/or tectonic setting, generally alters the hydraulic conductivity of the rock mass. The extent of alteration features like conductive and resistive fractures, and reduction staining, reflects the scale of influence of the change in setting. For example, a local fault is expected to result in local alterations to porosity and permeability of the rock mass, where as a regional fault is expected to regionally affect the rock mass. Characterizing features becomes a problem of scale, as seen in Figure 2.7. Cores may be sampled and hydraulically tested in the laboratory, but the sample volume is small relative to the volume investigated by geophysical measurements made in a borehole. The scale of these borehole measurements is also relatively small compared to the scale of hydraulic testing methods like drill stem testing and hydrophysical logging to measure features on an intermediate scale. The scale of investigation of the intermediate-scale testing is typically not large enough to confirm continuity of features between widely spaced boreholes and inference or interpretation using seismic data is required.

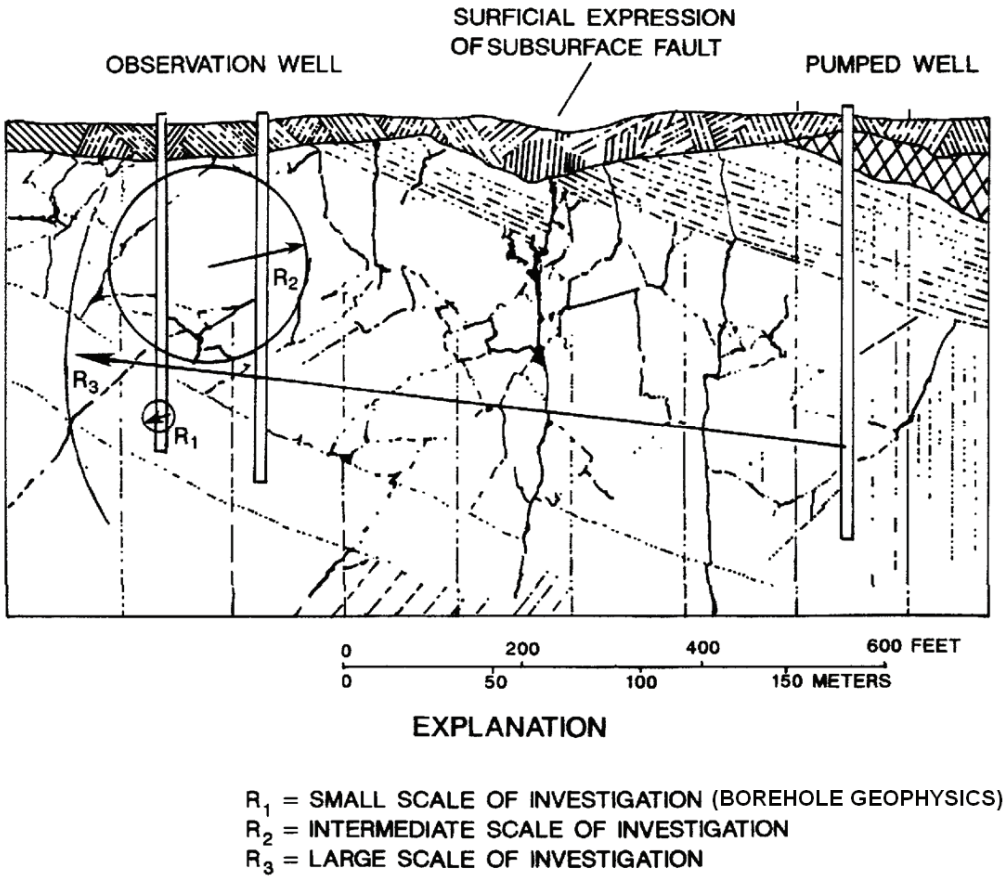

Figure 2.7 - Illustration of the effects of scale on measurements (after Paillet et al., 1993)

Two types of porosity can exist in a rock mass, primary and secondary porosity. In the case of clastic sedimentary rocks, primary porosity comprises void spaces existing between mineral grains (Tiab, 1999). The permeability associated with primary porosity is largely dependent on three factors: the size of the pore spaces or voids; infilling of pore spaces with smaller minerals (commonly referred to as cements); and, the interconnectivity of the pore spaces. The average size and the distribution of grains influence pore properties.

Coarser grained sediments, such as sandstones, typically have high matrix permeabilities when compared with finer-grained siltstones and claystones, as they possess larger pore spaces and better interconnectivity.

Secondary porosity can be created when a mineral originally present within a rock is dissolved by groundwater, increasing the overall porosity (Tiab, 1999). When large amounts of minerals are dissolved away, vugs are created. Vugs are pore spaces within the rock mass that were once occupied by mineral nodules. The presence of vugs is an indication that water has historically flowed through the rock mass to dissolve the original host minerals that occupied the vugs.

Secondary porosity may also be created if stress changes induce fractures and joints within the rock mass. Secondary permeability created by fractures, solution openings, and solution along bedding planes is quite possibly the single most important class of heterogeneity in sedimentary aquifers (Paillet et al., 1993).

A fracture within a rock mass is a feature that has potential to create significant permeability and is governed by its aperture, infilling and roughness. Fractures with large apertures result in high permeability. High permeability is decreased by reducing the aperture of the fracture either by the rocks physically moving closer together (compaction), sedimentation and/or precipitation within the fracture. Two methods of observing fractures within a borehole are FMI logs and drill cores. FMI logs allow one to visualize fractures based on an electrical conductivity image, while drill cores allow fractures to be seen with the naked eye. Further, fractures may be indirectly measured or inferred from borehole acoustic logs and caliper logs.

Overall, alteration of the original rock mass by means of dissolution of minerals, creation of fractures or joints and precipitation of minerals within original or secondary pore spaces affects the permeability of the rock mass. Alteration noted during characterization of a rock mass should not be considered confirmation of a permeable horizon and should be used as supporting evidence alongside hydraulic testing. When used alone, alteration features may create false positive predictions of permeable horizons. For instance, the presence of reduction staining does not confirm present day permeability within a reduction stained zone, but is an indicator that historically waters have flowed through

the zone to create the staining. Vugs that are visible in FMI logs as highly conductive patches do not necessarily confirm the presence of electrically conductive fluid. The conductive nature of vugs spotted on the FMI log may be caused by conductive fluid in a large void but it is also possible for the same result to be produced by highly conductive clays infilling pore spaces that had been vugs. As with reduction staining, using the FMI tool alone may not confirm permeability of a rock mass, and should only be used to support results of hydraulic tests.

A single hydraulic test, measuring water flow under pressure, should not be used to confirm regional hydrogeology, as this may be measuring local permeability. Permeability on a local scale is affected by local alteration features such as jointing, but may not represent the regional hydrogeology of the study area. Regional hydrogeology is characterized by large-scale flow paths. Large-scale flow paths and interconnections between fractures and solution openings are dependent on the large scale structure of the rock mass (Paillet, 1991a; as referenced in Paillet et al., 1993). These large-scale structures include faults and bedding planes in sedimentary rocks, and faults and lithological contacts for igneous and metamorphic rocks.

2.3.1 Tools for characterizing hydraulic zones

Tools that are used for downhole characterization of hydraulic properties and are relevant to this study include: drill stem tests (DST) and hydrophysical logging (HPL).

2.3.1.1 Drill stem tests

Drill stem testing provides an estimate of formation permeability and pore pressure by hydraulically isolating an interval of a borehole, drawing down pressure for a period of time by allowing formation fluid to flow into the drill stem, then measuring the pressure build-up that occurs after shutting in the tool, by closing a valve at the base of the drill stem (Chaudhry, 2004). Two types of tests can be performed: a bottom hole test, where the bottom of the well is sealed off at some upper level using a single packer; and a

packer or interval test, in which the bottom and top of an interval are isolated from the rest of the well using two packers.

Figure 2.8 presents a typical pressure plot associated with the four phases of a drill stem test: running the tool into the hole (A-B); flowing the well (C-D and F-G); shutting in the well (D-E and G-H); and pulling the tool out of the hole (H-I). A standard test consists of at least two flow periods, a pre-flow and final-flow, and at least two shut-in periods, an initial shut-in and a final shut-in period. The purpose of the often short pre-flow period is to clean out near-well damage and drawdown the formation pressure. This is often necessary because the mud column used while drilling creates a pressure differential causing the near-well area to become over pressured and damaged, as drilling fluid infiltrates the formation and causes a mud filter cake to be created on the borehole wall. The initial build-up allows a build-up of pressure to a natural state, prior to any flow periods that may be used in calculations.

The static pore pressure is extrapolated from a Horner Plot, which is created from shut-in pressures; usually those obtained during the final shut-in period. A Horner plot is a plot showing shut-in pressure versus Horner time (Reid, 2010), where Horner time is:

$$Horner\ time = \frac{t_p + \Delta t}{\Delta t} \tag{2.7}$$

where:

t_p = the total flowing time of the drill stem test prior to shut-in

Δt = the shut-in time

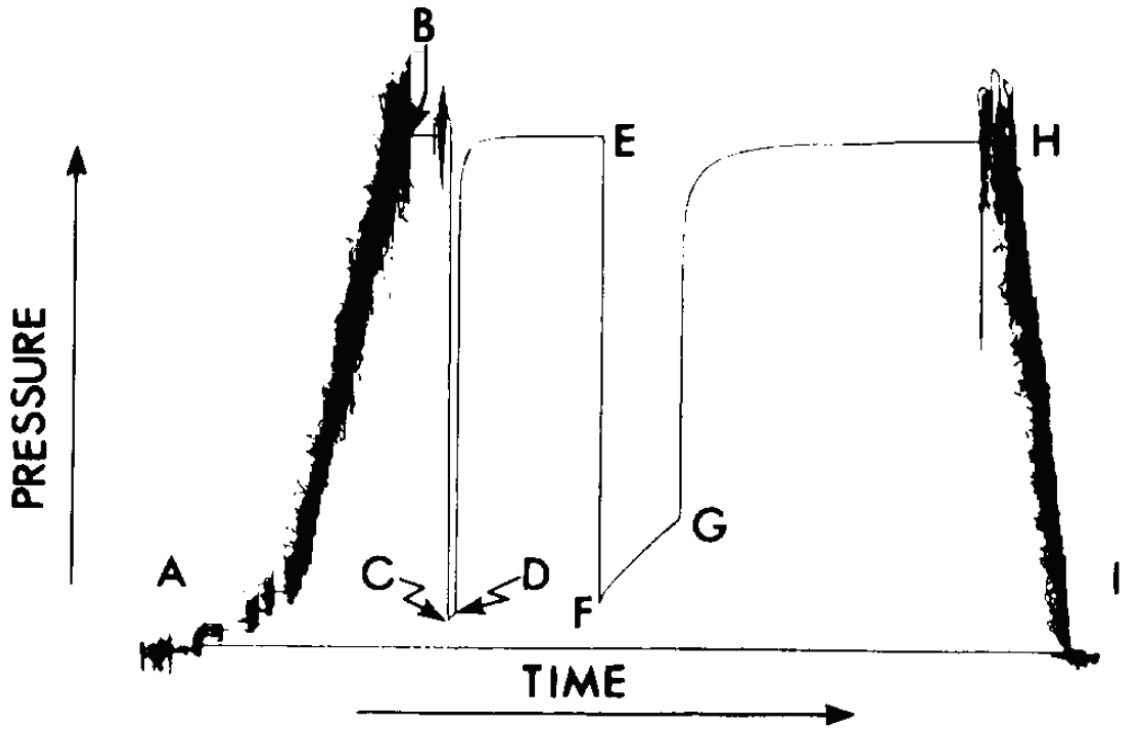

Figure 2.8 - Sample of DST pressure record (after Hackbarth, 1978)

The function of a Horner plot is to extrapolate shut-in pressures to infinite time, as a means of estimating the static formation pore pressure, and to also determine the slope (m) of the extrapolated pressure trend line over one log cycle of time as follows:

$$m = \frac{P_1 - P_{10}}{1 cycle} \tag{2.8}$$

where:

P_1 and P_{10} are pressures one log cycle apart on the extrapolated trend line.

The slope of the Horner plot is used for calculating the transmissivity (T) of the tested formation as follows:

$$T = \frac{kh}{\mu} = \frac{2149.4Q\beta_0}{m} \tag{2.9}$$

where:

T = Transmissivity (m^2/day)
Q = flow rate prior to shut-in (in standard cubic meters per day or Sm^3/D) measured from the preceding flow period(s)
β_0 = the formation volume factor (in "reservoir" or in-situ cubic metres per standard cubic metre; i.e., Rm^3/ Sm^3).

The permeability-thickness cross-product ($k \cdot h$) is simply obtained by multiplying the transmissivity by the viscosity of the flowing phase, μ (mPa·s). To calculate the permeability, the thickness of the flow zone must be known or estimated (e.g., from core or logs). A DST cannot differentiate between a 12 m thick, 10 md permeability zone and a 1 m thick, 120 md permeability zone, as they both would produce the same volume of fluids into the drill stem during a given flow period.

2.3.1.2 Hydrophysical logging

The hydrophysical logging tool is a specialized tool that characterizes fluid flowing into boreholes. "HydroPhysical logging was originally developed for application in very deep boreholes (>1500 m) associated with nuclear waste isolation studies" (Pedler et al., 1992). When developing the tool, the borehole conditions logged using the hydrophysical tool were validated using downhole flow metering, straddle packer testing, and downhole fluid sampling.

The hydrophysical logging tool is a temperature/conductivity array that is broken down into four sensors, each 6 inches apart with a 90 degree offset to minimize errors caused by borehole conditions. The purposes of the tool are to: identify the depth and location of water-bearing intervals; estimate the interval-specific fluid electrical conductivity (FEC) for each zone; evaluate the flow rates of each zone at two or more pressure states; and determine the permeability or hydraulic conductivity. [Note: Conventional DST interpretation practice, as presented in the preceding section, is to characterize flow properties in terms of permeability (k). Conventional practice for hydrophysical logging is to characterize flow in terms of hydraulic conductivity (K). Appendix A explains the process for converting between these parameters.]

Hydrophysical logging (HPL) is based on the principles of dilution, measured using a time-lapse series of electrical conductivity logging runs. For dilution logging to be effective, the borehole must initially be flushed of drilling mud and injected with water possessing a salt concentration different from the native formation water; deionised water is often used as this contrasting fluid. By 'setting up' the well with a contrasting fluid, the ion concentration of the borehole water is altered as fluid infiltrates the well through fractures, vugs, and/or matrix porosity.

Once a borehole has been flushed of mud and injected with a contrasting fluid, the borehole is then logged under ambient conditions in order to observe inflows and/or outflows occurring under natural fluid gradients. It is common practice to subsequently conduct a second series of logs while altering the pressure conditions in the borehole, in order to assess the changes in flow rates resulting from these altered conditions. For example, a common follow-up test involves lowering the fluid column in the borehole by pumping fluid out of the well before re-logging.

Variations of pumping conditions may be required in some boreholes, depending on the characteristics of the strata that it penetrates. When flow into the borehole is small, or a natural contrasting fluid is flowing into the bottom of the hole from a flow zone with anomalous salinity, then drawing down the water level in the borehole may be deemed to

be sufficient for characterizing the well under pumping conditions. However, if flow into the borehole from permeable horizons is too large, dilution may occur too quickly relative to the rate at which the well can be logged, hence preventing accurate hydrophysical characterization of the well. Under such a condition, an injection pump may be placed at the bottom of the well (pumping during injection), and a low flow rate of contrasting fluid (e.g., deionised water) injected at the base of the borehole. This is done to ensure that dilution of the contrasting of fluids in the borehole does not occur too rapidly, as multiple loggings are required for characterization of the inflow locations and their associated flow rates (Figure 2.9).

Using the time series of electrical conductivities from several passes of the logging tool, the fluid's salt concentration at each inflow interval into the borehole can be calculated for both ambient and pumping conditions. The calculations assume a one-dimensional steady state mixing model, in order to match incremental flows and salinities from individual flow zones to the salinity and flow rate being pumped out of the borehole at surface. The method takes a mass balance approach to calculate inflow and salinity at each inflow interval.

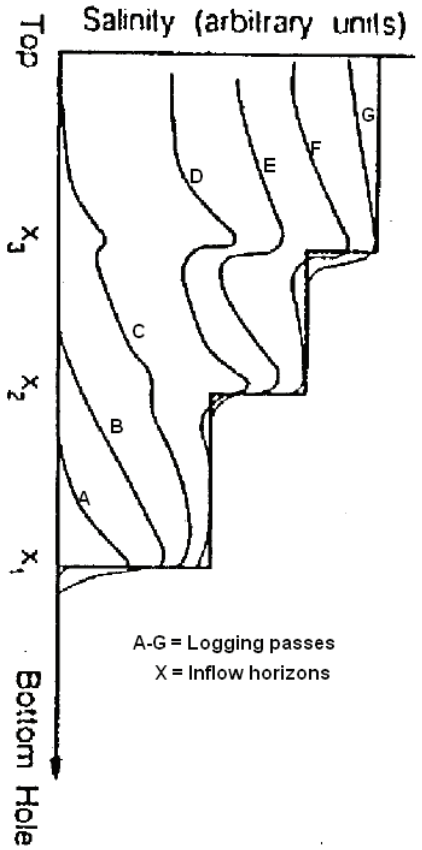

Figure 2.9 - Schematic of HPL logging passes (after Tsang et al., 1990)

At large time limits, each inflow interval results in an increase in salinity, which creates a step in the salinity profile. Smoothed corners are present, when it is assumed that minimal diffusion is present as shown by the dashed curve in Figure 2.10.

The modelling works strictly for a one-dimensional steady-state mixing model, because the initial flow and concentration, as well as the outflow and concentration, are known by surface measurements and are known variables, resulting in the same number variable as there are equations.

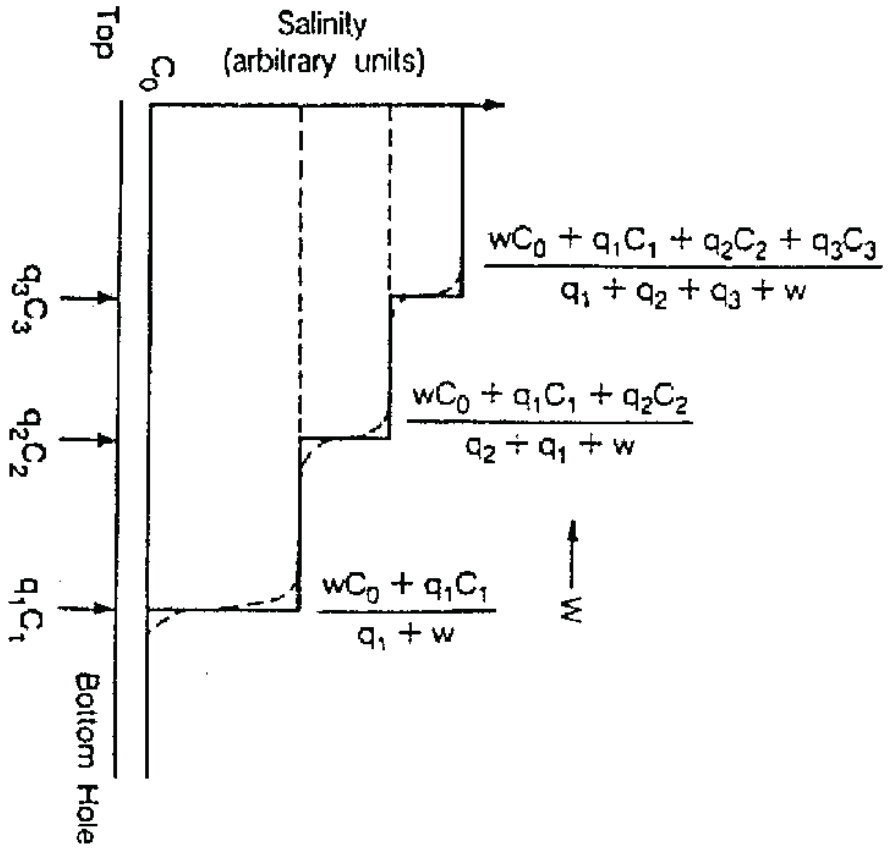

Figure 2.10 - Salinity concentration curves at large time limit (after Tsang et al., 1990)

The method uses a series of equations to calculate flow rate and salinity at each interval. If no permeable horizons are present, the outflow at surface is equal to the inflow at the bottom of the hole and the salinity at surface is equal to initial salinity of the wellbore water. When a single permeable horizon is present, the increase in flow rate and salinity at the surface is due to the permeable horizon. The increase in flow rate at surface is equal to the inflow rate of the permeable horizon. The increase in salinity at surface is equal to the salinity of the permeable horizon. A series of equations like Equations 2.10 and 2.11 (Tsang et al., 1990) are used to iteratively model the unknown variables at each step in the salinity profile.

$$flow\_rate\_at\_surface = w + q_i + q_{i+1} \tag{2.10}$$

$$C_{\max,i+1} = \frac{wC_o + q_i C_i + q_{i+1} C_{i+1}}{w + \sum_{n=1}^{i+1} q_n} \tag{2.11}$$

where:

w = borehole flow rate from below the surveyed section

C_o = the initial salinity of the wellbore water

q_i = inflow rate for interval i

C_i = fluid salinity for interval i

$C_{\max,i+1}$ = Salinity of fluid at surface

Combining the calculated flow rates with observations made during pumping of the well, the transmissivity of each fracture or flow zone may be estimated using the Theim equation (Pedler et al., 1992), as follows:

$$T = KL = \frac{\Delta Q_i}{2\pi\Delta h_w} \ln \frac{r_e}{r_w} \tag{2.12}$$

where:

T = transmissivity

K = hydraulic conductivity

L = length of tested interval

ΔQ_i = the change in flow rates from ambient flow conditions and pumping conditions

Δh_w = drawdown from ambient flow conditions and pumping conditions

r_w = radius of the well or tested interval

r_e = effective radius (if observation well data was not available, an effective pumping radius of 91 m (300 feet) is assumed (RAS, 2008b)).

2.4 Seismic reflection surveying

Seismic reflection surveying is relevant to this research, as it provides a means of characterizing stratigraphy and structures in the subsurface, and hence interpolating results between boreholes.

Seismic reflection surveys can be run in two and three-dimensions. Two-dimensional surveys provide a single cross section of an area of interest, while three-dimensional surveys create a three-dimensional image or a series of in-lines and cross-lines of the subsurface in the area of interest. The added costs associated with three-dimensional surveys are frequently considered to be acceptable, because three-dimensional seismic provides a more complete understanding of the subsurface during imaging (Biondo, 2006).

Seismic surveys are based on acoustic impedance changes in the subsurface. The acoustic impedance of a given volume of rock is proportional to the product of its acoustic velocity and density (Kleyn, 1983). As a practical point, it is useful to note that acoustic velocity is the reciprocal of the acoustic 'slowness' or interval transit time, which is the parameter that is typically presented on geophysical logs (Section 2.2.2.2).

When acoustic waves propagating through a rock succession encounter an interface between rock units with contrasting acoustic impedance values, a component of the wave is reflected by the interface and travels back towards ground surface; the sign and magnitude of the reflected wave is a function of the sign and magnitude of the impedance change occurring at the interface. Seismic reflection surveys take advantage of this behaviour to develop profiles of subsurface layers possessing different acoustic impedances (Figure 2.11-a).

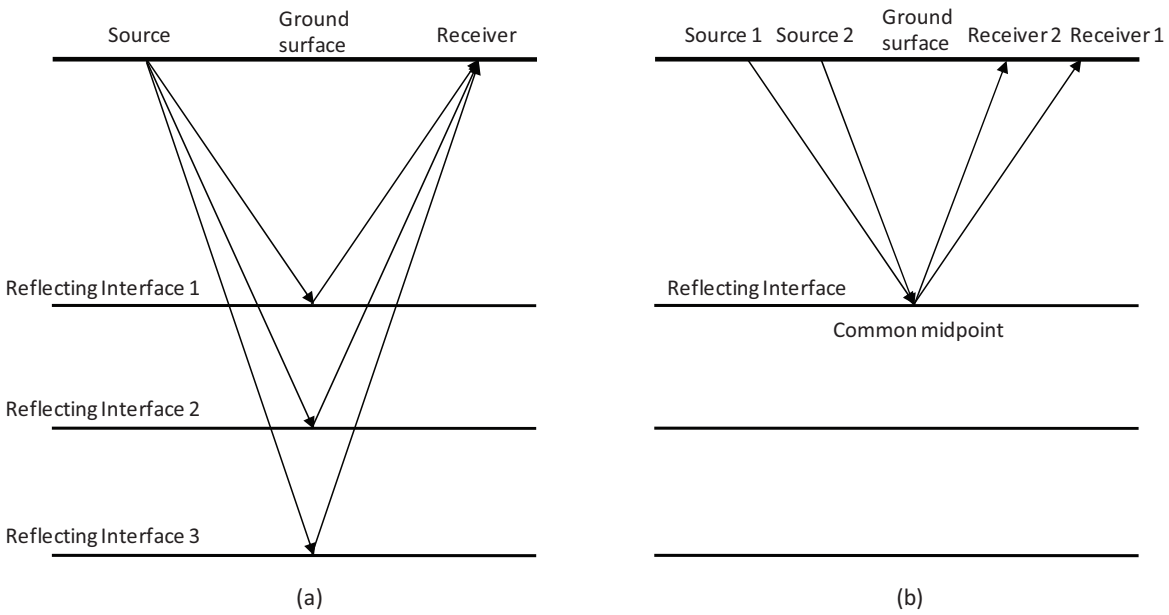

Figure 2.11 – (a) Basic 2D schematic of seismic reflection survey (after *Wightman, 2003)*; and (b) illustration of a common midpoint for two selected ray traces.

The sources used for seismic surveys are typically explosives that are set off in a line (2D) or grid (3D) of shallow holes, one hole at a time, or by use of one or more mechanical elastic wave generator (EWG) trucks. EWG's are used near pipelines and houses, or anywhere else that explosives are prohibited. Reflections generated at subsurface interfaces return to surface and may be detected by a line (2D) or grid (3D) of geophones (receivers) upon its arrival. The time required for the acoustic wave to travel down to the each interface and back is recorded.

When acquiring field data for a seismic reflection survey on land, acquisition parameters like the geometry of the geophones and source locations must be determined prior to conducting the survey in order to find an acceptable balance between cost and resolution, often with a particular depth interval in mind as the zone requiring the best quality data. Parameters such as bin size and fold, defined below, are central to the survey design.

Sorting the acoustic wave traces by common midpoint, as shown in Figure 2.11-b, is desirable and conceptually simple; however, due to the complexities arising during data acquisition (e.g., non-planar and/or dipping interfaces, irregular or complex combinations

of source and/or receiver spacings at surface), sorting by common-midpoints is not possible as the traces do not share the exact same midpoint coordinates (Biondi, 2006). To work around this obstacle, binning is performed prior to common-midpoint sorting. Binning at a given depth refers to placing a grid within a horizontal plane at that depth. All points located within a cell in the grid are assigned coordinates that correspond to the midpoint point of the cell (Figure 2.12). The size of each bin is determined by the acquisition parameters of the survey and can vary in length between the in-line and cross-line directions.

The term fold is used to refer to the number of traces that are assigned to a bin. If no irregularities in geometry occur, the number of traces falling into each grid is called the nominal fold (Biondi, 2006). Higher fold numbers generally give rise to better data quality.

The ultimate goal of seismic processing is to create an image of the subsurface . Formulating a subsurface image is the most data-intensive and computationally demanding aspect of the processing process. Two options for imaging are time imaging and depth imaging. Time imaging presents an image with the z axis as a function of time (i.e., the two-way travel time for acoustic ray traces), where depth imaging presents an image with the z axis as depth. To map a time image relative to depth an independent step often called map migration is required. For further differences between the two imaging techniques refer to Biondi (2006).

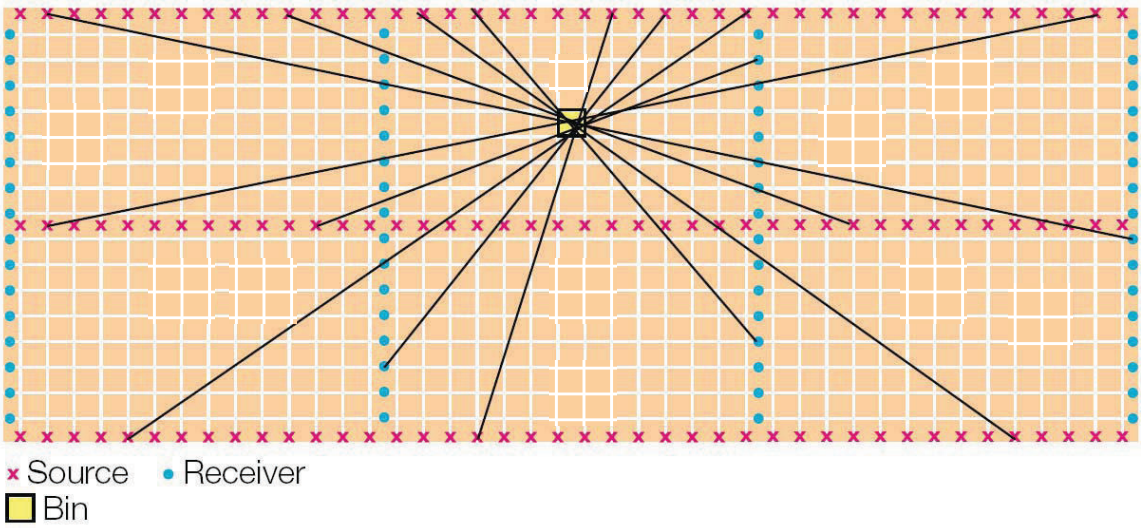

Figure 2.12 – Source and receiver offsets and azimuths in a common mid-point bin for a 3D seismic survey (after Ashton et al., 1994)

3 ASSESSMENT OF GEOPHYSICAL DATA

3.1 Overview of PCS's Borehole Data Collection Activities

Data collection for the Picadilly development has been ongoing for nearly a decade. The collection of data to characterize the hydrogeology started simultaneously with the beginning of the exploration program for the Picadilly area. A summary of the services performed in the drill holes used for this project is presented in Table 3.1, along with a map (Figure 3.1) displaying the location of the drill holes.

Table 3.1 - Drill hole summary table

Drill Hole	Date	Drill core and Photographs	DST	Geophysical logs		FMI	Cuttings	HPL
				Run by DGI	Run by Schlumberger			
PCS 0201	2002	x		x				
PCS 0202	2002	x		x				
PCS 0502	2005	x	x	x				
PCS 0504	2005	x	x	x				
PCS 0601	2006	x	x		x	x		
PCS 08105	2008				x	x	x	x
PCS 08107	2008				x	x	x	x
PCS 08113	2008				x	x	x	x
PCS 08115	2008				x	x	x	x

Where:

FMI = Fullbore Formation Microimager

HPL = Hydrophysical logging

DST = Drill stem test

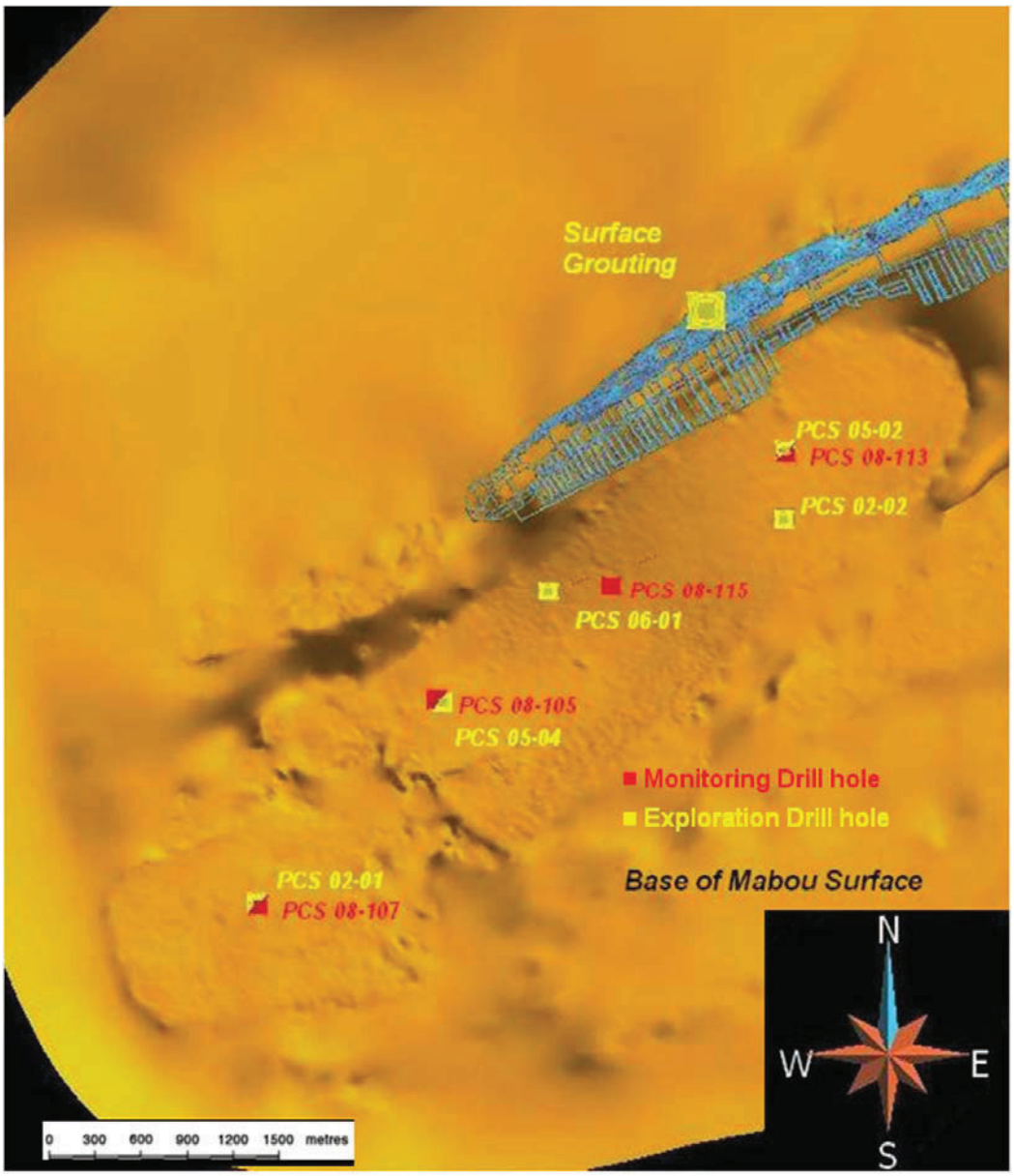

Figure 3.1 - Drill hole locations (the orange-gold surface is the current PCS interpretation of the base of the Mabou Group based on seismic reflection profiles and surface geology)

Due to the promising results obtained from the exploration in 2002, a second phase exploration program was undertaken in 2005, to better characterize and delineate the potash deposit. Further to coring and geophysical logging, this second phase was expanded to include drill stem tests (DSTs) at selected intervals to assess the flow potential of the overlying Mabou Group.

The two-phased exploration program provided sufficient data to create plans for the expansion of PCS potash assets in New Brunswick. The drilling of a pilot well (PCS 0601) for the purpose of sinking two mineshafts was executed to retrieve as much information as reasonably possible about the near-shaft area. The pilot hole was cored, a suite of geophysical logs was run by Schlumberger, including a formation micro image log (FMI), and DSTs were performed at selected intervals.

As the project continued, PCS put into place a program to drill several boreholes to establish potential inflow sources in the Picadilly region. The monitoring holes drilled during this program were located close to the previous exploration wells to reduce both the surface foot-print created by drilling operations and the size of the "sterilized" area; i.e., the area in which the resource will not be mined, in order to avoid mining too close to any potential flow conduits. The boreholes were grouted to mitigate the potential for such a scenario to occur, but the designation of sterilized areas is undertaken as an added precaution.

The monitoring drill hole program was designed to allow for a shallow drill hole and a deep drill hole to be drilled at each location. All of the deep drill holes drilled in 2008 were planned to be drilled to (or nearly to) the base of the Mabou. Due to complications, borehole PCS 08105 did not reach the base of the Mabou. It was tested and then abandoned further up hole within the Coarse Sandstone subdivision (defined in Section 4.2).

3.2 Borehole Data Assessment

Given that the borehole data used in this research had been collected prior to the commencement of the author's masters program, it was reviewed to assess its quality and to find errors that may have been previously overlooked. Borehole data included: borehole locations, depths, borehole deviations, characterization of core (RQD), wireline geophysical data, drill stem test results, and hydrophysical logging results. The

importance of this exercise quickly became apparent, as several minor errors were discovered within the data set. For example, incorrect calculations of RQD values, based on the length of recorded intact core over 10 cm relative to the length of the core run. To improve the reliability of the data and to improve its accessibility, a database was created for storing the data that had been verified.

The cores from the 2002 exploration wells were of use in providing insights into the stratigraphy and rock quality. However, the author's confidence in several of the geophysical logs obtained for these boreholes was low due to the inability of the logging company to produce repeatable data when selected sections were re-logged. The logs from these boreholes were not used in this study. Due to the subjective nature of the core strip logs, as mentioned in Section 4.1, only core photographs from these boreholes were used to help understand the stratigraphy of the area.

A significant outcome of the author's data assessment was the following: the geophysical data of the 2006 pilot well and the 2008 monitoring wells logged by Schlumberger are of higher quality when compared with the earlier exploration boreholes' logs. Aspects of the Schlumberger logs that led to this assessment include the following: pre- and post-verifications were presented on the well logs, showing that the tools were working properly before and after logging; repeat sections were run (according to standard procedure in the oil and gas industry), and these demonstrated that each tool could generated reproducible results; and comparisons of the total depths recorded by the drilling and the logging company (Schlumberger) were presented, thus explicitly demonstrating accurate depth control.

Results for several of the geophysical logs from the 2005 exploration program were also questionable for the same reasons as given above. As a result of the lower confidence, these geophysical logs were also not used. The wells' drill core photographs were used to visualize the stratigraphy of the area and to provide a starting point for understanding attributes of the zones chosen by PCS for DSTs. The DST testing program included bottom hole DST tests for the lower portion of all the holes, and packer tests, or interval-

specific testing, performed at chosen sections. The need to select discrete intervals to test gives rise to the possibility of missing potential flow zones such as fractured zones that were often not tested, but observed in core directly above and below intervals that measured flow.

Using the hydrophysical tool of RAS Inc. in the 2008 monitor wells provided the opportunity to improve the confidence in the interpreted DST permeable zones. The continuous nature of the log provided the opportunity of logging any missed flow zones from previous DSTs. The continuous nature also provided a better vertical resolution for the identification of flow zones in the borehole when compared with the 12 metre packed off intervals for the interval drill stem tests. Also, to improve confidence and check the quality of the drill stem test results, a sample transient analysis calculation of the drill stem test data was performed and is discussed later in Section 5.4.2.

3.3 Overview of PCS Seismic Reflection Survey Data Acquisition

A three dimensional seismic program conducted by Boyd PetroSearch was run in 2004 over the Picadilly region. Both explosives and an elastic wave generator (EWG) truck were used to create source waves within the study area, which covered an areal extent of 43.4 square kilometers. The design of the survey was for a minimum fold of 800% at an offset of 500 metres using a 20 x 20 metres bin size (Boyd PetroSearch, 2005).

4 DEVELOPMENT OF A GEOLOGICAL FRAMEWORK

To develop the geological framework for this study, a field investigation was initially undertaken to gain a better general understanding of Mabou stratigraphy, and was followed by compiling strip log data, geophysical data and core photographs from exploration and monitoring drill holes within the study area. The locations of the drill holes within the study area were previously presented in Figure 3.1.

4.1 Field Investigation

A field excursion was undertaken October 13 to 17, 2009 by: the author; Nazrul Islam (PhD. Candidate at the University of New Brunswick); Dr. Douglas Milne; Dr. David Keighley; and Dr. Chris Hawkes. The purpose of the excursion was to view Mabou Group outcrops and gain a better general understanding of its stratigraphy, coupled with an inspection of PCS 0502 drill core, the only accessible drill core.

Most of the field work focussed on the shoreline of Pecks Point, in the Cumberland Subbasin, roughly 75 km east of the Picadilly study area (see Figure 4.1). At Peck's Point, a continuous outcrop the Mabou roughly 1 km in length exists. The major points of relevance noted at this type section pertained to reduction staining and the spatial attributes of conglomerate strata.

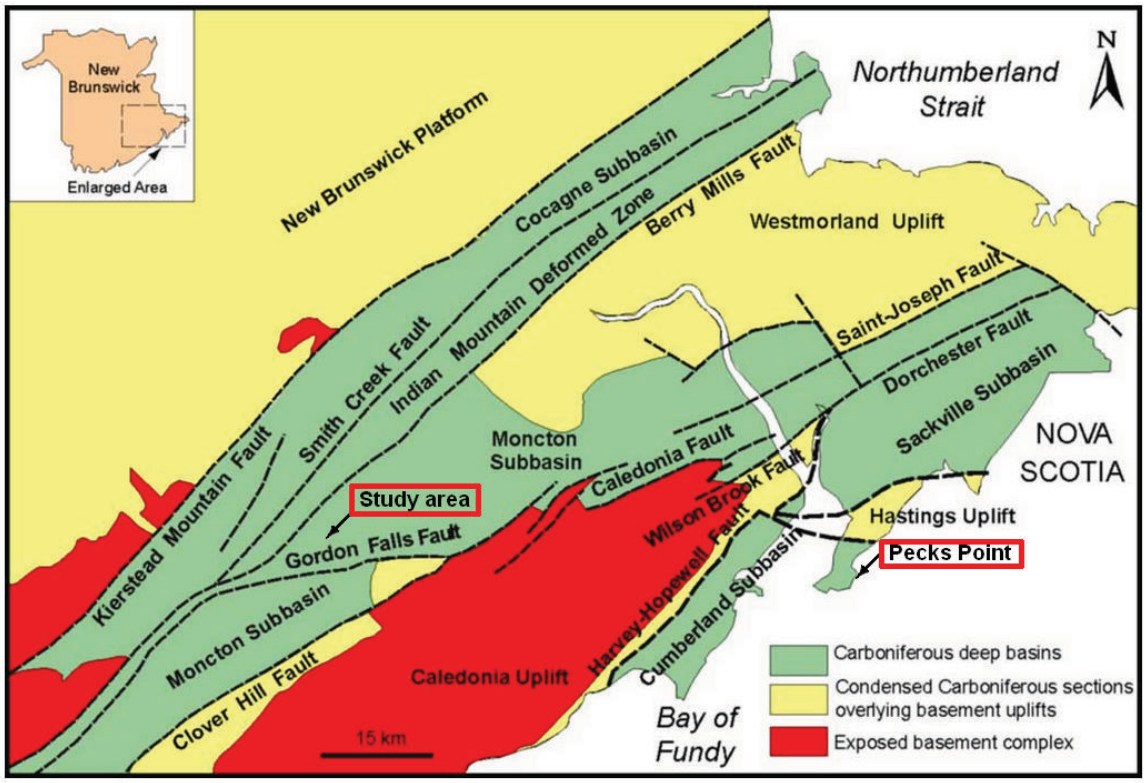

Figure 4.1 - Location of Mabou type section at Pecks Point relative to study area (after DNR, 2011)

Reduction staining, readily visible as localized green-coloured features within the predominantly red beds of the Mabou, was observed predominantly on two of the three orthogonal joint sets present at the site (Figure 4.2). The reduction stained joints were sub-vertical and at right angles to the sub-horizontal bedding. This staining suggests that these features have been conduits for flow, at some point in the past, hence enabling the reaction of through-going water with the rocks adjacent to the joints. With no major outcrop sections in the study area and the only presence of rock being cores, the author did not expect to see the detail of reduction staining on joint sets within the study area, merely the ability to observe its presence.

In a manner typified by the conglomerate unit identified in Figure 4.3, several conglomerates in the outcrop were observed to pinch out; i.e., they occur as lenses rather than laterally continuous layers. This is consistent with the complexity of the Mabou lithology mentioned in Section 2.1. This is relevant to a hydrogeological characterization, as it suggests that individual conglomerates found in the Mabou Group

are not likely to serve as laterally continuous, high-permeability flow units over the scale of kilometres.

Figure 4.2 - Dr. Milne pointing out the presence of reduction staining

Figure 4.3 - Dr. Milne pointing towards a conglomerate unit which is pinching out

A second set of Mabou outcrops was visited in the Millstream area roughly 15 km southwest of the Picadilly study area. Outcrops of the order of a few metres in length were found along small creeks that run through the area. The transition from Windsor Group strata to the overlying Mabou Group was observed in these outcrops. Though the Mabou at this location was felt to be a good analogue for the Picadilly study area, a key difference at this location was the absence of an evaporite sequence in the Windsor. Mabou Group sandstones present in these outcrops are known to contain calcite (personal communication, D. Keighley). This observation is relevant when considering the theories for the origin of the gypsum present in the study area, presented in Section 2.1.1. The plausibility of the second theory, in that gypsum is the result of a sea water advance, is supported by the presence calcite in the lower section of the Mabou Group in Millstream.

The importance of calcite is that calcium concentrations in seawater and fresh water are too low for gypsum precipitation. However, during a seawater intrusion, sodium and

magnesium cations from the seawater are able to displace calcium ions on exchange sites (Gomis-Yagues et al., 2000). The result is that calcium goes into solution. If the advancing seawater reaches a high enough calcium concentration in solution, gypsum precipitation is possible, because the only requirements for gypsum precipitation are sufficiently high sulphate and calcium concentrations to reach the solubility product of gypsum. Sea water has a relatively high sulphate concentration and the other requirement has been filled by cation exchange process.

4.2 Informal lithological subdivisions

Given that no formal subdivisions of the Mabou Group have yet been interpreted for the study area, the interpretation of informal subdivisions was undertaken in order to provide a framework for hydrogeological characterization. Initial work on subdividing the group focused on the use of strip logs (seen in Figures 4.4, 4.5, 4.6, 4.7 and 4.8) available for the exploration wells, the pilot well, and their associated lithological descriptions.

When studying the lower section of each of the strip logs, it quickly became evident that inconsistencies existed in the subjective criteria used by the geologists when interpreting the lower half of the strip logs. The inconsistency occurred between the interpretation of the 2002 exploration drill holes (Figures 4.4 and 4.8) and the later drill holes (Figures 4.5, 4.6 and 4.7). The strip logs for PCS 0201 and PCS 0202 portrayed a ~50 m thick, medium to coarse-grained sandstone in the lower portion of the borehole (~400 m depth). Although this ~50 m thick sedimentary unit has not been explicitly identified on the strip logs generated for wells drilled since 2002, lithological descriptions presented for these more recent wells do include mention of grain-sizes coarsening (to ‘medium’ grained sandstones) over a section in the lower portion of the boreholes.

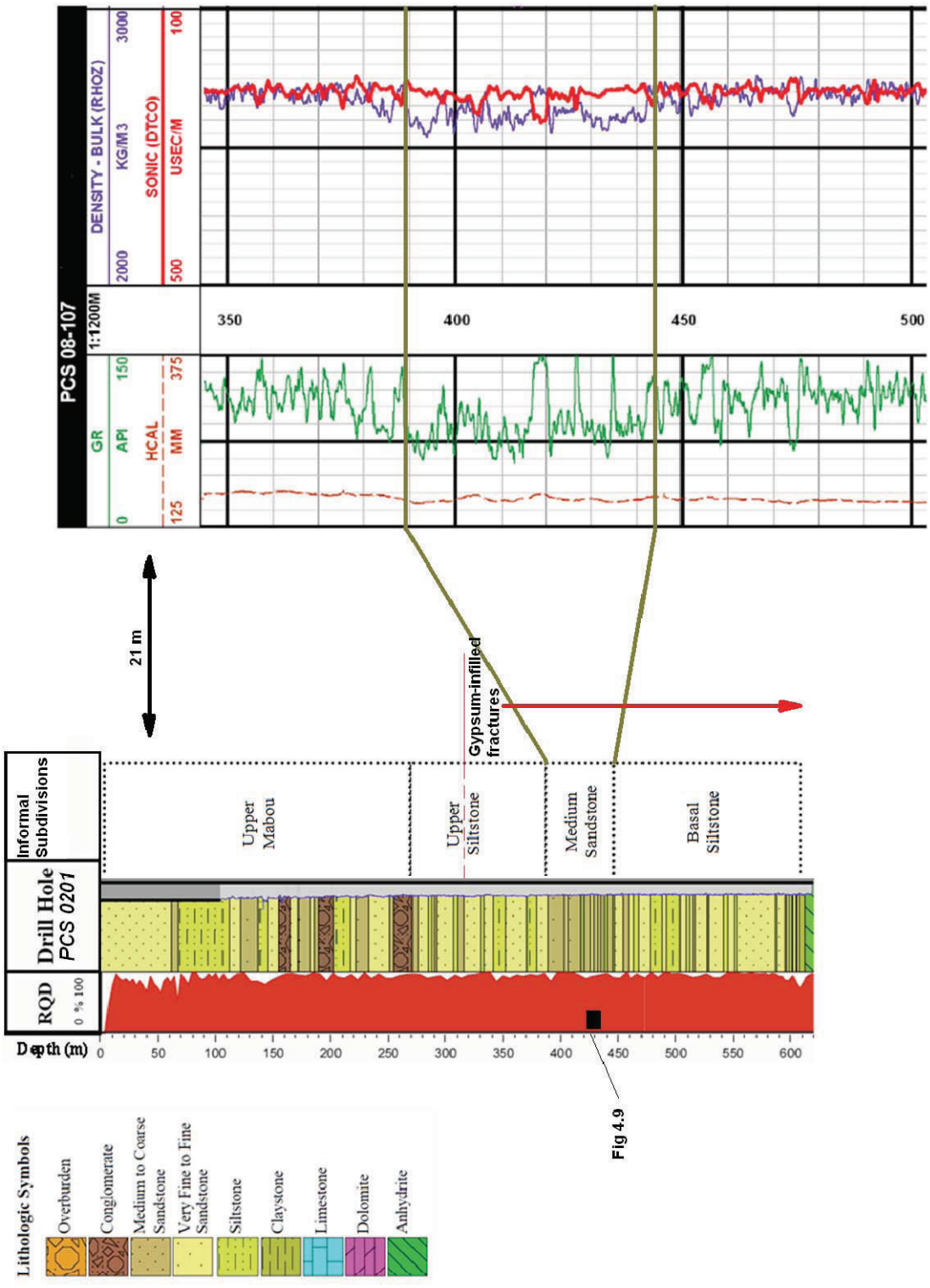

Figure 4.4 –Medium Sandstone subdivision within PCS 08107 geophysical log referenced to the strip log of PCS 0201 (after PCS, 2002a)

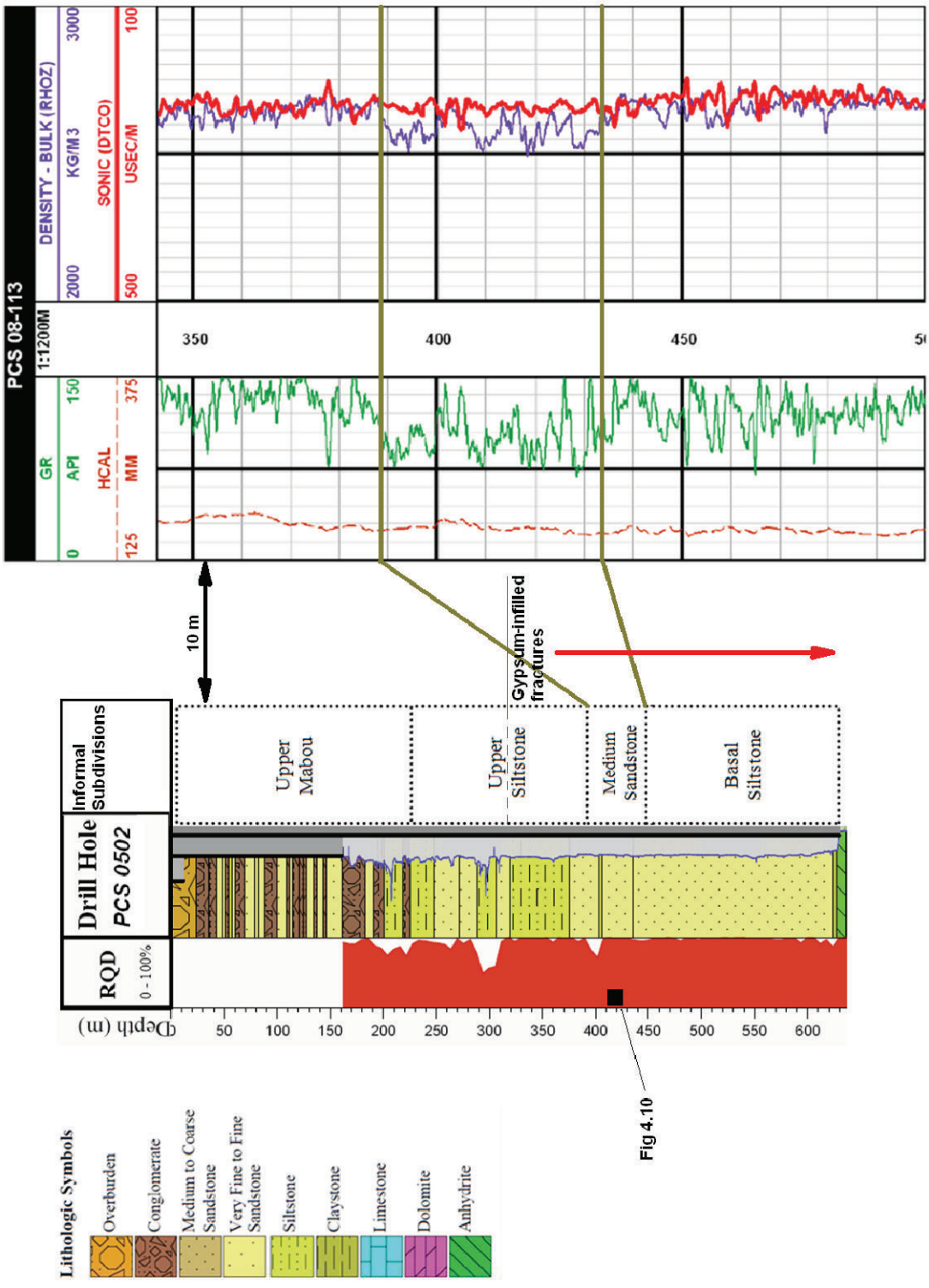

4.5 - Medium Sandstone subdivision within PCS 08113 geophysical log referenced to the strip log of PCS 0502 (after PCS, 2005a)

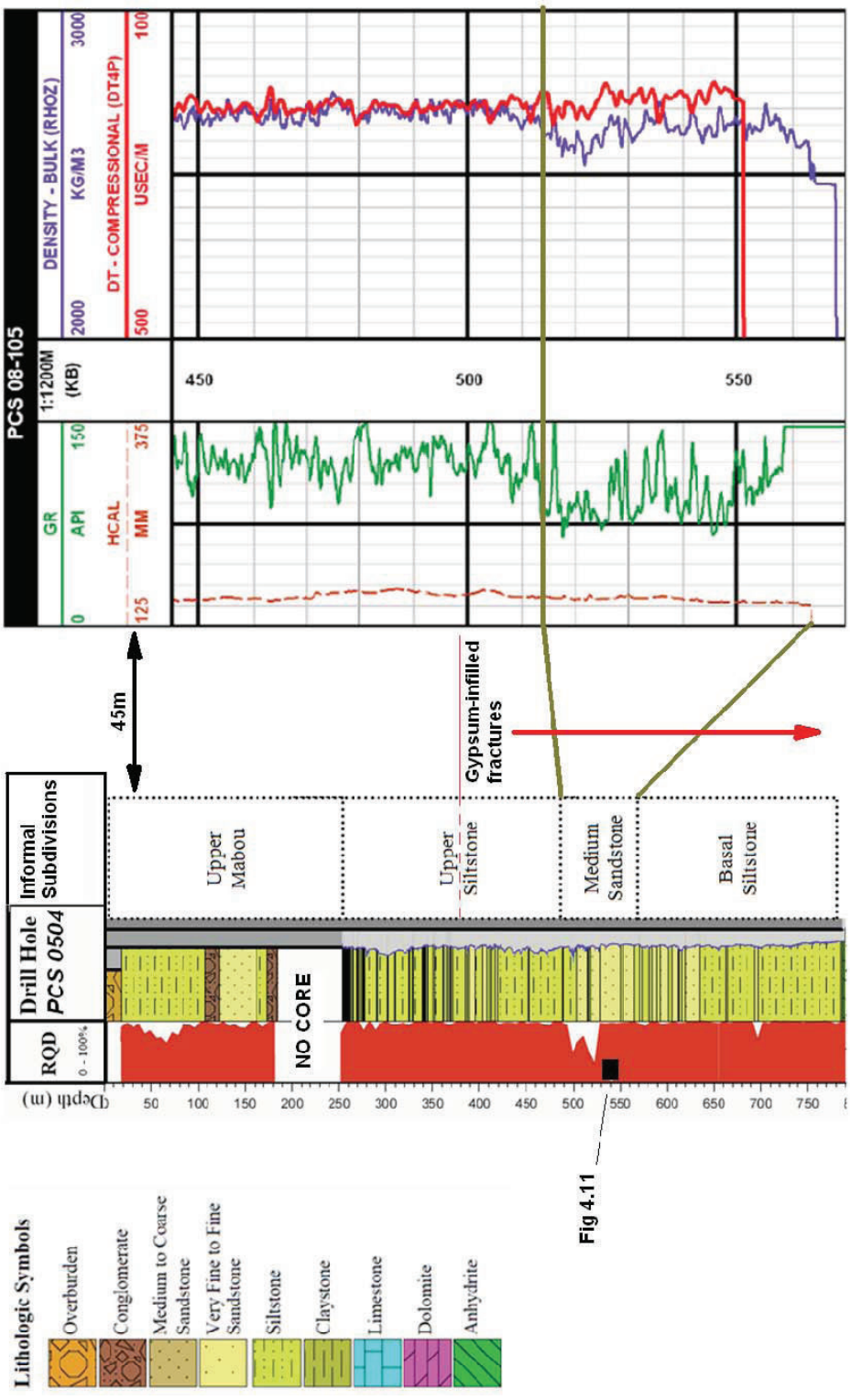

4.6 - Medium Sandstone subdivision within PCS 08105 geophysical log referenced to the strip log of PCS 0504 (after PCS, 2005b)

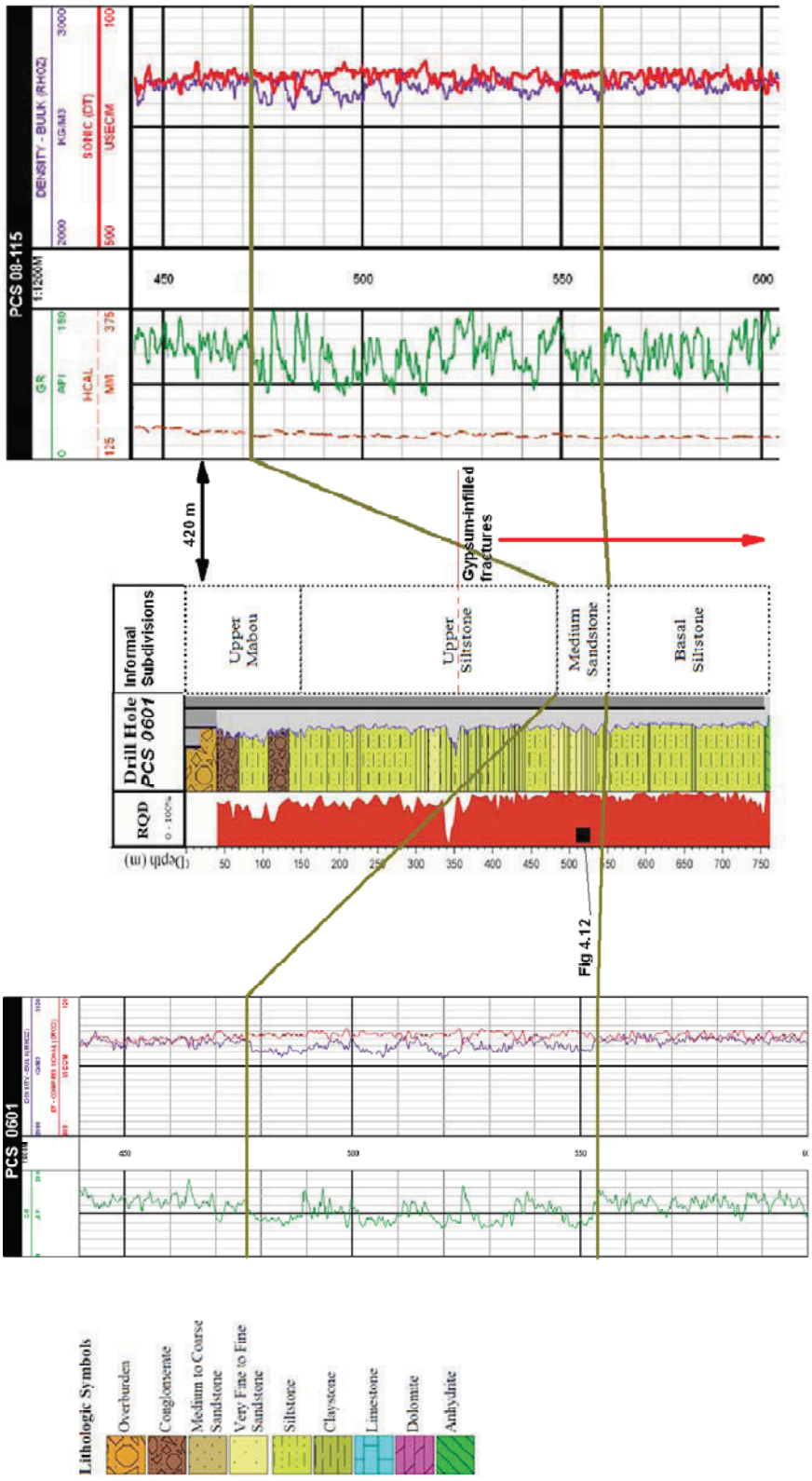

Figure 4.7 - Medium Sandstone subdivision within PCS 0601 and 08115 geophysical logs referenced to the strip log of PCS 0601 (after PCS, 2006)

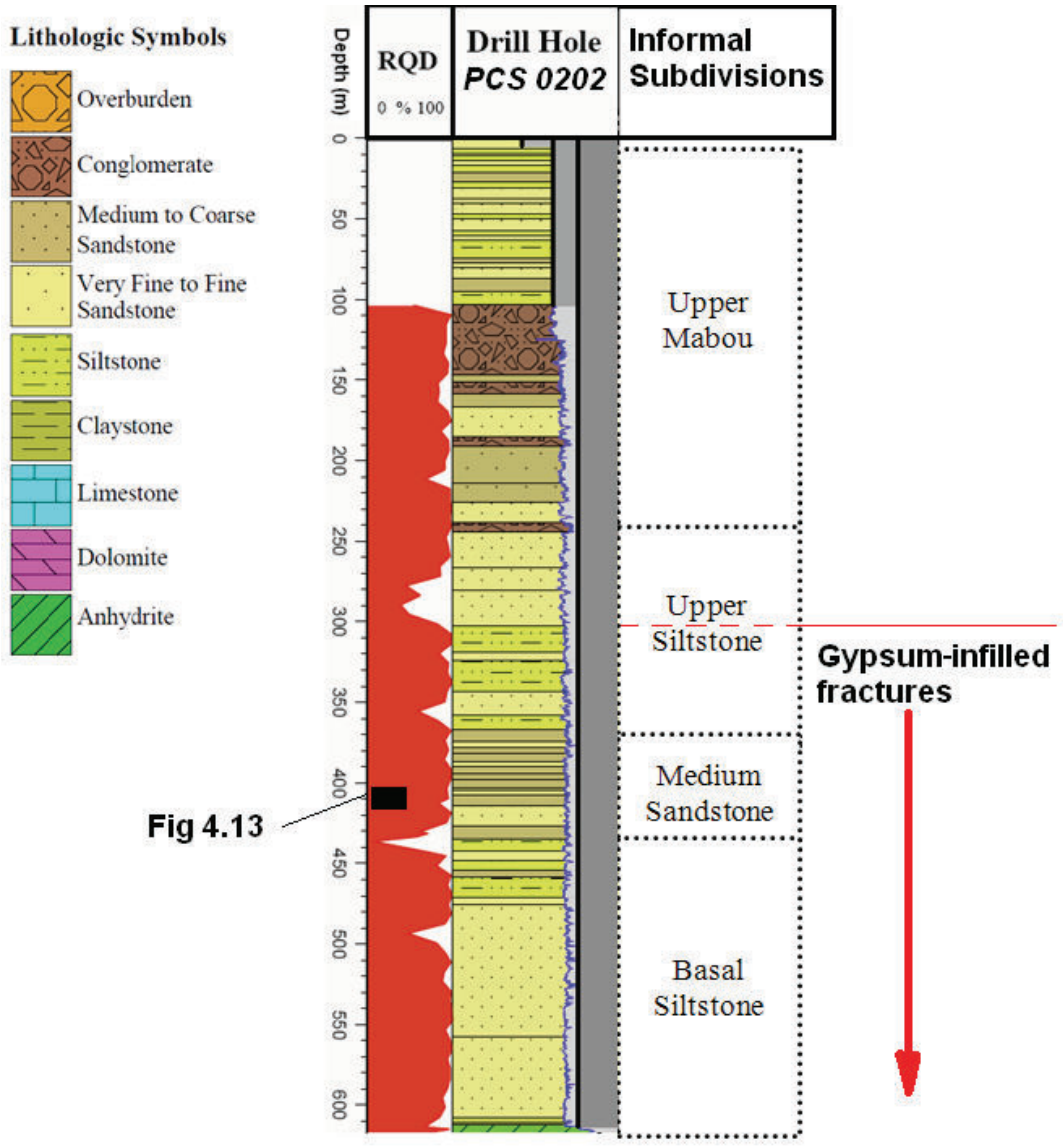

Figure 4.8 - PCS lithological strip log (after PCS, 2002b)

To confirm that the discrepancy was based on the interpretations of the geologists logging the core and not truly a distinct change in grain size, core photographs from all five wells within the 50 m thick horizon of expected medium to coarse-grained sandstone unit were compared (Figures 4.9, 4.10, 4.11, 4.12 and 4.13). Visual comparisons of the core photographs appear to suggest that all the photographs could be part of the same sedimentary package. Geophysical logs of nearby monitoring drill hole were investigated to attempt to resolve whether or not the ~50 m thick medium to coarse-grained sandstone unit existed throughout the study area; this was done by determining if all wells in the study area with high quality logs showed a consistent geophysical signature throughout

the zone in question. Geophysical logs (Figures 4.4, 4.5, 4.6 and 4.7) from the wells paired to the exploration striplogs present a separation in a sonic-density overlay (i.e., a marked decrease in density occurs while sonic transit time remains approximately constant) at the expected depth of the medium to coarse-grained sandstone.

A likely explanation for the aforenoted sonic-density separation is an increase in primary porosity in the sandstone, along with a decrease in matrix (mineral grain) transit time that more-or-less counteracts the effect of the increased porosity on the sonic transit time. Such a reduction in transit time (i.e., increase in velocity) is consistent with the transition to a high quartz-content / low clay-content in this subdivision. This is consistent with the gamma-ray log response over the intervals with sonic-density separation, as the gamma-ray tends to read low (i.e., reduced clay content) in these intervals. Based on the consistency of the sonic-density separation in the geophysical logs it was decided to define this 50 m as a sandstone unit, in spite of being described as siltstone.

Only the upper section of all four strip logs presented conglomerates interbedded with siltstones and/or fine grained sandstones. Since conglomerates were only present in the upper portion of each drill hole, a subdivision was created using the deepest location of conglomerates as the lower boundary.

Figure 4.9 - PCS 0201 medium to coarse grained sandstone (Photograph courtesy of PCS)

Figure 4.10 - PCS 0502 'medium' grained sandstone (Photograph courtesy of PCS)

Figure 4.11 - PCS 0504 'medium' grained sandstone (Photograph courtesy of PCS)

Figure 4.12 - PCS 0601 'medium' grained sandstone (Photograph courtesy of PCS)

Figure 4.13 - PCS 0202 medium to coarse grained sandstone (Photograph courtesy of PCS)

Following on the two aforementioned distinctions, four informal subdivisions were interpreted and used for this work (Figure 4.14). The four subdivisions, from bottom to top, include: the Basal Siltstone, the Medium Sandstone, the Upper Siltstone, and the Upper Mabou. The selection of these subdivisions was based on lithological changes and is consistent with the approach used by Anderle et al. (1979) in the Marchbank syncline.

The deepest subdivision (Basal Siltstone) is defined as an interbedding of siltstone and fine-grained sandstones. Above this subdivision, grain size transitionally increases to the second subdivision. The second subdivision (Medium Sandstone) is composed of medium to coarser sandstone with minor interbeds of fine-grained sandstone and siltstone.

GROUP	INFORMAL SUBDIVISIONS	GENERAL LITHOLOGIES
MABOU	Upper Mabou	Cgl, SiltS, fine SS
	Upper Siltstone	SiltS, fine SS
	Medium Sandstone	med SS, coarse SS
	Basal Siltstone	SiltS, fine SS

Figure 4.14 - Informal subdivisions and general lithologies of the Picadilly area in the western Moncton Subbasin, as interpreted in this work

The third subdivision (Upper Siltstone) constitutes interbedded siltstones and fine-grained sandstones. The last and shallowest subdivision (Upper Mabou) is defined as an interbedding of conglomerates, siltstones, and fine-grained sandstones. The transition between the last two subdivisions is defined by the deepest occurrence of interbedded conglomerate.

4.3 Presence of gypsum in the study area

The presence of gypsum was identified but not subdivided into the general lithologies because infilling of fractures by gypsum was considered the result of an alteration process and not relevant to original deposition and lithology. The relevance of gypsum and the informal subdivisions will be demonstrated in chapter 5. Its location is characterized by its presences in core photographs and descriptions, and the presence of resistive fractures in tadpole plots created from FMI logs.

Tadpole plots (Figures 4.15, 4.16 and 4.17) present a large number of resistive fractures in the lower half of the Mabou Group, in the study area. Evidence of gypsum infilling starts within the Upper Siltstone subdivision and ranges down to the base of the Basal Siltstone subdivision.

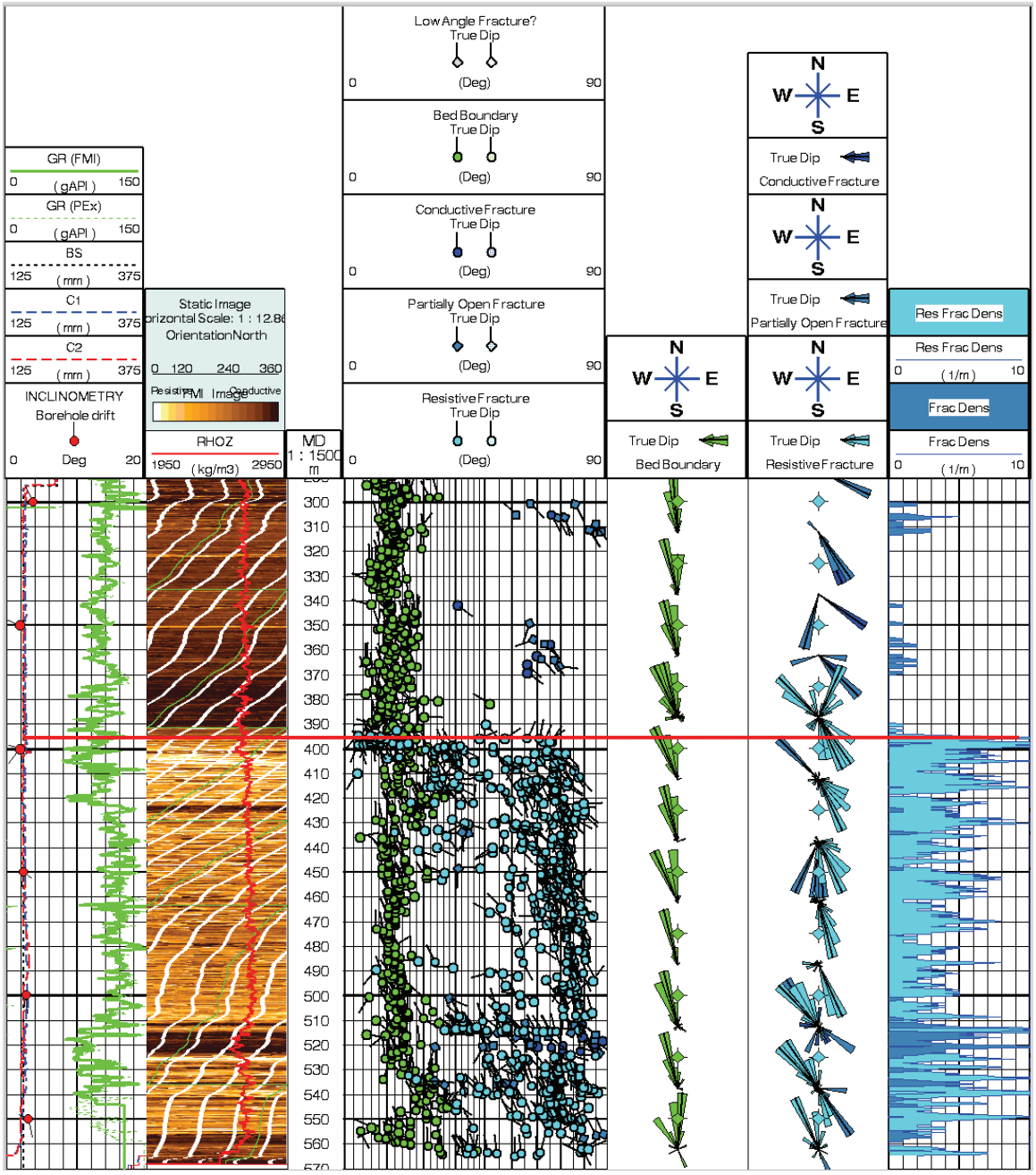

Figure 4.15 - PCS 08105 - FMI Tadpole plot. Top of gypsum-infilled fractures denoted by the red horizontal line (after Schlumberger, 2008a)

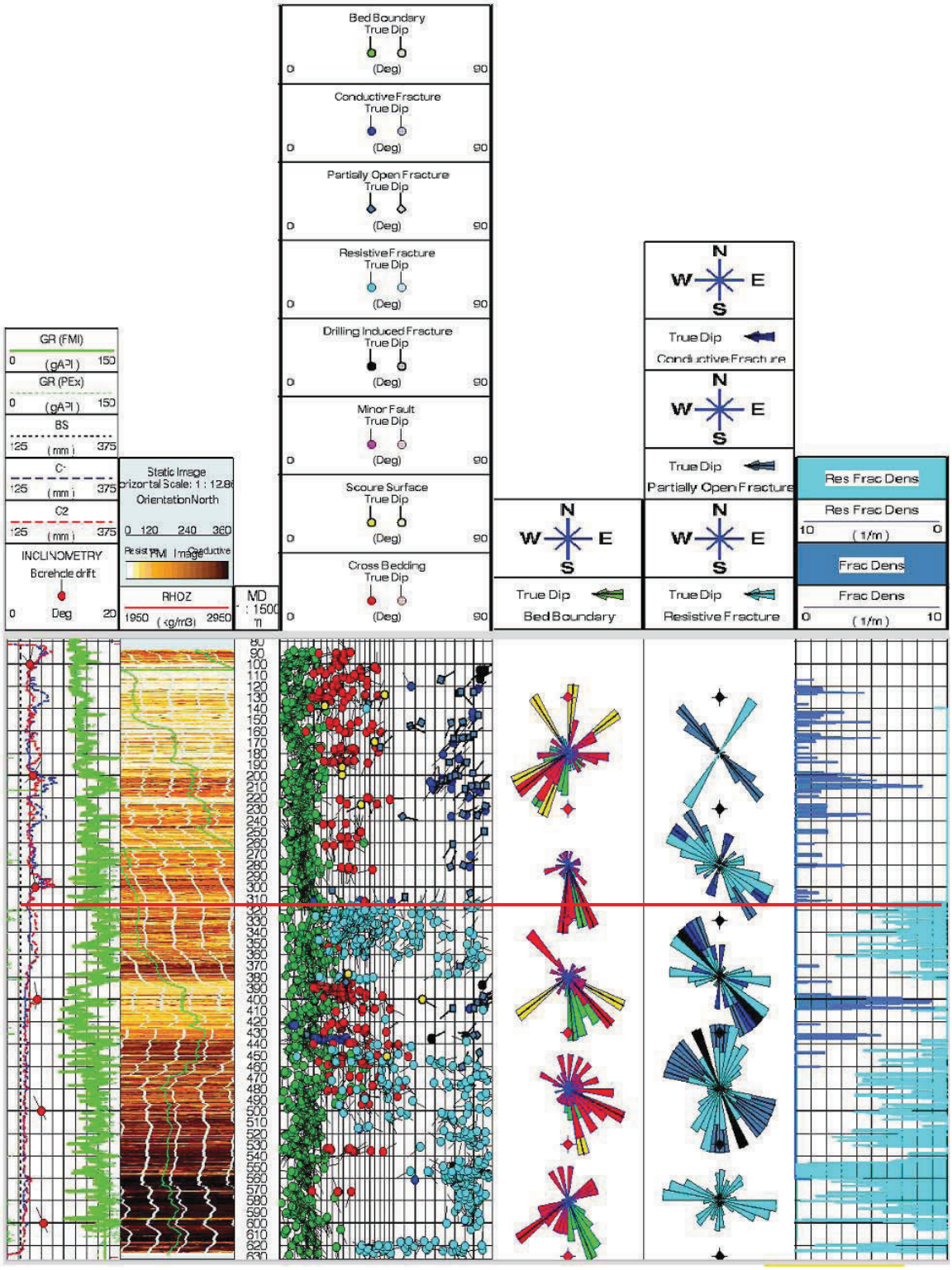

Figure 4.16 - PCS 08113 - FMI Tadpole plot. Top of gypsum-infilled fractures denoted by the red horizontal line (after Schlumberger, 2008b)

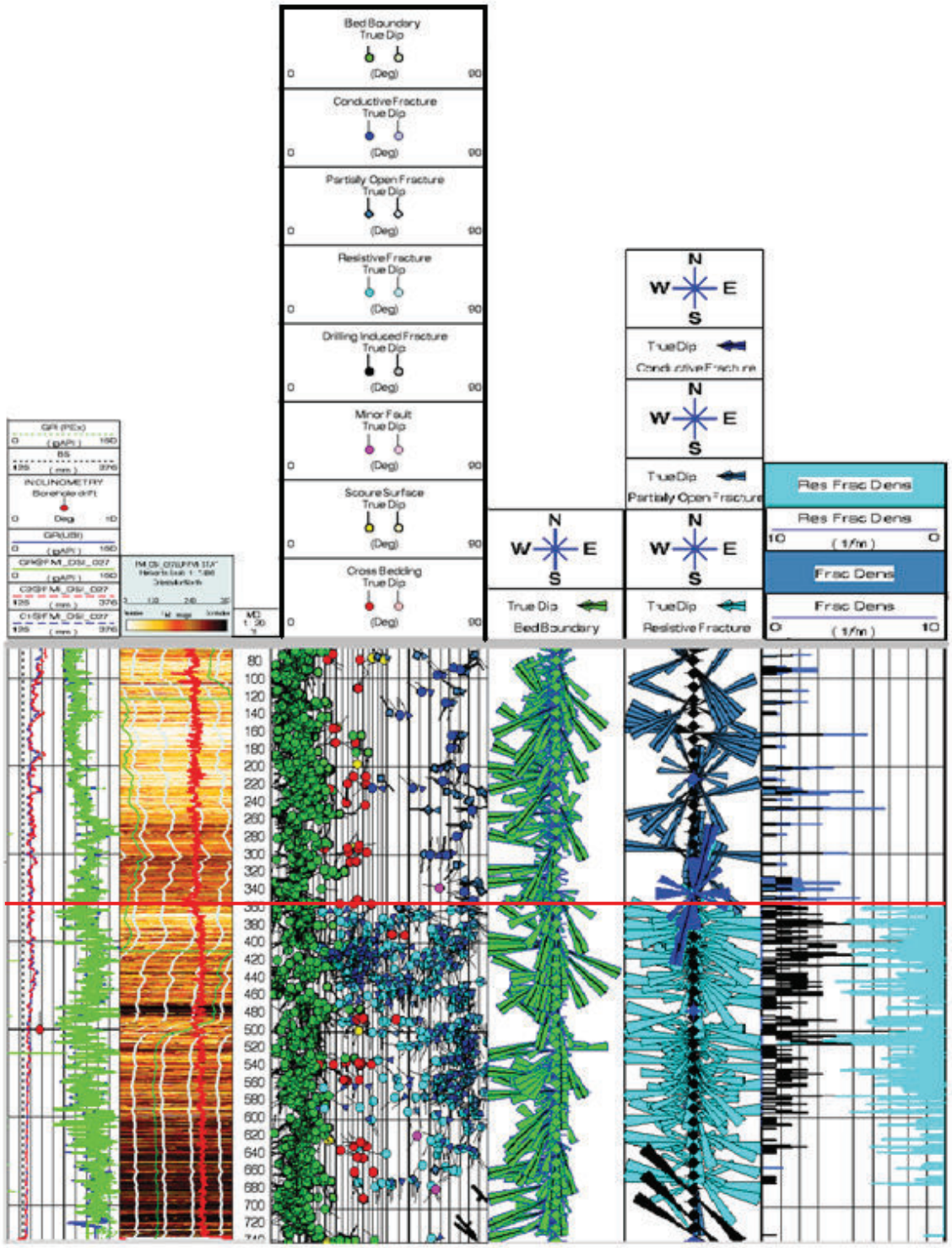

Figure 4.17 - PCS 08115 - FMI Tadpole plot. Top of gypsum-infilled fractures denoted by the red horizontal line (after Schlumberger, 2008c)

Visible dissolution to form vugs does occur periodically in core located directly above the contact of gypsum-infilled fractures and within the Medium Sandstone subdivision. RQD presented in Figures 4.4, 4.5, 4.5 4.7 and 4.8, indicates low RQD above the gypum-infilled fractures in PCS 0202, PCS 0502 and PCS 0601 and zones of low within the Medium Sandstone of PCS 0202 and PCS 0504.

4.4 Porosity

The only porosity measurements within the study area were taken by means of geophysical logs. No laboratory porosity measurements were taken on Mabou Group cores within the study area. However, laboratory porosity values for Mabou Group samples were obtained by PCS from cores obtained adjacent to the study area, above the Penobsquis operation. These measurements were made as part of a testing program conducted by the University of Saskatchewan's Rock Mechanics Laboratory, prior to commencement of the research project presented in this thesis. The average porosity for five conglomerate samples measured in the Penobsquis – Mabou testing program was 4.6 %, with values ranging from 3.14 to 7.17 %. The 12 siltstone cores tested had porosities that ranged between 0.3 % and 5.4 %, with an average of 1.65%. .

Neutron, density and sonic logs were used in this research to calculate porosities in the Mabou Group. The results are presented in figures 4.18, 4.19, 4.20, 4.21, and 4.22. On these figures, the second track displays the neutron and density log-derived porosities provided by Schlumberger, based on algorithms for clean sandstone. The third track displays the averaged neutron-density porosity that was calculated using Equation 2.1, and the sonic porosity that was calculated using Equation 2.2. For the latter calculation, a constant (C) of 0.6 was used, as well as the matrix transit time of quartz, 180 μS/m (55 μS/ft) (Schlumberger, 1991).

The neutron-density and sonic porosity curves shows in track 3 yielded porosities ranging, on average, between 9 and 18 %. These values seem unrealistically high compared to the aforementioned laboratory testing results. To obtain more realistic

values, corrections for shale content were implemented using equations 2.3 – 2.5 (neutron-density) and 2.6 (sonic).

The study area lacked definitive clean sandstone and shale layers to use as baselines, hence values of 15 GAPI for clean sandstone and 135 for shale were assumed to calculate the shale content and the volume fraction of shale based on personal communication with Don Gendzwill (2011).

The corrected or effective neutron-density porosity is presented in track 4
The corrected sonic porosity, also presented in track 4, was calculated using an assumed sandstone matrix travel time of 180 μs/m and an assumed shale transit time of 250 μs/m. The latter value is deemed realistic for shale (Magara, 1978), and was found to yield porosities in the upper section of each borehole that were comparable to 0 and 5 % range observed in cores from the Penobsquis area (adjacent to the study area).

A comparison of these log-derived porosities to permeabilities interpreted from hydrophysical logging (track 5) is given in Chapter 5.

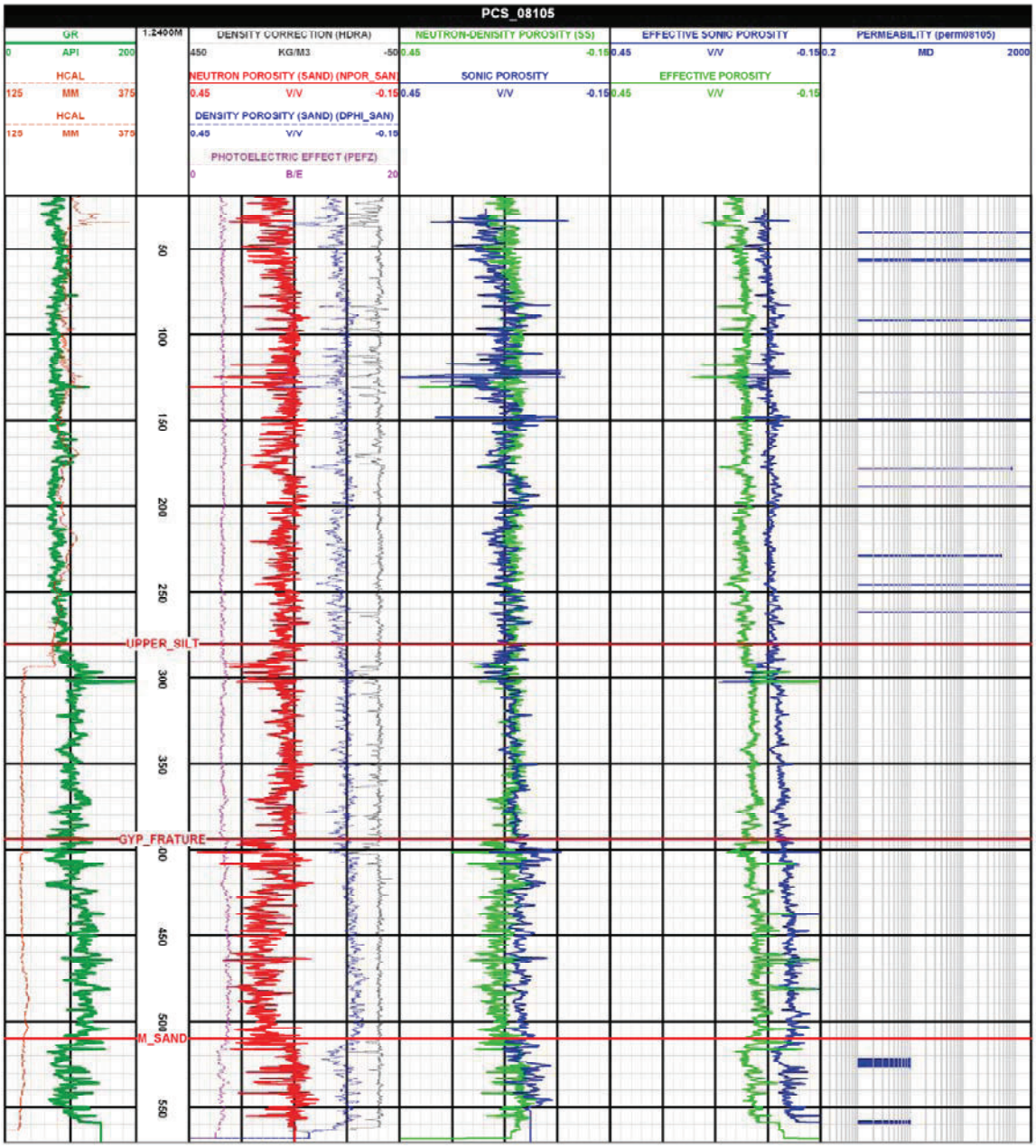

Figure 4.18 - Geophysical log-derived porosity curves for borehole PCS 08105, and permeability measurements discussed in Chapter 5

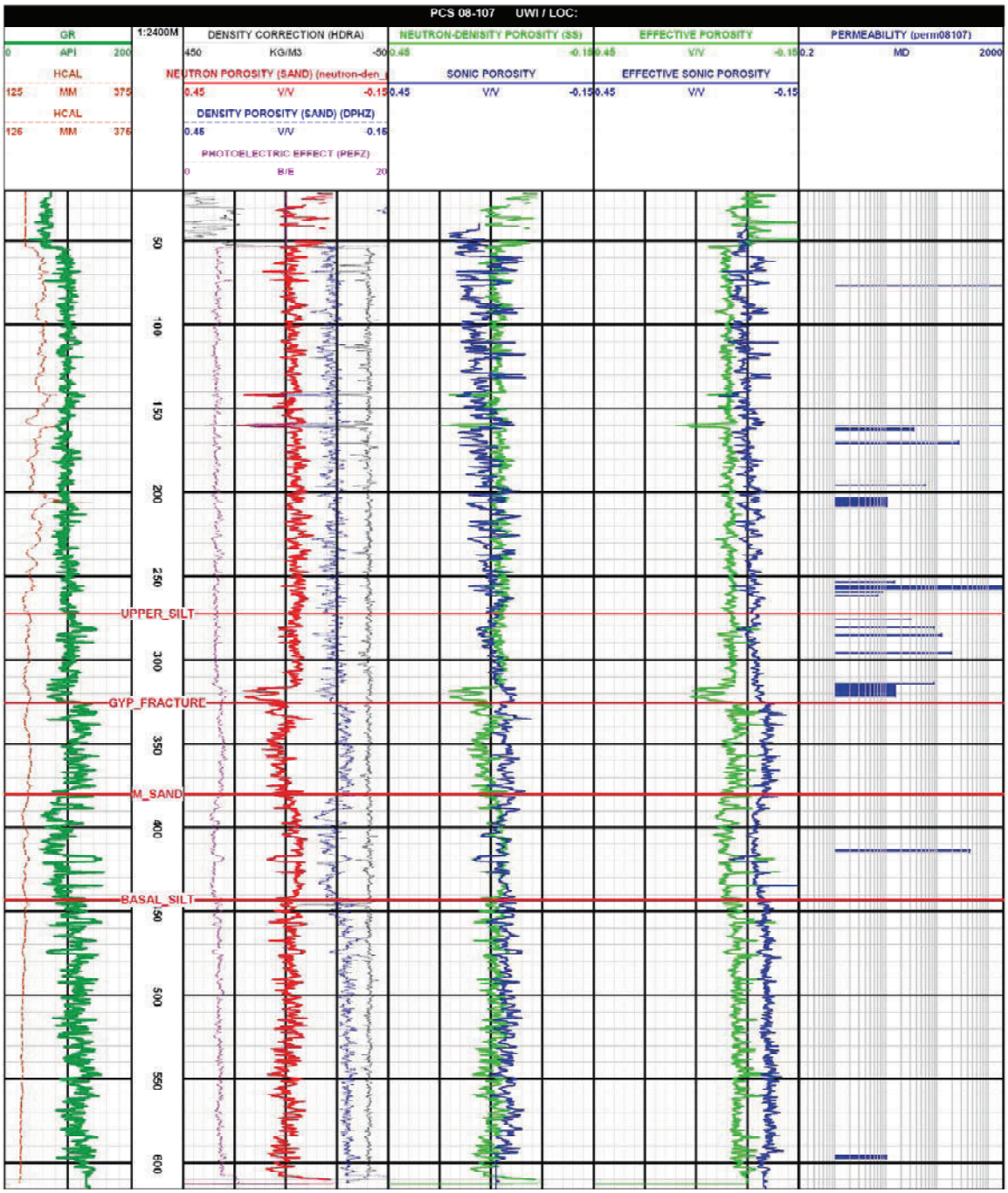

Figure 4.19 - Geophysical log-derived porosity curves for borehole PCS 08107, and permeability measurements discussed in Chapter 5

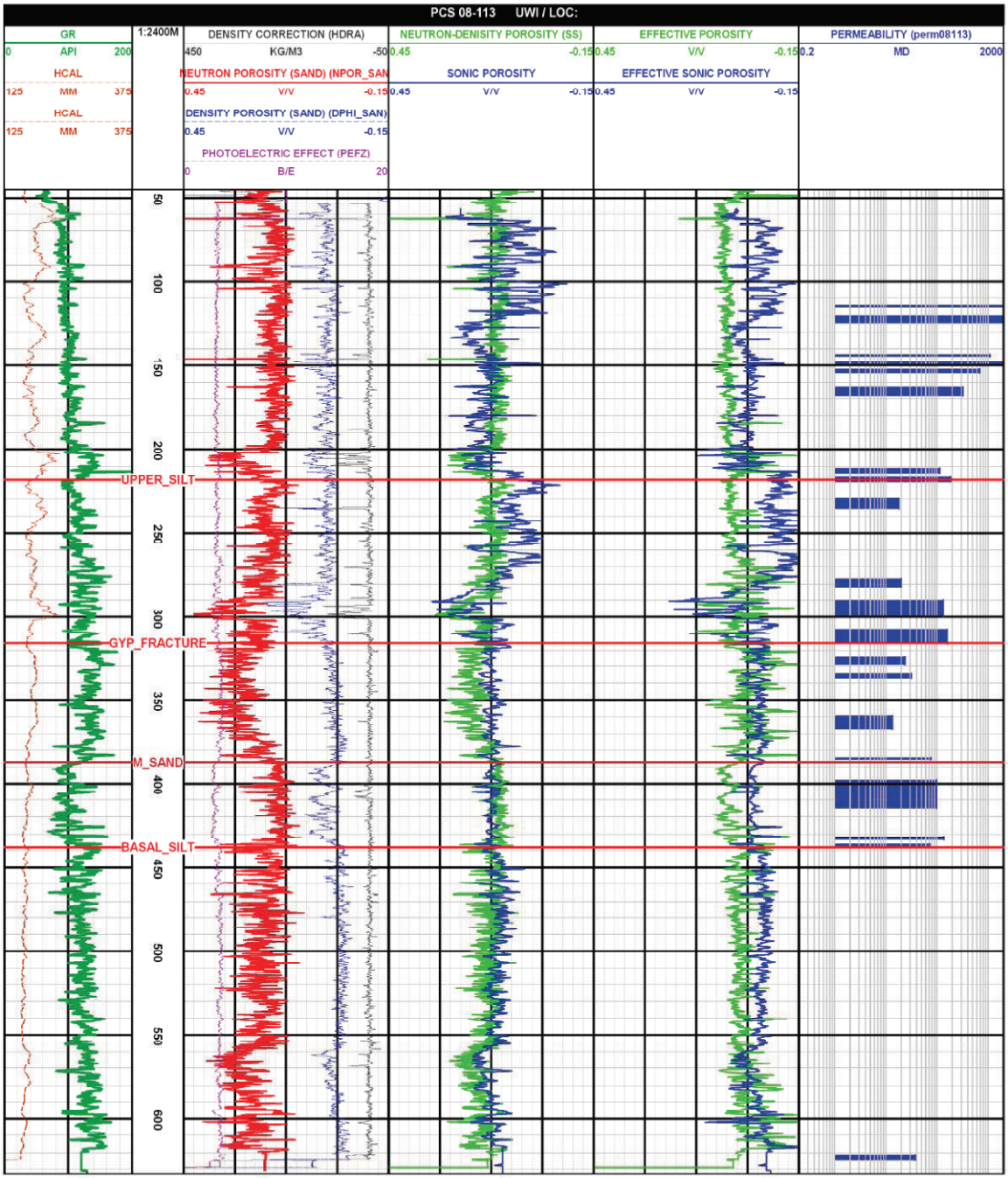

Figure 4.20 - Geophysical log-derived porosity curves for borehole PCS 08113, and permeability measurements discussed in Chapter 5

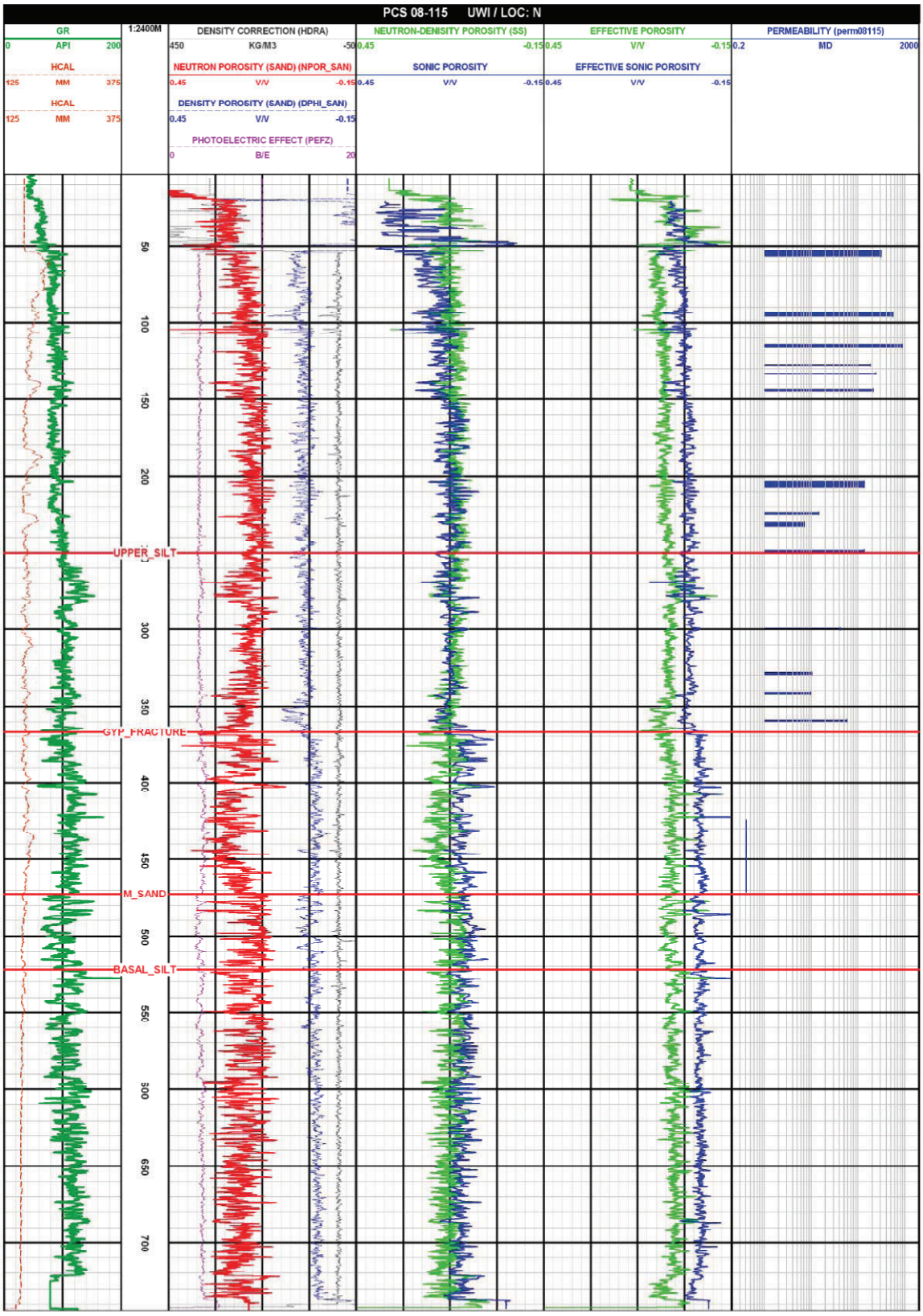

Figure 4.21 - Geophysical log-derived porosity curves for borehole PCS 08115, and permeability measurements discussed in Chapter 5

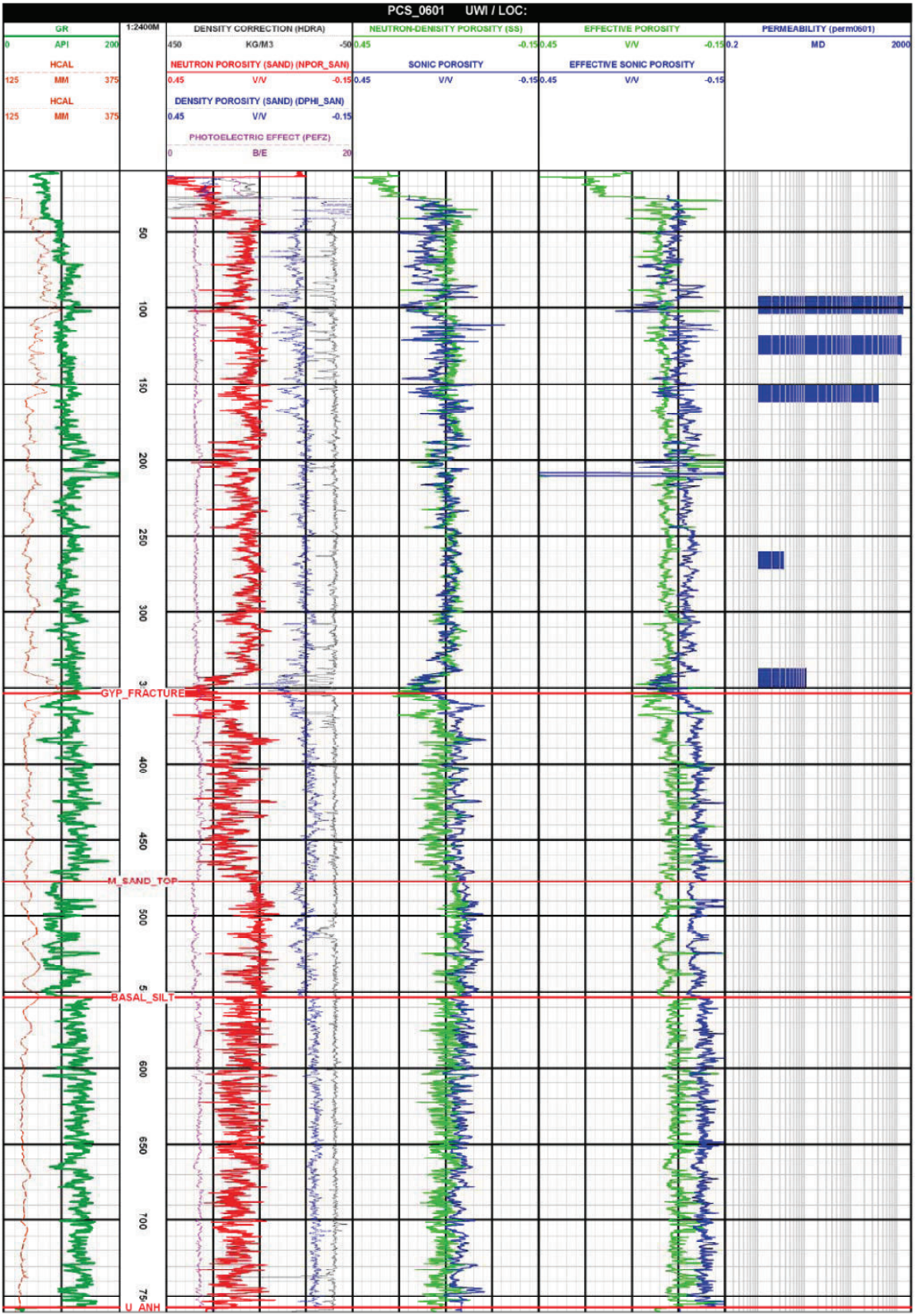

Figure 4.22 - Geophysical log-derived porosity curves for borehole PCS 0601, and permeability measurements discussed in Chapter 5

4.5 Structure

The structure surrounding the study area is a system of faults and folds as identified in Section 2.2 in the geological map and cross section created by Wilson and White (2006) (Figures 2.5 and 2.6) . Information indicates that the study area is synclinal, with the strike of the syncline following parallel to the strike of the regionally interpreted Penobsquis thrust fault.

All of the boreholes presented appear to be near the axis of the syncline based on the shallowly dipping bedding, with the exception of PCS 0601. PCS 0601 is anomalous and regionally closer to the Penobsquis thrust fault. The borehole possess' significant differences in orientation of bedding planes between the bottom and top sections of the hole. Figure 4.23 shows the changes in dip from 15-20 degrees in the lower half of the borehole to averaging 45 degrees in the upper section of the borehole. The transition depth does not correlate to the upper limit of gypsum-infilled fractures which occurs approximately 30 meters up hole from bedding dip transition. It is not certain whether the change in bedding dips is the result of halokinesis and/or thrusting of the Penobsquis fault.

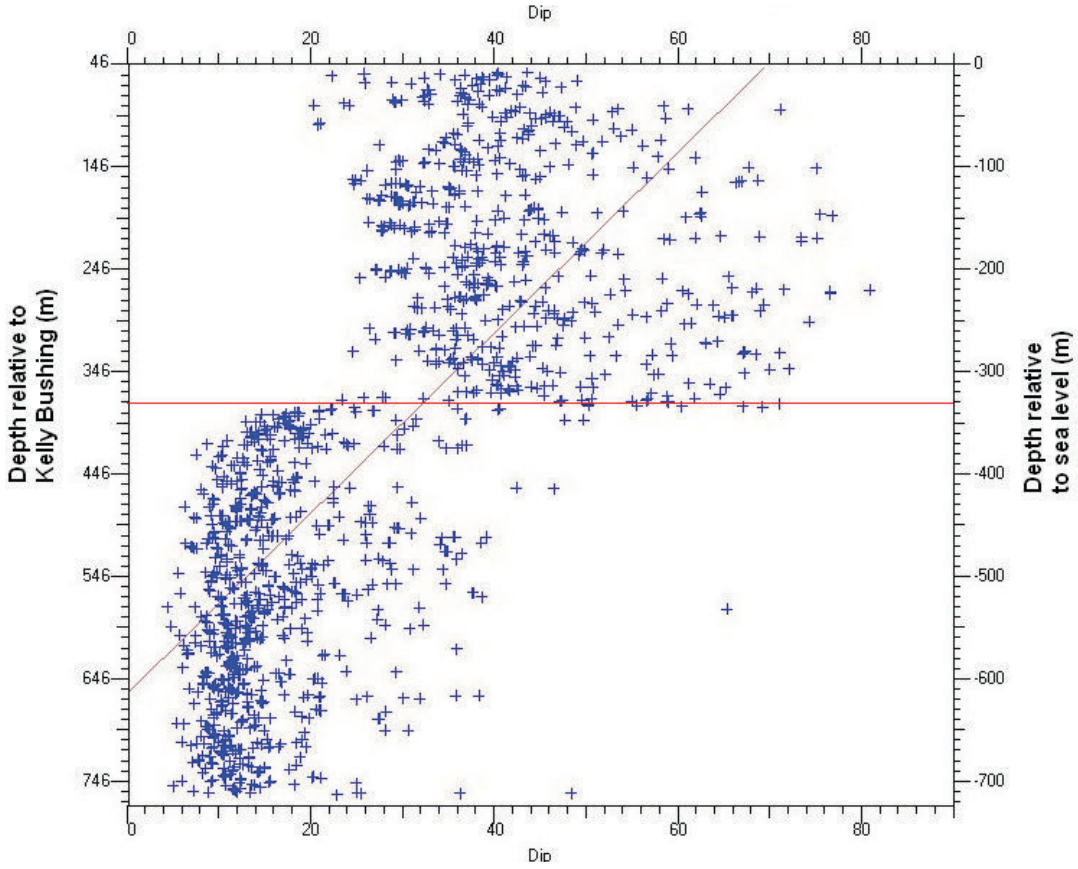

Figure 4.23 - PCS 0601, Bedding dips versus depth from FMI results. Red line denotes an abrupt change in the dip orientation of bedding layers

To visualize the structure parallel to strike (Figure 4.24), a cross section of the geophysical logs is presented in Figure 4.25. The geophysical logs presented in the cross section include the gamma ray log, a caliper log of the borehole, the bulk density of the formation, the sonic 'slowness' log, a calculated acoustic impedance curve, the pumping volumes during hydrophysical logging, and the hydraulic conductivities presented by hydrophysical logging.

The cross section suggests the north-eastern section of the study area plunges to the south west, while the lower half of Mabou in the south-western corner plunges north east.

When considering the synclinal structure along strike coupled with the plunges found on the north-eastern and south-western edges of the study area, it may be hypothesized that this area was once a small basin that was later filled with sediment. Additional

information on large scale features is discussed in the next section on seismic reflection surveys.

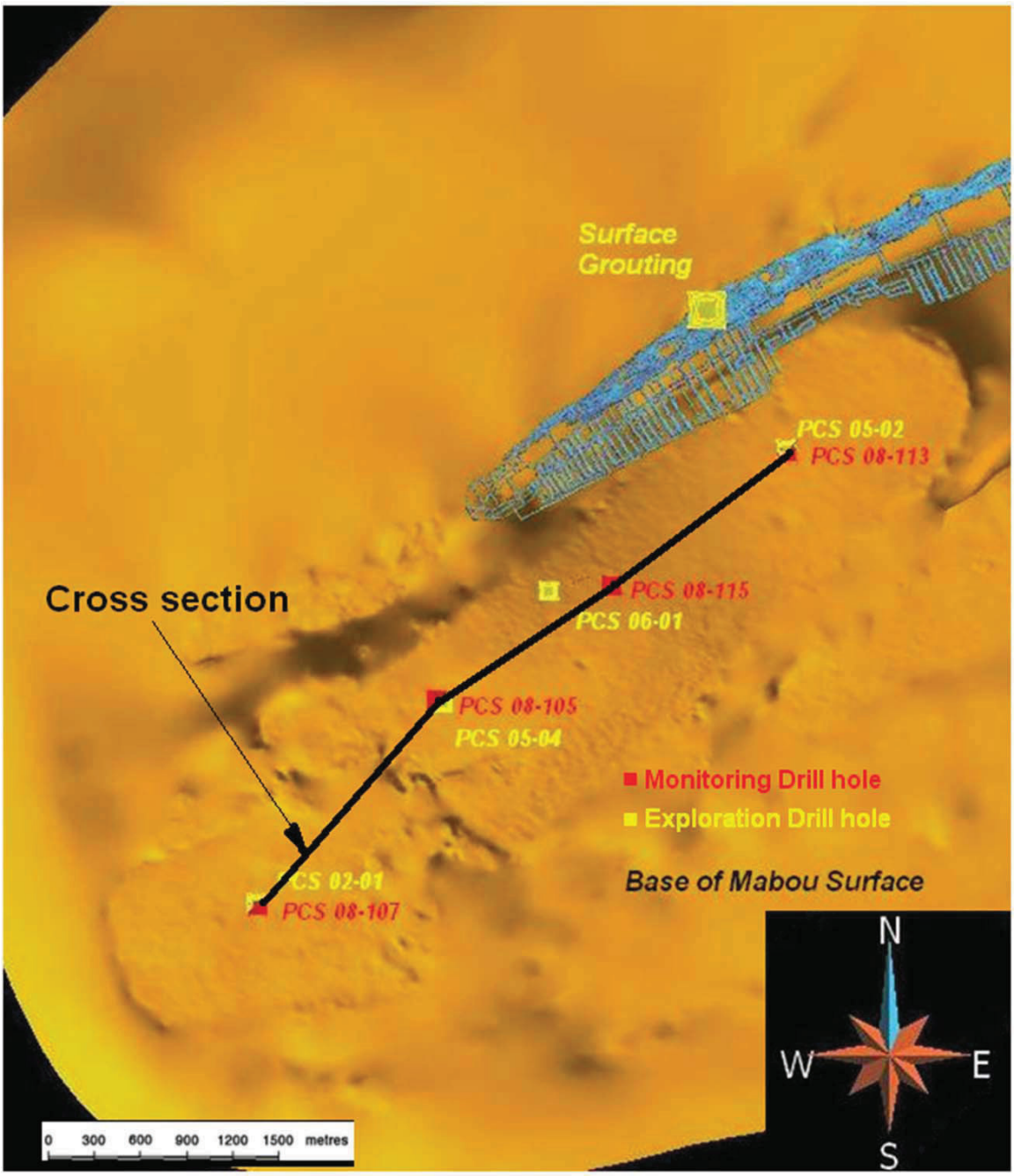

Figure 4.24 - Plan view of cross section created by geophysical log
(The orange-gold surface is the current PCS interpretation of the base of Mabou Group, based on seismic reflection profiles and surface geology)

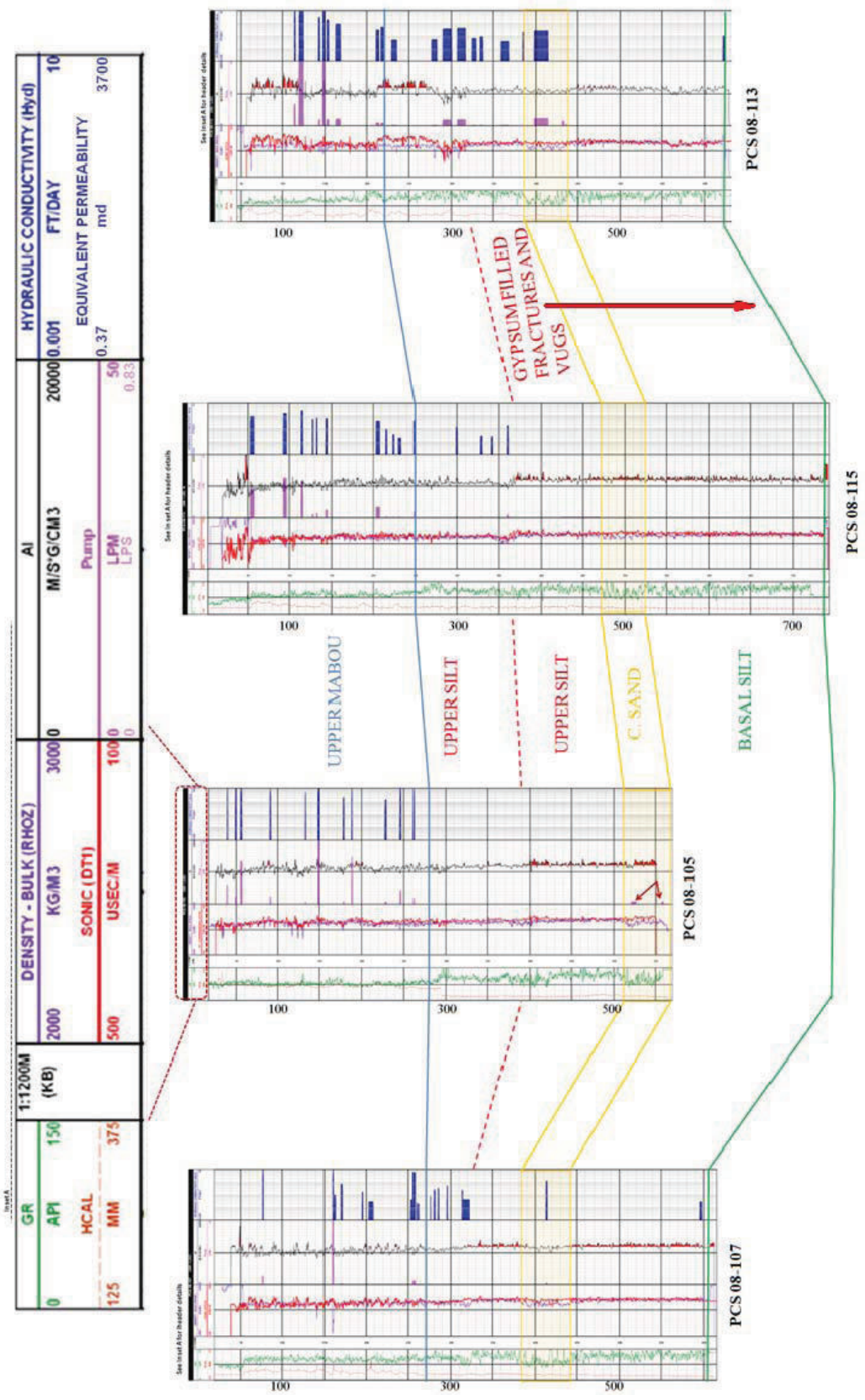

Figure 4.25 - Two dimensional geophysical cross section with subdivisions presented

4.6 Seismic reflection survey

The seismic survey was executed by Boyd PetroSearch in 2004. The data was time-migrated using a combination of FOCUS 5.1, a processing package developed by Paradigm Geophysical, and Arcis processing's proprietary software (Boyd PetroSearch, 2005). The time-migrated data was later depth stretched by a geophysicist employed at Potash Corporation of Saskatchewan Inc.. The base of the Mabou interpreted by PCS geologists and geophysicists is identified as an orange-gold surface in Figure 4.26. The interpretation made use of seismic reflection profiles and surface geology to produce the current model for the base of the Mabou. The interpretations made by the author were made by comparing Mabou Group continuous reflectors within the depth-stretched, time-migrated seismic volume to features present in the boreholes studied during the research.

Changes in colour and intensity on the coloured seismic profile represent changes in the acoustic waves recorded by the geophones. The colours used in this study to portray the waveforms are blue, red and white. Blue indicates the trough of an acoustic wave; a darker blue signifies larger amplitudes. Red denotes the crest of an acoustic wave; a darker red shows larger amplitudes. White indicates the zero crossing or zero amplitude

The seismic processing presented two continuous reflectors between boreholes: the base of Mabou reflector (contact with the upper anhydrite caprock); and a continuous reflector within the Mabou connecting wells PCS 08113 and PCS 08115 (Figure 4.27). Overlain on the seismic fence diagram (Figure 4.27), are the borehole trajectories, with associated HPL inflow results, to be discussed in Section 5.3.

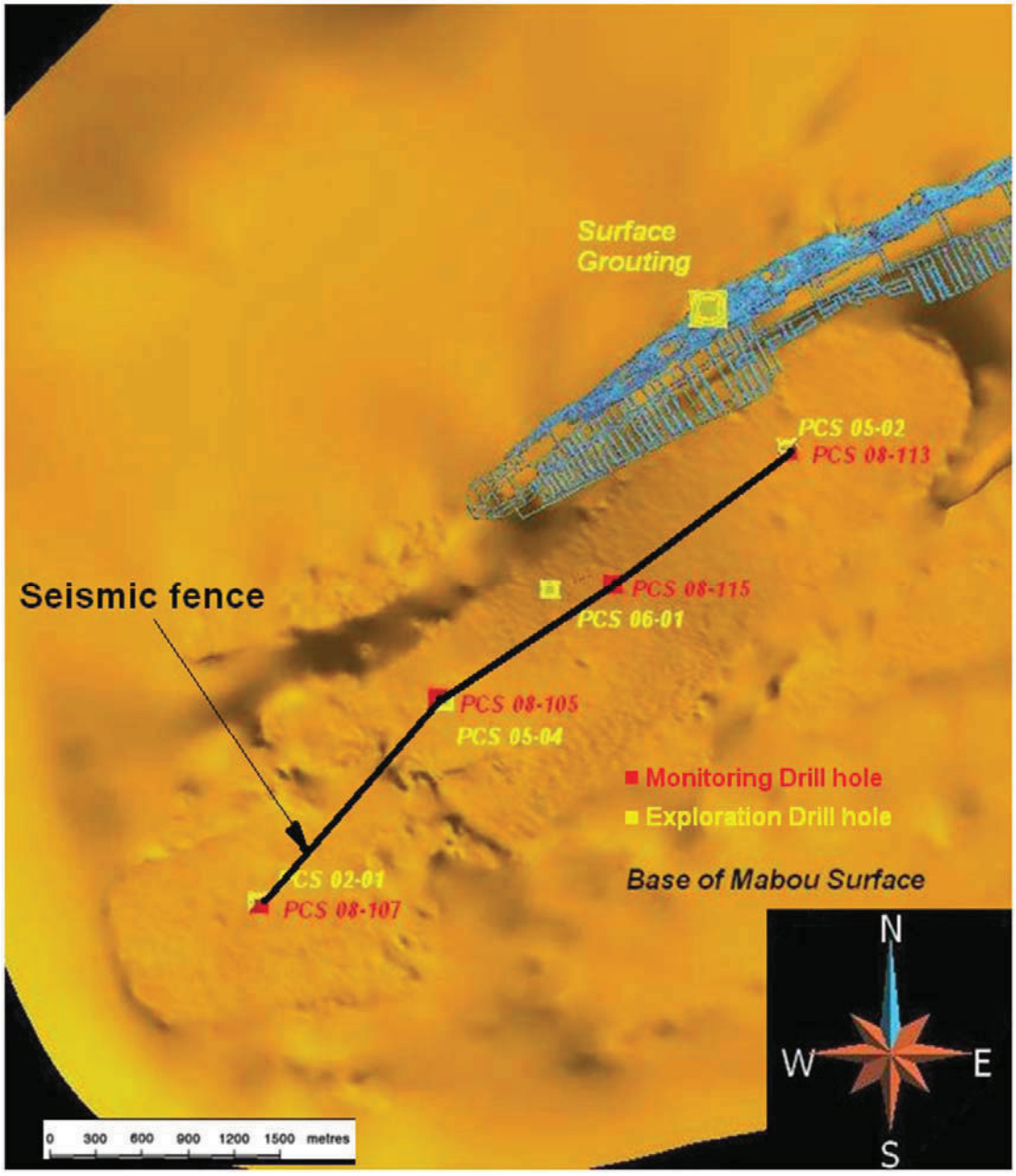

Figure 4.26 - Plan view of seismic fence

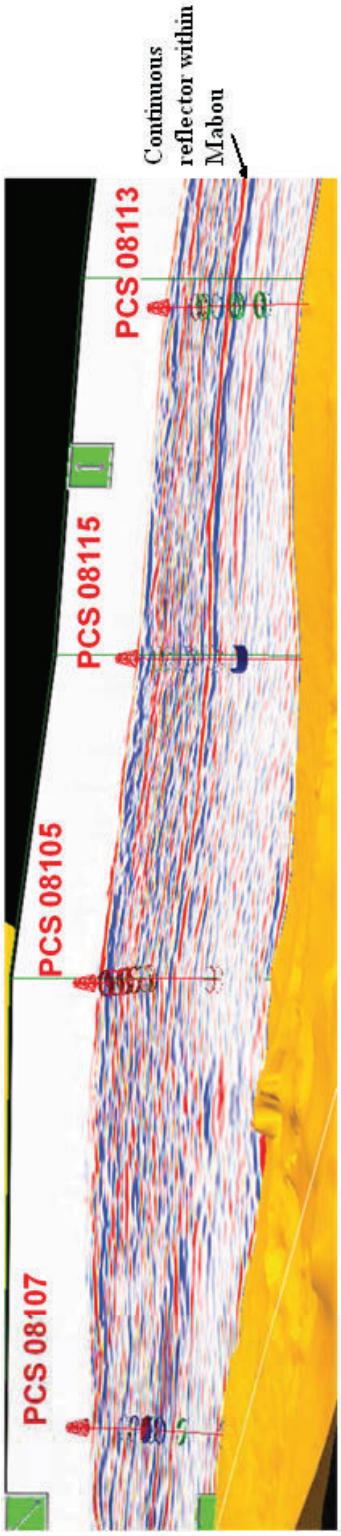

Figure 4.27 – Perspective view of seismic reflection survey fence diagram of study area with monitoring wells, overlain with HPL inflow zones, inflow color scale red=high inflow during pumping, blue=low but measurable inflow

To determine what the continuous reflector in the Mabou is associated with, this author calculated the monitoring wells' acoustic impedance by multiplying density times velocity and then plotted the result with associated geophysical logs.

The plot of the acoustic impedance of PCS 08113 shows, distinct changes in the trend observed at depths of 215 m and 316 m (Figure 4.28). The contact of gypsum-infilled fractures coinciding with the depth of 316 m. Further down hole at a depth of 440 m (Figure 4.29), a subtle increase in the acoustic impedance is seen in the wireline logs, approximately where the base of the Medium Sandstone Subdivision grades to the Basal Siltstone Subdivision.

PCS 0601 and 08115 also presented acoustic impedance trend changes at the contact of gypsum-infilled fractures. The change in the trend of acoustic impedance found at 340 m and 360 m in PCS 0601 is presented in Figure 4.30. The change in trend at 360 m correlates to within 7 m below the contact of gypsum infilling fractures. A large washout, not presented in Figure 4.30, occurred in the zone and likely influenced the calculation of acoustic impedance in the wellbore. As such, the exact depth of the trend changes may only be estimated to be between 340 to 360 meters.

The changes in trends of the acoustic impedance in PCS 08115 occur at 340 and 370 meters (Figure 4.31). The changes of acoustic impedance between the two major trends are not as drastic in PCS 08115 as in PCS 0601. This may be attributed to the lack of washing out of the borehole wall in the PCS 08115 borehole.

The acoustic impedance changes at 215 m and 440 m in PCS 08113 were not observed in PCS 08115 or PCS 0601. The one continuous seismic reflector trace observed halfway down the Mabou Group, presented in Figure 4.27, occurs at the contact of gypsum-infilled fractures. The change is present in acoustic impedance logs of PCS 0601, PCS 08113 and PCS 08115.

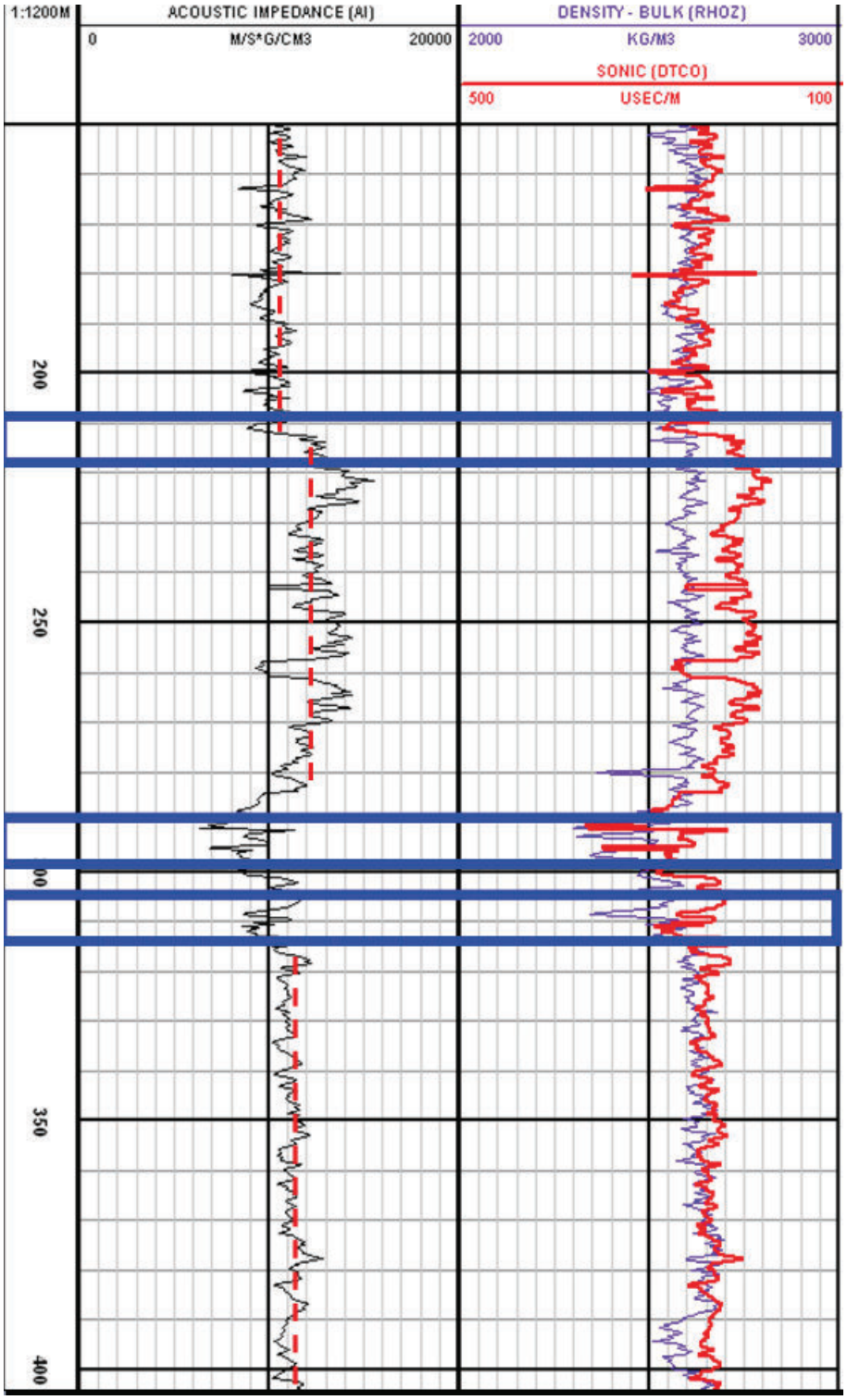

Figure 4.28 - PCS 08113 acoustic impedance upper section, blue boxes indicate zones of high flow measured during HPL logging

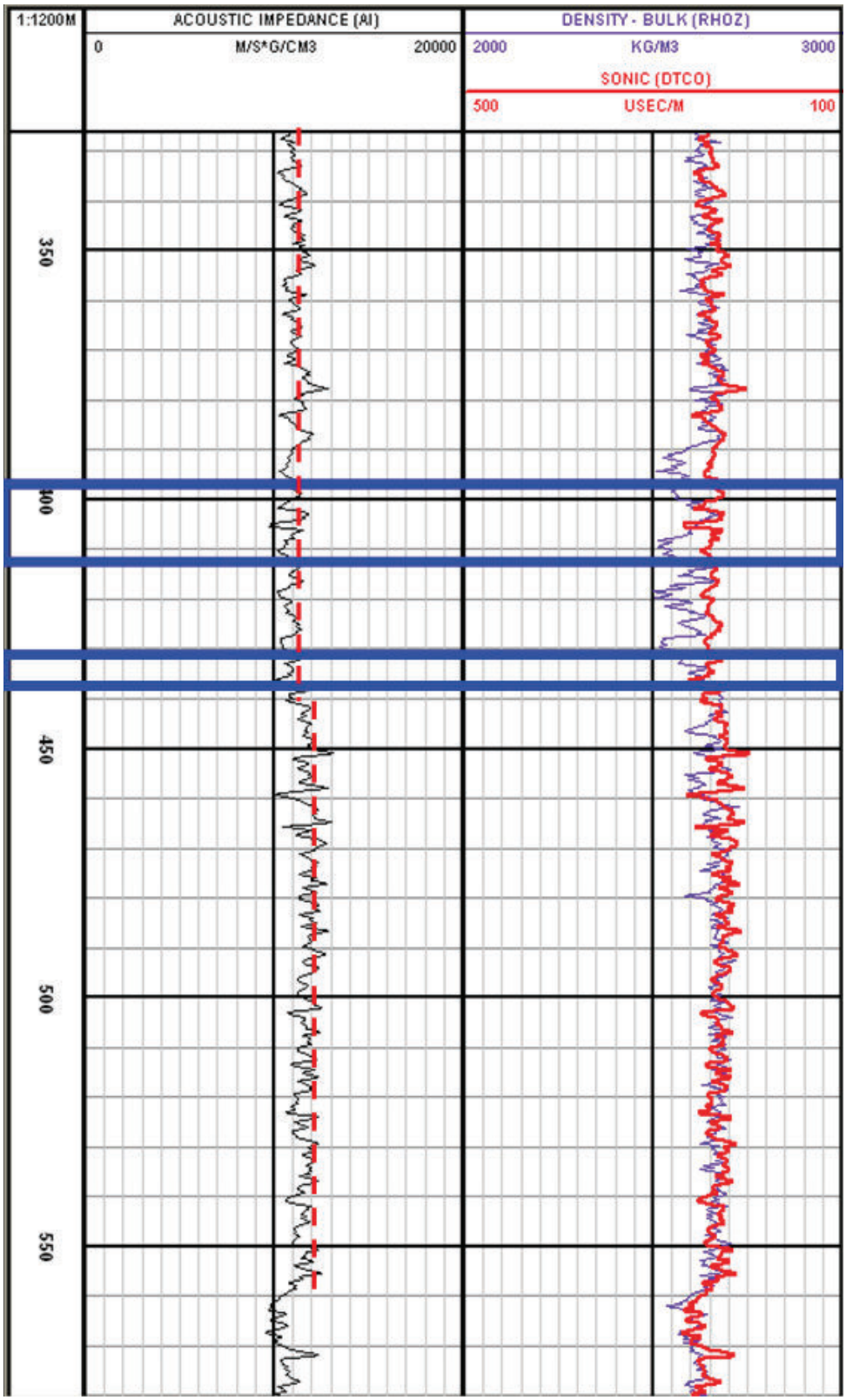

Figure 4.29 - PCS 08113 acoustic impedance lower section , blue boxes indicate zones of high flow measured during HPL logging

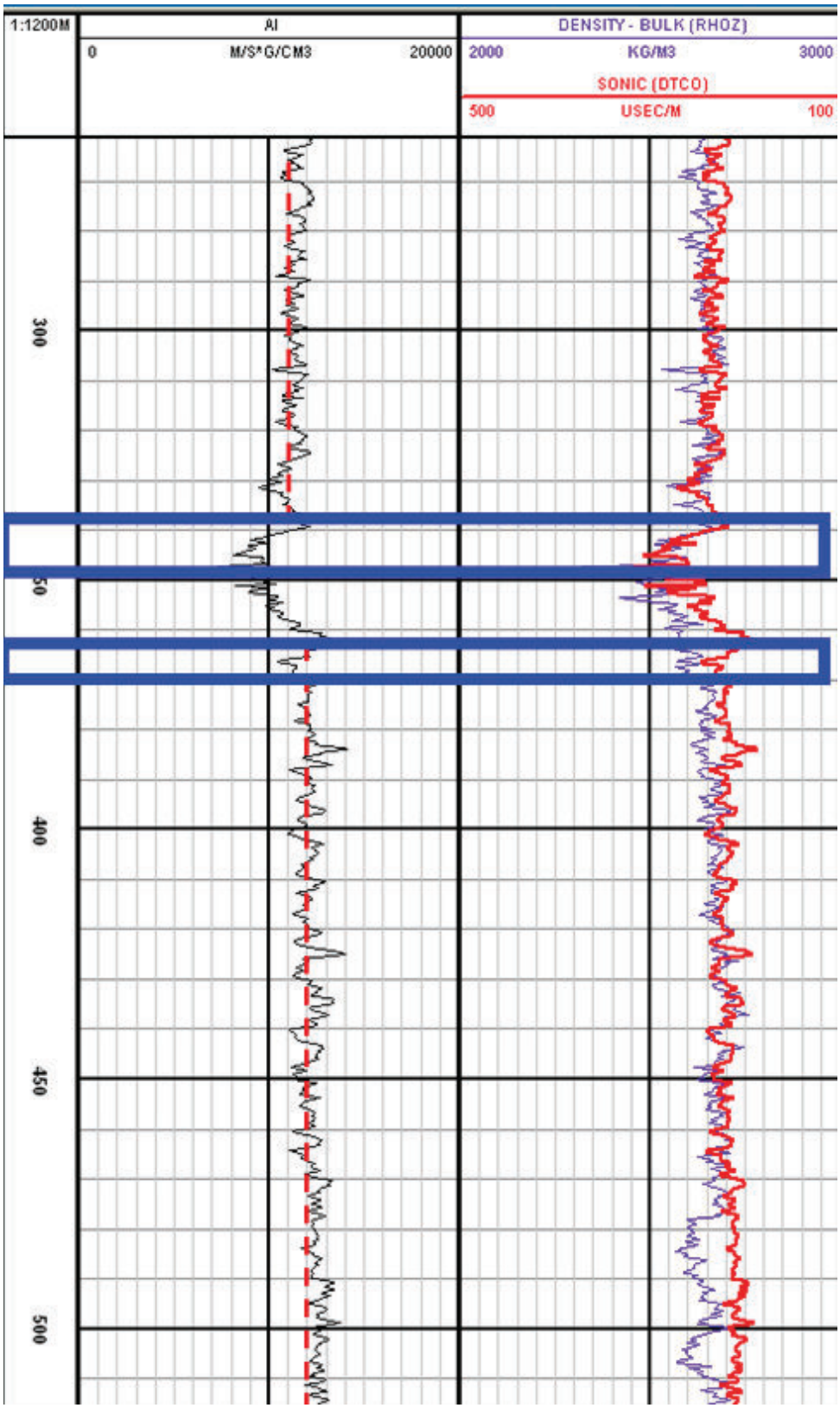

Figure 4.30 - PCS 0601 acoustic impedance upper section, blue boxes indicate zones of high flow measured during HPL logging

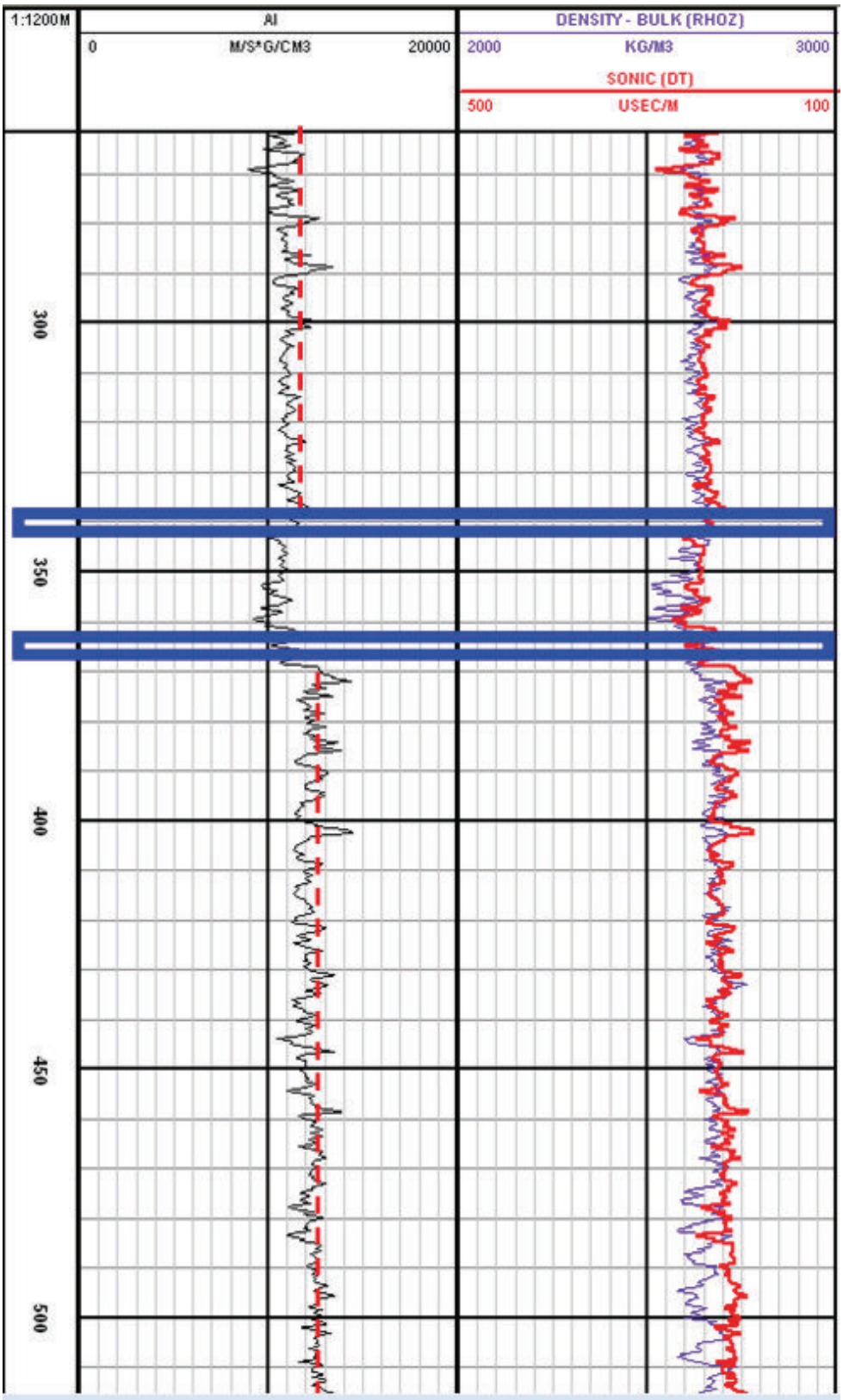

Figure 4.31 - PCS 08115 acoustic impedance upper section , blue boxes indicate zones of high flow measured during HPL logging

5 ANALYSIS OF HYDRAULIC TESTING RESULTS

5.1 Introduction

This chapter presents the results of hydraulic tests performed to characterize the hydrogeology of the Mabou Group. The hydraulic tests include: permeability testing of core samples at the University of Saskatchewan's Rock Mechanics Laboratory, which was conducted by the author; assessment of in-situ permeabilities by comparison of hydrophysical logs and drill stem tests (DSTs) conducted by PCS' service companies in neighbouring wells; and analysis of pore pressure distributions based on the results of DST's.

5.2 Permeability testing of core samples

5.2.1 Sample Selection: Rationale for samples selected

Laboratory testing was conducted to estimate the permeability of core samples from PCS 0502 that contained vugs. Drill core from PCS 0502 was selected as it was the only exploration hole core accessible at the time of the field investigation. Core boxes from other drill holes, from which samples may have been selected for testing purposes, were at a remote storage site and could not be viewed at the time of the field investigation.

Laboratory testing provided a controlled environment to assess the hypothesis that zones exist which possess sufficient interconnectivity of vugs to possess high permeability, at the centimetre scale. The samples chosen for testing contained vugs that were visible to the naked eye in hand specimens, and were located within hydraulically conductive zones identified by DSTs that are discussed in Section 5.3.

Several pieces of core were taken from PCS 0502 (Figure 5.1), three of which were ultimately selected for testing. One core interval was located in the Upper Siltstone subdivision, within a vuggy interbedded siltstone located directly above the contact with gypsum-infilled fractures and vugs. The other two sections of core were selected from within the Medium Sandstone subdivision.

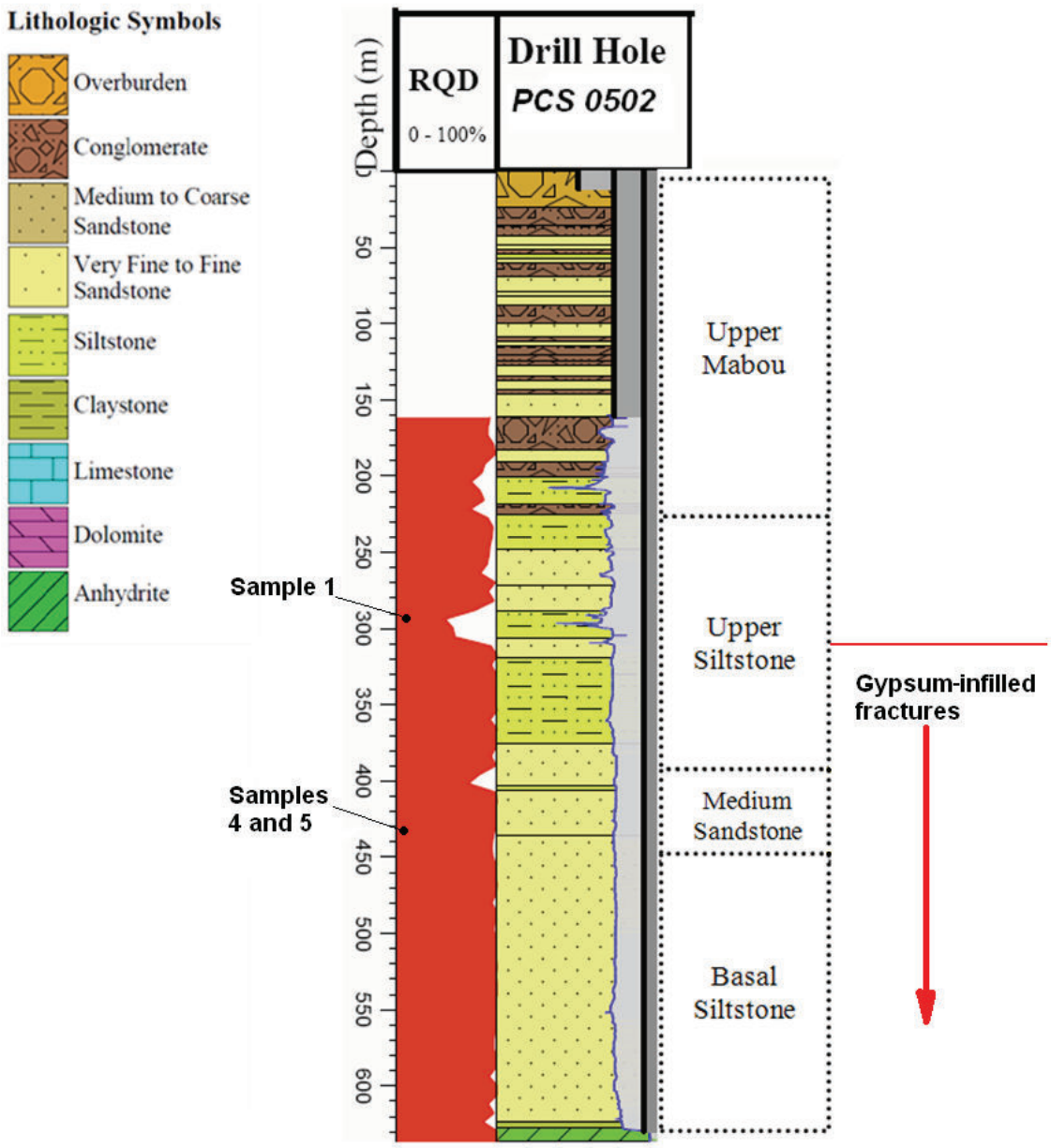

Figure 5.1 - Location of laboratory testing samples taken from PCS 0502 drill hole

Given that the test apparatus used for this work requires 2.54 cm (one-inch) sample diameters, four 2.54 cm (one-inch) plugs were drilled from the three core samples noted above. Two of these 2.54 cm (one-inch) plugs were drilled out of an interval of the Upper Siltstone in which bedding laminations were visible, at a depth of 290.10 to 290.21 m (labelled Sample 1). In order to determine if bedding influenced the flow characteristics, one of the plugs (shown in Figures 5.2 and 5.3) was cut parallel to the bedding while the second plug (shown in Figure 5.4) was cut perpendicular to bedding.

The third and fourth plugs were cut from the Medium Sandstone samples taken at 432.43 m to 432.47 m depth (Figure 5.5, labelled Sample 4) and 433.05 to 433.12 m (Figure 5.6, labelled Sample 5), respectively. Both of these sandstone samples were drilled parallel to bedding.

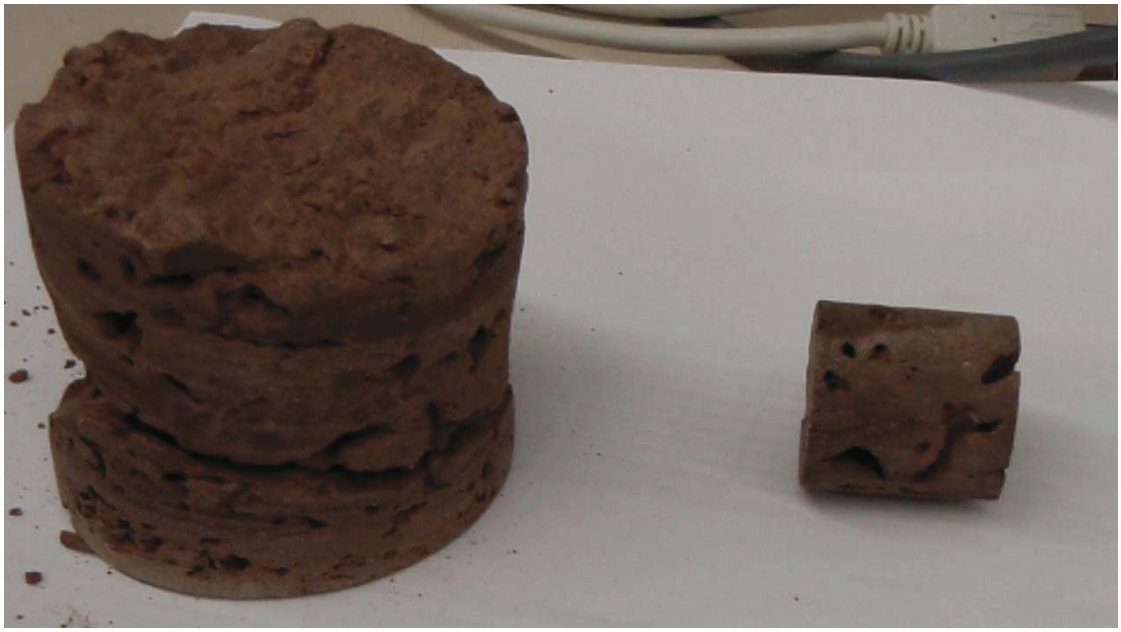

Figure 5.2 - Sample 1, cut parallel to bedding planes, prior to testing (Scale: diameter of the plug on the right is 2.54 cm)

Figure 5.3 - Sample 1, cut parallel to bedding, post testing (Scale: diameter of plug is 2.54 cm)

Figure 5.4 - Sample 1, cut perpendicular to bedding planes (Scale: diameter of plug is 2.54 cm)

Figure 5.5 - Sample 4; sandstone with some vugs (Scale: diameter of the plug on the right is 2.54 cm)

Figure 5.6 - Sample 5; sandstone with well-connected vugs (Scale: diameter of the plug on the left is 2.54 cm)

5.2.2 Testing Procedures

Two types of permeability tests were considered: liquid permeability and gas permeability. Due to concerns that the plugs could be adversely affected by exposure to water (e.g., clay hydration), gas permeability testing was selected. A Ruska gas permeameter (Figure 5.7), with a maximum operating pressure of 100 kPa (gauge), was used to conduct the permeability tests using nitrogen gas as the flowing fluid.

Details regarding testing procedures and data interpretation are included in Appendix B.

Figure 5.7 - Ruska gas permeameter

5.2.3 Results

The permeabilities interpreted for the four samples tested are presented in Table 5.1. As expected, the results for the siltstone with visible bedding laminations demonstrated anisotropic permeability. Permeabilities measured parallel to bedding were 590 md and

740 md. The higher value measured on the second test is likely attributed to a bedding-parallel crack that developed during the course of testing (see Figure 5.3).

The permeability measured normal to bedding was approximately 1 md; the true value may be smaller than this, as the flow rate measured for this sample (at the maximum pressure rating possible with the equipment used) was at the lower end of the recommended range for the permeameter's flow-meter.

The average permeability interpreted for sample 4 was 6 md.

It was not possible to interpret permeability for Sample 5, as the permeability was greater than the capabilities of the testing equipment, the upper limit of which was calculated to be 2500 md. Visual inspection of the plug showed interconnectivity of vugs along the outside edge of the sample. The same interconnectivity was present in the core sample in which the plug was cut (Figure 5.6), suggesting that the interval from which this sample was taken has the ability to sustain high flow rates, in the presence of a hydraulic gradient.

Unpublished liquid permeability test results generated for vug-free Mabou Group siltstone samples from the neighbouring Penobsquis area were of the order of 10^{-3} md and smaller (personal communication, Z. Szczepanik). Those results, compared with the 1 md and greater permeabilities measured on vuggy samples by this author, directly support the expectation that permeabilities should be significantly higher in zones containing secondary porosity in the form of vugs. It is further suggested that these results indirectly support the expectation that higher permeabilities should be expected in fractured zones.

Table 5.1 - Corrected permeabilities measured on core samples

Sample label and description	Corrected Permeability (md)
Sample 1 - plug cut parallel to bedding planes (290.10-290.21)	590-740
Sample 1 - plug cut perpendicular to bedding planes (290.10-290.21)	<1
Sample 4 - sandstone with some vugs (432.43-432.47)	6
Sample 5 - sandstone with lots of vugs (433.05-433.12)	>2500

Figure 5.8 - Light passing through a vug within drill core associated with sample five

5.3 Permeable zones interpreted from well pairs

As noted in Chapter 3, drill stem tests (DSTs) and hydrophysical logging (HPL) have both been used in the Picadilly study area, though never in the same well. Drill stem testing was performed by Baker Hughes Inc. in exploration boreholes and the pilot well, while hydrophysical logging was performed by RAS Inc. in the monitoring boreholes. In order to compare results obtained by the two methods, and to gain insights into the lateral extents of permeable zones, three pairs of wells were selected for analysis. These pairs were selected based on their proximity and on the fact that DST results were available for one well and HPL results were available for the other. To facilitate a direct comparison of the two methods, the hydraulic conductivities interpreted by RAS based on

hydrophysical logging results were converted into permeabilities expressed in millidarcies (md), following the example presented in Appendix A.

The well pairs studied were PCS 0502 and PCS 08113; PCS 0504 and PCS 08105; and PCS 0601 and PCS 08115. The relative locations of these wells are presented in Figure 5.9. The distance between the wells in each pair varied between 10 m and 420 m.

A fourth well pair, located in the southwest portion of the study area and consisting of PCS 08107 (monitoring well) and PCS 0201 (exploration well), was considered for analysis but was deemed unsuitable. Although PCS 08107 was subjected to HPL measurements, well pair PCS 0201 offered no basis for comparison because no DSTs had been performed in it.

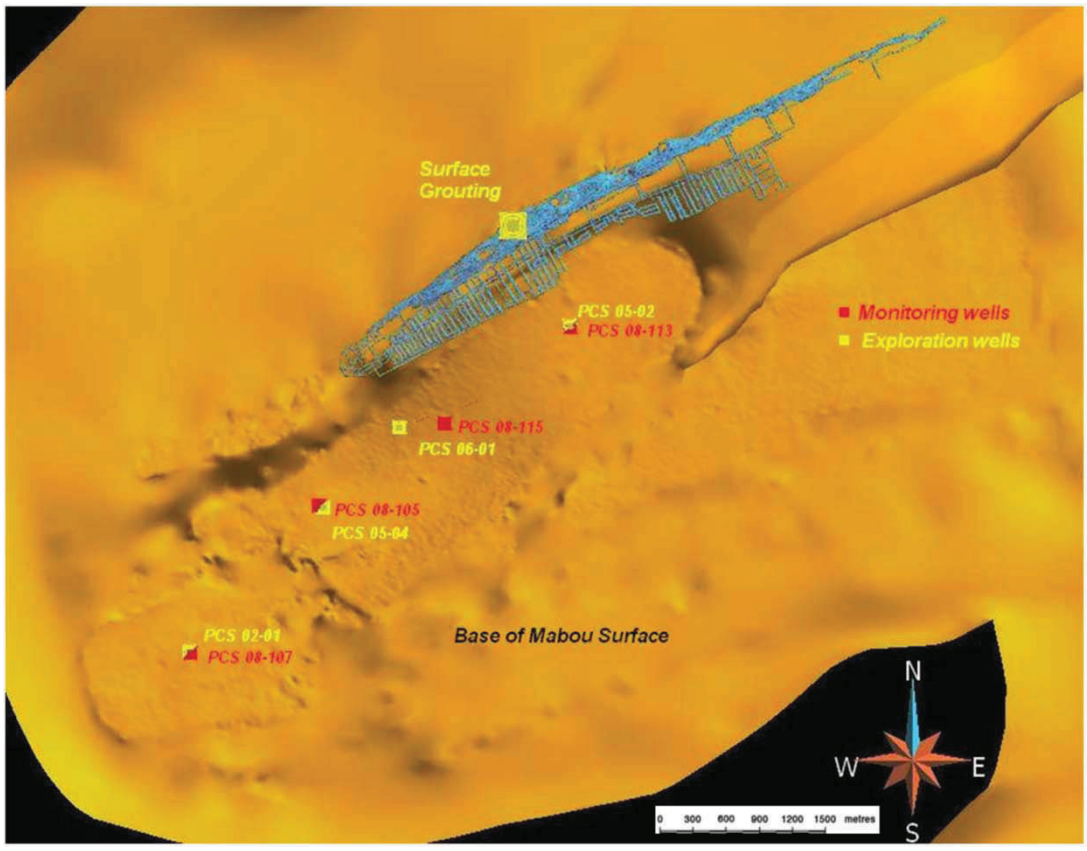

Figure 5.9- Well pairs in the Picadilly study area used to identify permeable zones in the Mabou (The orange-gold surface is the current PCS interpretation of the base of Mabou Group based on seismic reflection profiles and surface geology)

5.3.1 Well pair PCS 0502 and PCS 08113

Well pair PCS 0502 and PCS 08113 was analyzed first, given that the 10 m separation between these wells was smaller than any of the other pairs. Given the proximity of these wells and the fact that bedding dips were only 10-15 degrees in this part of the study area, a strong correlation between hydrogeological attributes was expected for this pair. The results for these wells, presented in Table 5.2 and Figure 5.10, are consistent with this expectation. Specifically, four of the five "permeable" zones (i.e., permeability = 1 md or greater), and one less "permeable" zone (i.e., permeability < 1md) identified in drill stem tests appear to correlate with "permeable" zones identified using the hydrophysical logs. Gaps in between the permeable horizons presented by HPL are below the tool's measurement threshold during both ambient and pumping conditions, indicating they have very low permeabilities.

Analysis of the HPL data performed by RAS Inc. (2008c) suggests that under ambient wellbore conditions, the upper permeable zones (168 m depth up to surface) in PCS 08113 are either thieving or below the hydrophysical logging tool's sensitivity threshold limit. Upon completion of ambient condition testing, pumping during injection (injection of a contrasting fluid at the base of the well while pumping from the top to keep the fluid level depressed) was initiated and the six uppermost intervals ceased to behave as thieving zones or zones of negligible inflow; rather RAS Inc. interpreted that they accounted for 93 percent of the total flow into the wellbore during pumping. The uppermost drill stem test in PCS 0502, at a depth interval from 201 m to 213 m, was not shallow enough to compare against the HPL results for these uppermost zones.

Table 5.2- Comparison of PCS 0502 drill stem test results with PCS 08113 hydrophysical logging results. Yellow highlighting indicates zones that correlate between the two wells

DST depth (m)	kh (md*m)	PCS 0502 permeability (md)	HPL depth (m)	PCS 08113 HPL Ambient Condition (l/s)	PCS 08113 HPL Pumping Condition (l/s)	PCS 08113 permeability (md)
			113.7 to 115.2	Thieving zone -1.0E-01	2.8E-01	5.1E+03
			119.5 to 125.0	<6.7E-04	3.6E+00	1.3E+04
			143.0 to 144.5	<6.7E-04	8.2E-02	1.1E+03
			147.5 to 150.0	<6.7E-04	1.2E+00	1.0E+04
			152.1 to 154.5	<6.7E-04	8.2E-02	6.7E+02
			162.8 to 168.3	<6.7E-04	8.8E-02	3.2E+02
201.0 to 213.0	2.0E+01	1.30E+02	210.9 to 214.3	1.8E-02	3.8E-02	1.1E+02
			216.7 to 219.8	3.8E-03	3.2E-02	1.8E+02
			229.2 to 235.6	<6.7E-04	<6.7E-03	1.8E+01
250.0 to 262.0	1.7E+03	1.70E+03				
			276.8 to 282.6	<6.7E-04	<6.7E-03	2.0E+01
284.0 to 296.0	1.8E+03	1.80E+03	289.6 to 300.2	5.7E-03	7.5E-02	1.3E+02
			306.9 to 316.7	6.3E-03	8.2E-02	1.6E+02
			324.3 to 329.2	<6.7E-04	<6.7E-03	2.4E+01
			333.8 to 337.4	<6.7E-04	<6.7E-03	3.1E+01
			359.1 to 367.6	<6.7E-04	<6.7E-03	1.3E+01
			384.1 to 385.6	<6.7E-04	<6.7E-03	7.5E+01
395.0 to 407.0	2.0E+00	1.00E+00	397.8 to 414.5	1.5E-02	9.7E-02	9.7E+01
431.0 to 443.0	7.7E+02	1.90E+03	431.3 to 433.7	3.8E-02	5.8E-02	1.4E+02
			435.9 to 437.4	8.8E-03	1.7E-02	7.2E+01
590.0 to 630.0	6.2E+00	1.60E-01	621.8 to 624.8	<6.7E-04	<6.7E-03	3.8E+01

Note: Additional bottom hole tests were conducted and not shown. Pressure results from the bottom hole tests not shown are presented in Section 5.4.3.

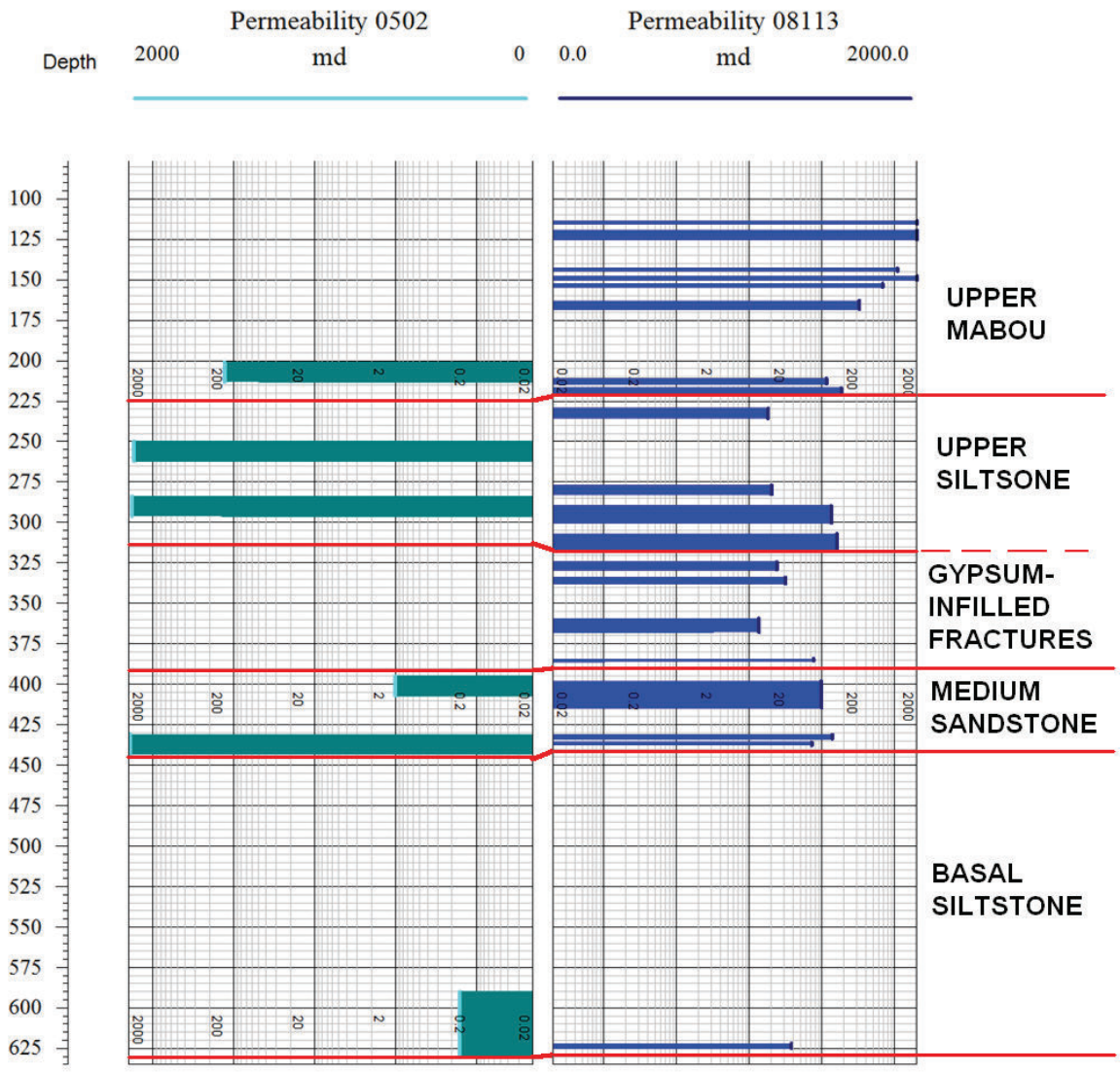

Figure 5.10 - Graphical representation of permeable horizons in PCS 0502 and PCS 08113

In PCS 0502 DST testing from 201 to 213 m depth, a permeability of 1.3E+02 md was interpreted. The hydrophysical log of PCS 08113 shows a flow zone of similar depth from 210.9 to 214.3 m and an interpreted permeability of 1.1E+02 md. Core from PCS 0502 presents several horizontal fractures with no reduction staining, and sub-vertical fractures with reduction staining (Figure 5.11). The lack of reduction staining suggests that the horizontal fractures were likely not original flow paths and could have potentially been induced by drilling operations. The presence of reduction staining on the sub-vertical fractures confirms that water has passed through them at some point in geologic time. This, coupled with the high angled conductive fractures in the FMI log presented in

Figure 5.11, suggests that the high-angled features within this zone are the source of its high permeability.

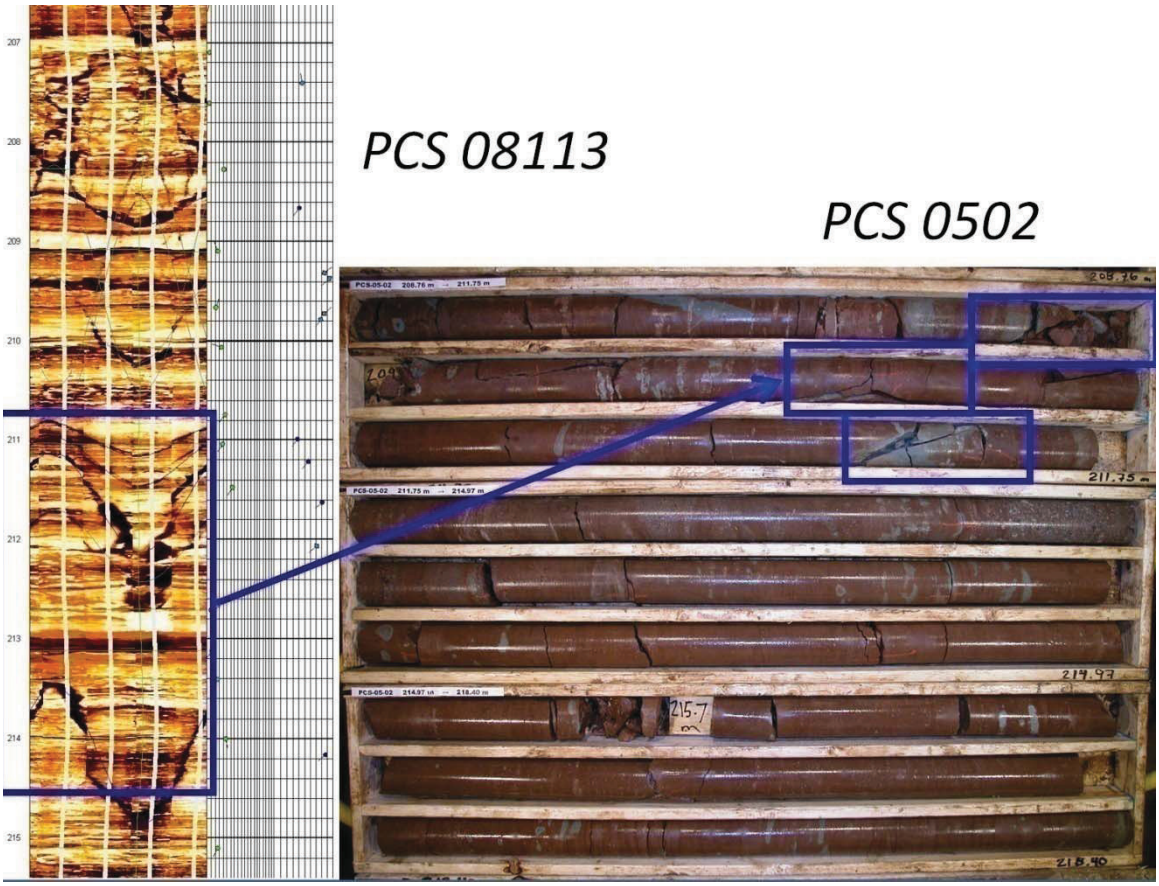

Figure 5.11 - Comparison of FMI from DST 08113 and drill core from PCS 0502 with the DST zone 201 to 213 m below KB (FMI : after Schlumberger, 2008b . Photograph courtesy of PCS)

A permeable zone from 250 to 262 m in PCS 0502 identified from the drill stem testing does not horizontally correlate with any flow zones identified in PCS 08113 by hydrophysical logging. The zone tested with a hydrostatic initial pressure and an interpreted permeability of 1.7E+03 md. Drill core reveals the presence of 2 sub-vertical fractures that do not exhibit any reduction staining on their surfaces. Therefore, it appears that the high permeability zone observed in PCS 0502 is not laterally continuous.

The next permeable zone tested occurs above the contact of gypsum-infilled fractures in the Upper Siltstone subdivision. It is significant to note that this zone as presented in Figure 4.5 possesses low RQD values in the core. A portion of this low RQD zone was packed off from 284 to 296 m in PCS 0502 and interval-tested. Results indicate a hydrostatic pressure and an interpreted permeability of 1.8E+03 md (Baker Hughes, 2005a). The intact core shows that vuggy porosity is present within the zone. During the field investigation and inspection of the PCS 0502 core, small broken pieces of core showed vuggy porosity indicative of a weak rock getting broken up, likely during drilling and coring operations. A 10.6 m zone, identified from 289.6 to 300.2 m in HPL logging of PCS 08113, appears to correlate to the aforenoted DST interval in PCS 0502. The HPL zone in PCS 08113 produced 7.5E-02 litres per second (l/s) under pumping during injection conditions, resulting in an interpreted permeability of 1.3E+02 md. FMI logging results for PCS 08113 (Figure 5.12) suggest that no fracturing within the zone of flow is present. Rather the high-resolution image of electrical conductivity on the wellbore surface generated by this logging tool shows only the presence of bedding planes. The FMI results suggest that flow must be occurring through vugs, which are present as dark electrically conductive features in the log, and/or along bedding planes which dip shallowly towards the south-southeast. In comparing the FMI log to drill core extracted from PCS 0502, the lack of fracturing in this interval is not clearly evident in the core; i.e., comparison of the log (which represents in-situ conditions) to the core suggests that many of the fractures present in the core may have been induced by drilling and core handling (Figure 5.13).

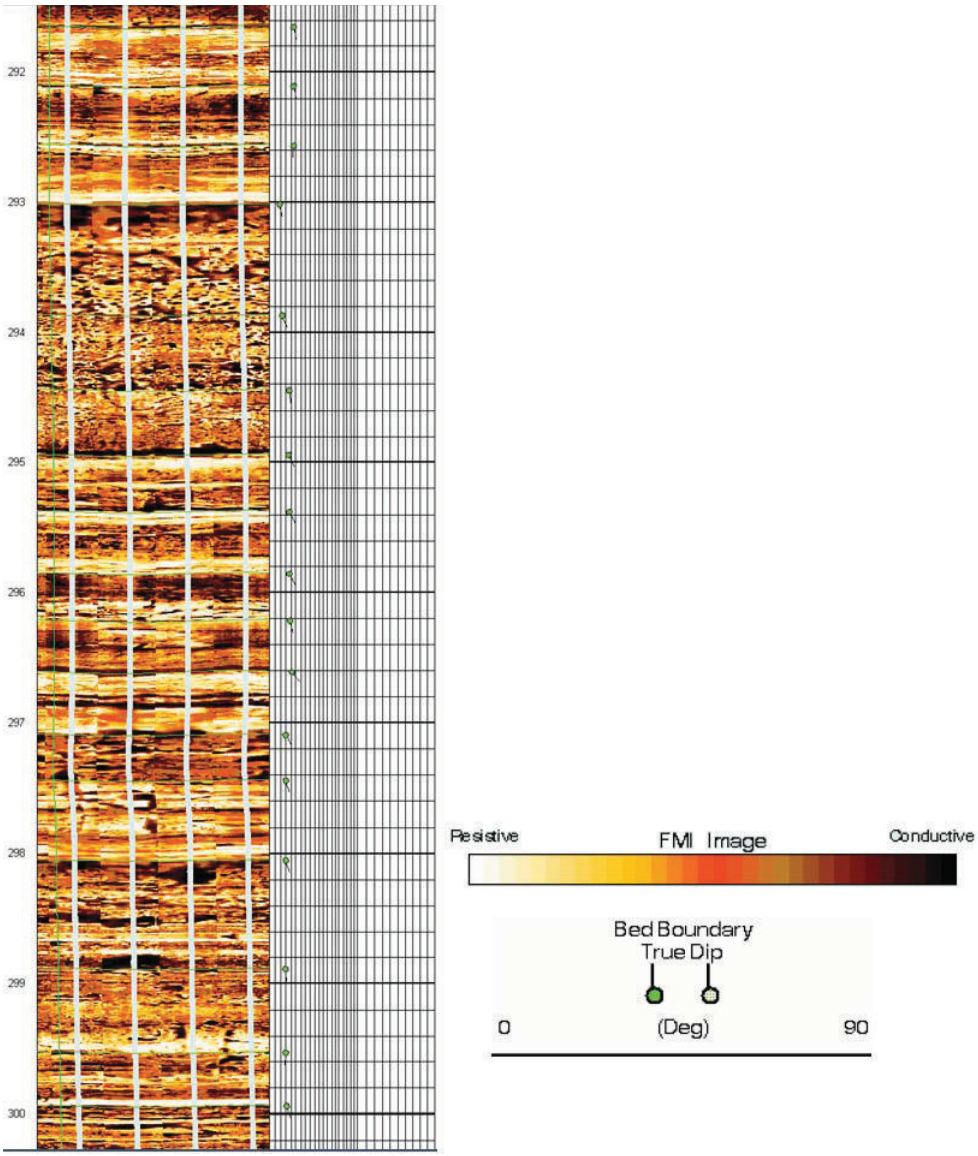

Figure 5.12 –FMI log of permeable zone within PCS 08113.
In the image track on the left, dark colours denote zones of high electrical conductivity (e.g., porous zones filled with saline drilling fluids). In the track shown on the right, bedding plane orientation is indicated by the green "tadpoles". The position of each tadpole "head" indicates dip angle; the direction in which the "tail" points indicates dip direction (with the upwards direction on the page representing north). (FMI : after Schlumberger, 2008b . Photograph courtesy of PCS)

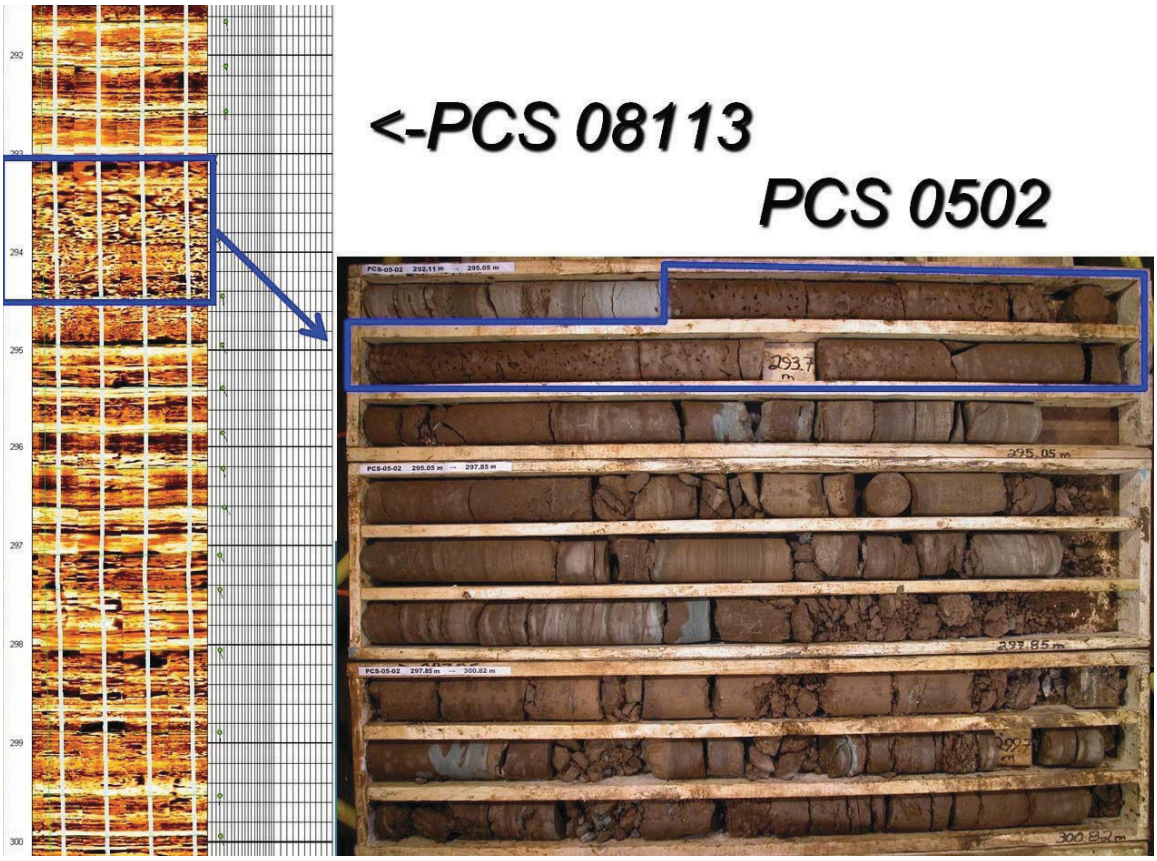

Figure 5.13 - Comparison of FMI from DST 08113 and drill core from PCS 0502 above gypsum-filled fractures (FMI : after Schlumberger, 2008b . Photograph courtesy of PCS)

A high-permeability zone above the gypsum-infilled fractures was identified by hydrophysical logs but appears to have been missed by drill stem tests. The HPL zone produced from 306.9 to 316.7 m in well PCS 08113 and was able to produce a flow rate (8.2E-02 l/s under pumping during injection conditions) of the same magnitude as the HPL zone above (289.6 to 300.2 m). Core from PCS 0502 also suggests that a permeable zone may have existed in this well, though it was not subjected to drill-stem testing (the closest interval being 284 to 296 meters), as shown by the low 48% RQD core in Figure 5.14 from 297.85 to 300.82 m.

It cannot be concluded from the isolated and non-contiguous DSTs conducted in PCS 0502 whether or not the entire permeable zone directly above the gypsum-infilled fractures was tested in this well. Fractures filled with gypsum are first observed in drillcore of PCS 0502 at a depth of 312.5 meters, which is 16.5 meters below the closest drill stem test.

Figure 5.14 - PCS 0502 Core photo 297.85 to 300.82 m (RQD of 48%) (Photograph courtesy of PCS)

A drill stem test was conducted by Baker Hughes Inc. within the top section of the Medium Sandstone subdivision over an interval of 395 to 407 m. The test was performed to measure flow from a large 2.7 m sub-vertical fracture observed in the core. Results indicate that the permeability was 1.0E+00 md. Reduction staining on this large sub-vertical fracture was not present. In PCS 08113, a flow of 1.5E-02 l/s was produced from 397.8 to 414.5 m under ambient conditions. Pumping conditions resulted in a noticeable increase in flow from the HPL zone, and a calculated permeability of 9.7E+01 md.

The deepest drill stem test zone which measured significant permeability in well PCS 0502 was near the base of the Medium Sandstone subdivision. Core indicates that vuggy porosity and/or fracture porosity could be associated with this high permeability zone. The laboratory testing presented in Section 5.2 supports the notion that high permeability due to flow through vugs is possible. Reduction stains observed on fractured surfaces further indicates that fracture flow is also possible.

The drill stem test performed from 431 to 443 m in PCS 0502 was located near the base of the Medium Sandstone subdivision. A permeability of 1.9E+03 md was interpreted over this interval (Baker Hughes, 2005a). Hydrophysical logging in PCS 08113 discovered two inflow zones with depths that appear to correlate with the aforenoted DST. The first of these zones was identified between 431.3 and 433.7 m, and produced the most flow for the entire well in PCS 08113 under ambient conditions. The FMI log (Figure 5.15) for this wellbore indicates the presence of partially conductive fractures and

vugs. The second permeable zone identified from the HPL in PCS 08113 was located from 435.9 to 437.4 m, which is only slightly offset from the conductive fractures identified in the FMI log between 434.3 and 435.6 m. Comparison with drill core from PCS 0502 (Figure 5.16) suggests that the conductive fractures identified by the FMI logging tool is more consistent with the depth of the second inflow logged by HPL.

Below the Medium Sandstone subdivision, from 621.8 to 624.8 meters, a zone of modest permeability was shown in the HPL log for PCS 08113. An inflow rate below 6.7E-03 l/s under was recorded in this zone under pumping conditions, resulting in an interpreted permeability of 3.6E+01 md. The small flow observed in this zone appeared to be coming from the base of Mabou (claystone clasts) just above the caprock of the upper anhydrite. Two bottom-hole drill stem tests in PCS 0502 indicated 1.6E-01 md of permeability.

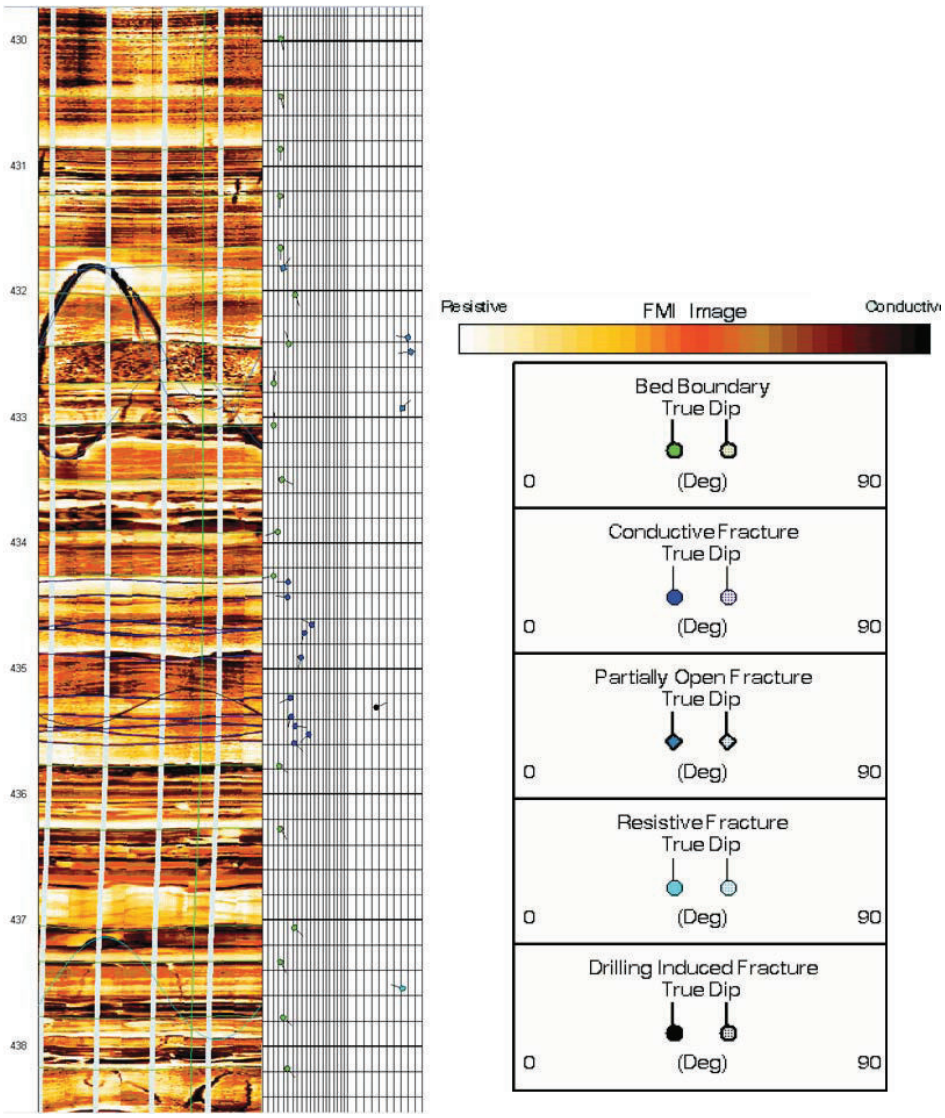

Figure 5.15 - FMI log for PCS 08113 from 430 to 438 m.
In the image track on the left, dark colours denote zones of high electrical conductivity (e.g., porous zones, fractures or vugs filled with saline drilling fluids). In the track shown on the right, the orientations of planar features are shown as "tadpoles". Bedding planes are indicated by the green tadpoles, partially open fractures are indicated by light blue tadpoles with diamond-shaped "heads", and conductive (i.e., open) fractures are indicated by dark blue tadpoles. (after Schlumberger, 2008b)

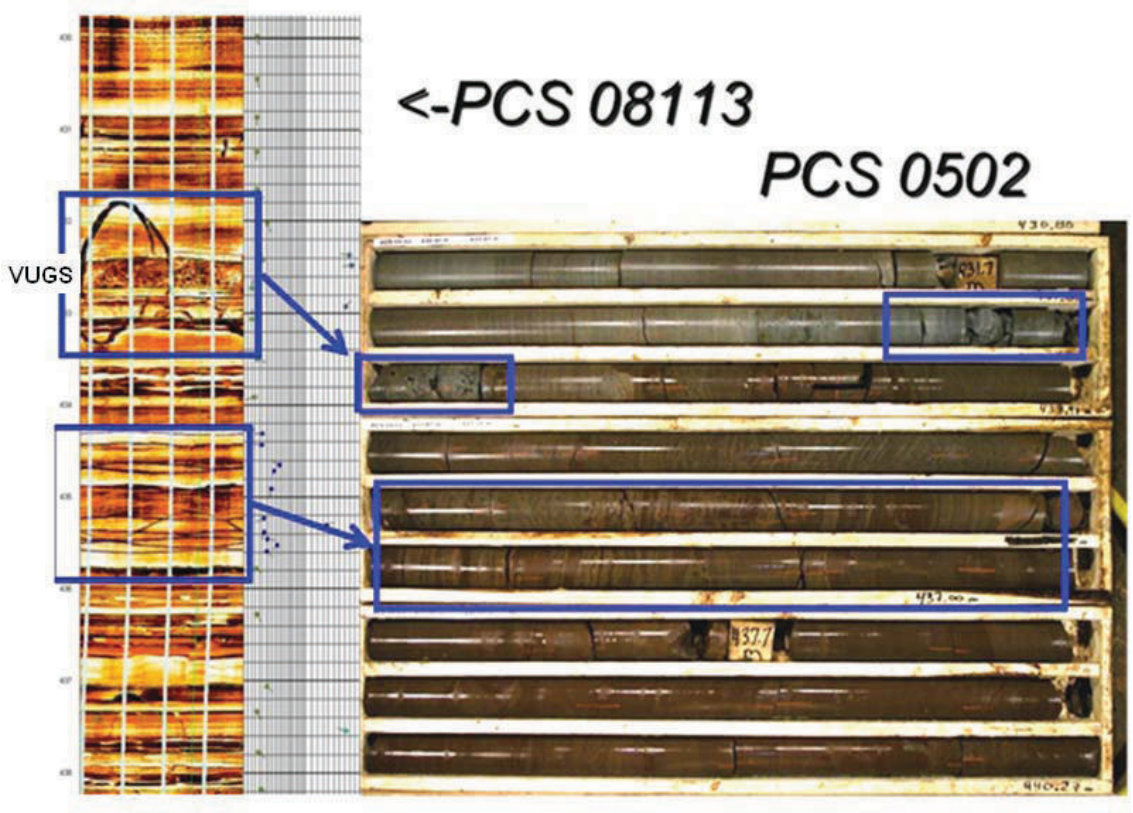

Figure 5.16 - Comparison of FMI from DST 08113 and Drill core from PCS 0502 within the Medium Sandstone subdivision (FMI : after Schlumberger, 2008b . Photograph courtesy of PCS)

Comparison of the two wells infers at least four laterally continuous and potentially mappable zones. These four zones are: (i) the inflow seen in both wells at 200 m; (ii) the vuggy porosity present directly above gypsum-infilled fractures within the siltstone; (iii) the two zones found within the Medium Sandstone subdivision (mapped as one); and (iv) at the base of the Mabou (claystone clasts). The fourth zone is at least an order of magnitude less permeable than the first three zones and similar to many other "zones" identified in HPL logging which have not been discussed in this work. This zone is considered worthy of mention, however, because of its presence immediately above the anhydrite caprock.

5.3.2 Well pair PCS 0601 and 08115

The drill collars of well pair PCS 0601 and 08115 are located approximately 420 meters apart. Depth correlation of permeable zones was expected to be weaker than the previous well pair due to this relatively large separation, and the fact that dips vary significantly in PCS 0601 (as presented in Section 4.4). Table 5.3 and Figure 5.17 illustrate the comparison of hydraulic zones between the two wells.

A thieving zone which correlates with the thieving zone of PCS 08113 may be present in the upper portion of 08115, but given

> "the very low inflow rates, and the extended period of time for the high FEC [fluid electrical conductivity] front to reach the upper flow zones (estimated to be several days), logging was terminated before an outflow location could be identified and confirmed. However the analysis of the data does suggest (as based on review of the AFC [ambient fluid condition] logs and the FEC logs collected during pumping) that the most likely candidates for the outflow location occurred above 153 meters depth, and the interval was most likely located between 52.7 and 116.1 meters" (RAS, 2008d).

No distinct correlations above the highlighted drill stem test in Table 5.3 could be made for the well pair with any sort of confidence, presumably due to the 420 meter separation. The DST depths that did match up with HPL logs could not be confidently correlated given the lack of distinct stratigraphic markers.

Table 5.3 - Comparison of PCS 0601 drill stem test results with PCS 08115 hydrophysical logging results. Yellow highlighting indicates zones that correlate between the two wells

DST depth (m)	kh (md*m)	PCS 0601 permeability (md)	HPL depth (m)	PCS 08115 HPL Ambient Condition (l/s)	PCS 08115 HPL Pumping Condition (l/s)	PCS 08115 permeability (md)
			52.7 to 57.3	<6.7E-04	3.9E-01	3.1E+02
92.0 to 104.0	1.6E+04	1.3E+03	92.7 to 96.3	<6.7E-04	5.2E-01	5.5E+02
			114.0 to 116.1	<6.7E-04	4.9E-01	8.8E+02
118.5 to 130.5	1.4E+04	1.2E+03	127.4 to 128.3	<6.7E-04	4.4E-02	1.8E+02
			132.6 to 133.5	<6.7E-04	5.7E-02	2.4E+02
150.0 to 162.0	4.6E+03	3.9E+02	143.0 to 144.8	<6.7E-04	1.0E-01	2.1E+02
			203.6 to 207.6	<6.7E-04	1.4E-01	1.3E+02
212.0 to 224.0	3.2E-02	3.0E-03	214.9 to 216.4	<6.7E-04	1.3E-02	3.0E+01
			223.4 to 224.9	<6.7E-04	6.3E-03	1.4E+01
			230.1 to 233.2	<6.7E-04	6.3E-03	7.2E+00
260.0 to 272.0	4.4E+01	3.6E+00	248.1 to 250.2	<6.7E-04	7.6E-02	1.4E+02
			299.0 to 300.5	3.2E-03	2.0E-02	4.2E+01
			327.7 to 329.8	<6.7E-04	6.3E-03	1.0E+01
337.5 to 349.5	1.3E+02	1.1E+01	340.8 to 342.3	2.5E-03	6.3E-03	9.6E+00
			358.8 to 360.3	8.8E-03	3.8E-02	5.8E+01
362.0 to 374.0	2.6E-02	2.0E-03 well below hydrostatic pressure (680 kPa)				
391.0 to 760.5	8.1E-01		424.3 to 471.2	1.3E-03	6.3E-03	4.2E-01

Note: Additional bottom hole tests were conducted below 391 m and are not shown as they have no added value to the comparisons. Pressure results of tests not shown are presented in Section 5.4.3.

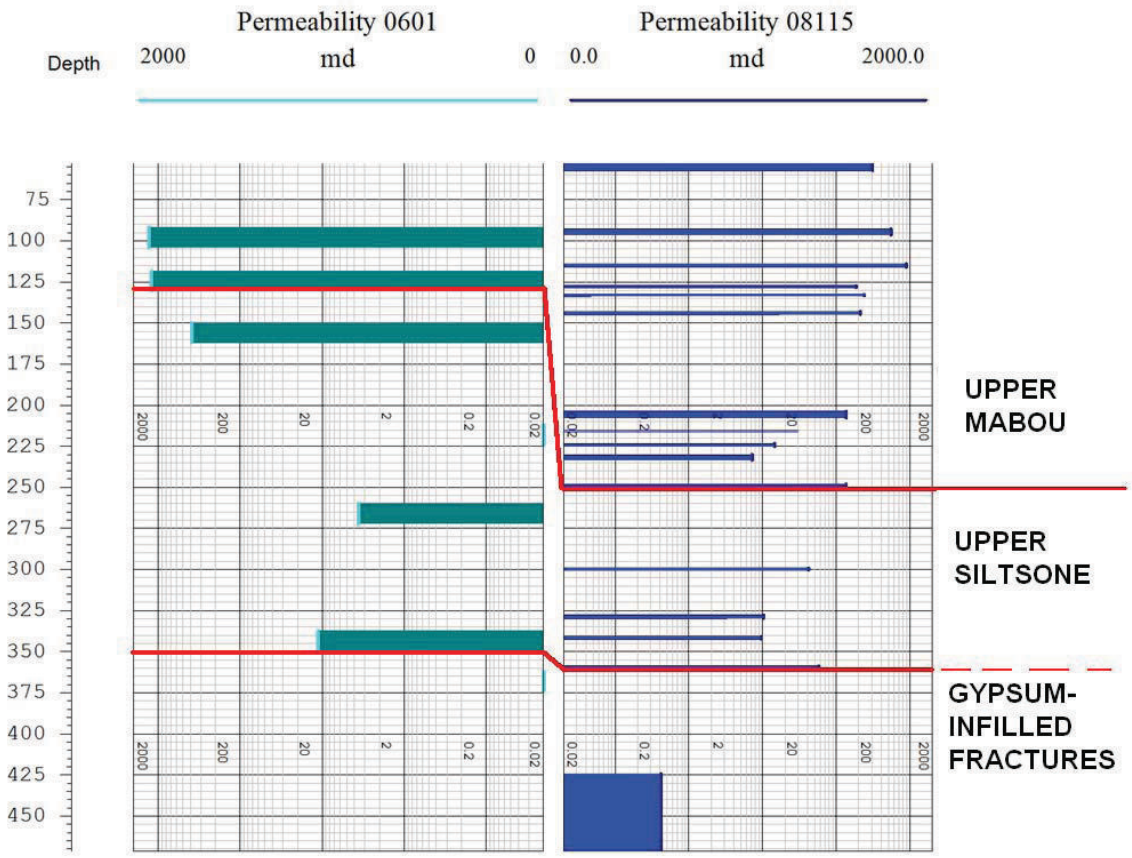

Figure 5.17 - Graphical representation of permeable horizons in PCS 0601 and PCS 08115

The correlation of the zone highlighted in Table 5.3 is postulated based on the fact that the zone is located above the upper limit of the zone of gypsum-infilled fractures. The first presence of gypsum-infilled fractures in PCS 0601 occurs at 353 m, as seen in Figure 5.18. The DST in PCS 0601from 337.5 to 349.5 m infers that the correlating zone possesses a permeability of 1.1E+01 md. Core photographs and FMI data in Figures 5.19 and 5.20 show a vuggy nature to the siltstone within the drill stem test interval. A permeability of 9.6E+00 md was recorded at a depth of 340.8 to 342.3 m in PCS 08115. The strip log for well PCS 08115 describes trace gypsum in the drill cuttings starting at a depth of 364 m, which is less than 2 meters below the base of the most productive interval (as measured under ambient conditions) in PCS 08115; this being a zone that possesses a permeability of 5.8E+01 md.

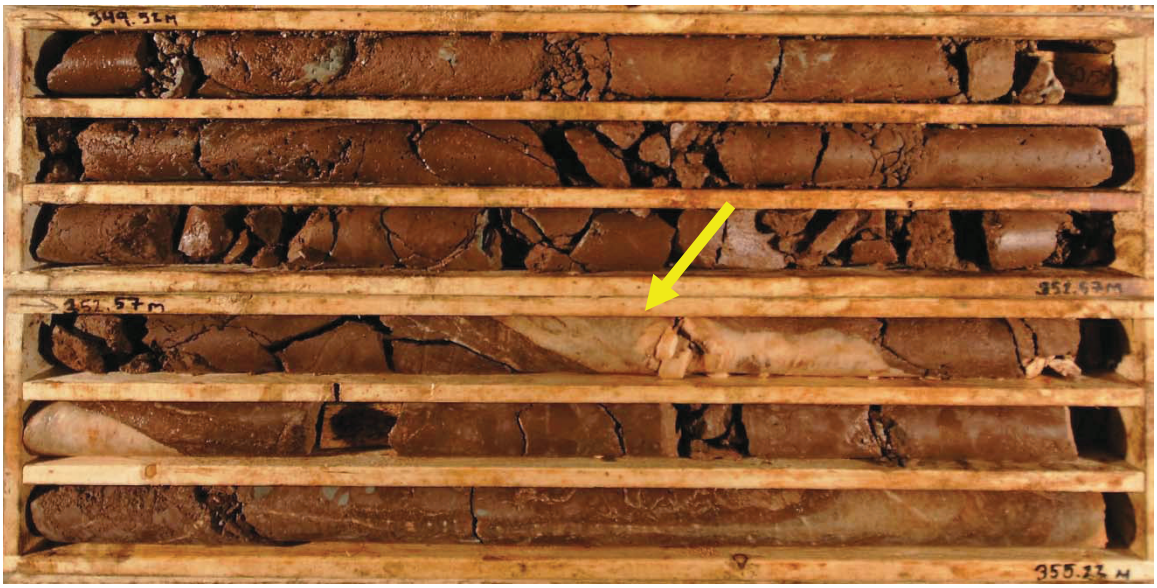

Figure 5.18 - PCS 0601 core from 349.52 - 355.22 m. The yellow arrow indicates the top of the gypsum-infilled zone (Photograph courtesy of PCS)

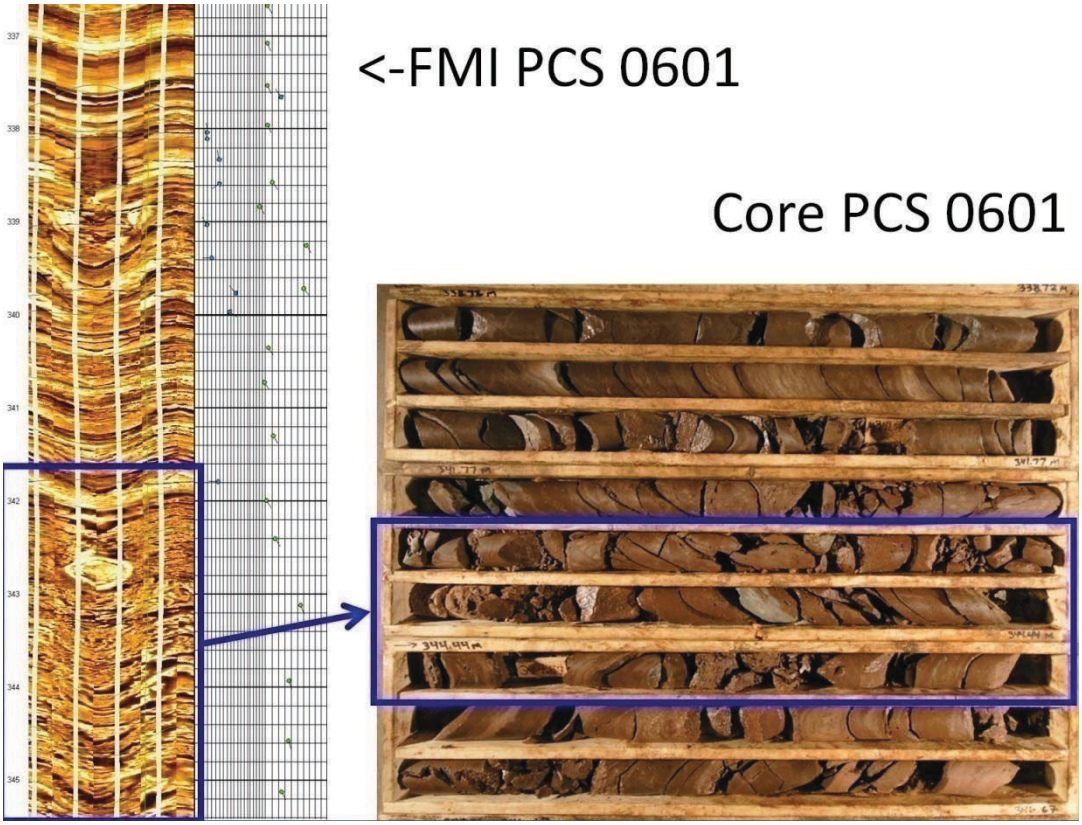

Figure 5.19 - Core and FMI log data from upper section of DST from 337.5 to 349.5 m (FMI: after Schlumberger 2006. Photograph courtesy of PCS)

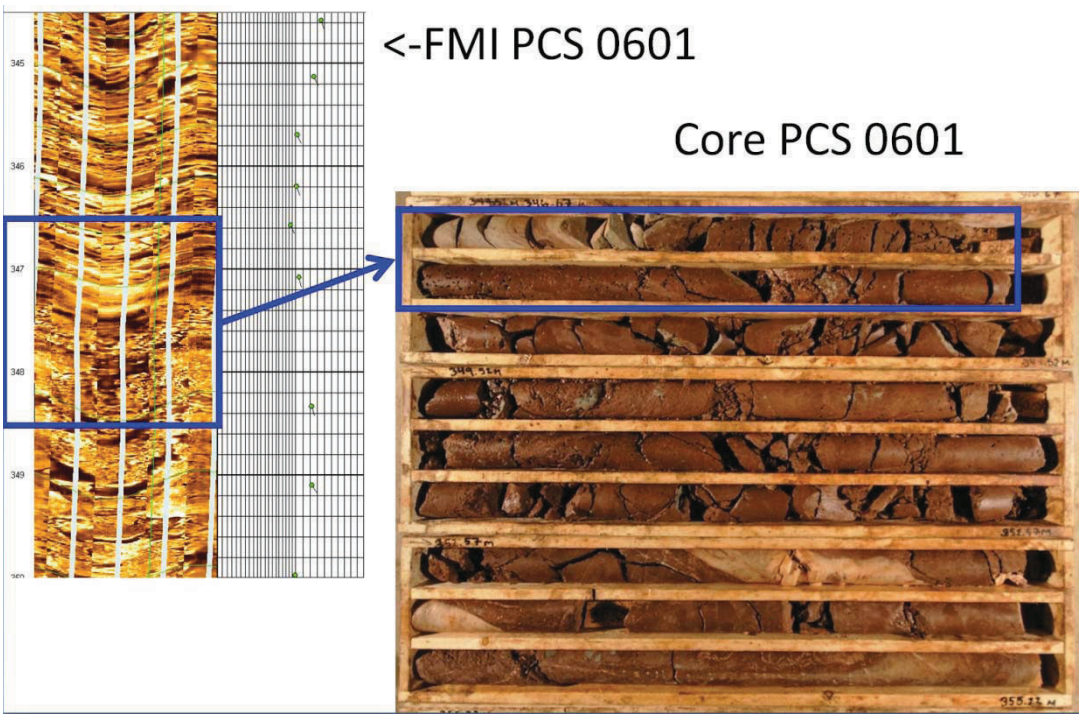

Figure 5.20 - Core and FMI log data from lower section of DST from 337.5 to 349.5 m (FMI: after Schlumberger 2006. Photograph courtesy of PCS)

A drill stem test was performed by Baker Hughes Inc. below the contact of gypsum-infilled fractures, as a zone of lower quality rock was present (Figure 5.21), with 0.5 m of core missing (i.e., lost recovery). The drill stem test interval from 362 to 374 m recorded an initial hydrostatic pressure and was interpreted by Baker Atlas to have a relatively low permeability of 2.0E-03 md.

Hydrophysical logs in PCS 08115 observed a 47 m thick zone of restricted flows within the Upper Siltstone subdivision below the gypsum-infilled fractures contact. Analysis of borehole PCS 08115 "suggests that the interval of extremely low ambient flow, occurring over the larger interval from 424.28 to 471.22 meters, had an inflow rate of 0.08 lpm [1.3E-03 l/s] during ambient pressure conditions" (RAS, 2008d). The HPL results indicate a 4.2E-01 md permeability within the gypsum-infilled fractures of the Upper Siltstone subdivision.

Figure 5.21 - PCS 0601 core from 364.35 to 368.04 m (Photograph courtesy of PCS)

Hydraulic properties near the base of the Mabou could not be assessed using FEC logs in PCS 08115. During field operations, the RAS field crew discovered that the maximum cable depth achievable was 653 m, which was insufficient to reach the total depth of the hole of approximately 740 m. Based on DST results from PCS 0601, no significant flow zones are interpreted in the borehole between 390 m and the bottom of the hole (in the upper anhydrite). At the location of this well pair, the Medium Sandstone subdivision does not appear to possess the relatively high permeabilities observed further to the northeast (i.e., in well pair PCS 0502/PCS 08113).

5.3.3 Well pair PCS 0504 and 08105

The drill collars of well pair PCS 0504 and 08105 are approximately 45 meters from each other. The comparison of the results are shown in Table 5.4 and Figure 5.22.

Drill stem testing was not performed within the upper section of the PCS 0504 borehole. No flow zones could be tested because the drilling rig lost circulation (the formation was thieving the mud). Drilling required the use of a tricone bit until circulation had been regained. As a result, the well could not be cored from 183 m to 253 m, and intermediate casing was installed to a depth of 253 m (PCS 2005b). The inability to drill stem test and collect data due to outflow of drilling mud into the formation correlates with results obtained in the hydrophysical logging of PCS 08105 in that a large outflow or thieving zone was logged from 227.9 to 261.9 under ambient conditions (RAS, 2008a).

Following the trend of the previous two well pairs, it would be expected that the contact of gypsum-infilled fractures would be the next potentially correlatable flow interval to be encountered with increasing depth. A drill stem test from 360 to 372 m indicated that no permeable zone is present directly above the gypsum infilling contact, which occurs at a depth of 374.3 m in PCS 0504. The transition from open fractures to gypsum-infilled fractures in core (Figure 5.23) does not show vuggy porosity as did the previous well pairs. No permeable zones were interpreted to exist in PCS 08105 at similar depths.

The correlation of low permeabilities and the absence of vugs above the zone of gypsum-infilled fractures should be noted, as this also correlates to the profile of the lone continuous reflector identified in Section 4.5, connecting PCS 80113 and PCS 08115 but not extending out to PCS 08105. This is based on the observation that the first two well pairs compared possessed vugs above the zone of gypsum–infilled fractures contact and were found to have high permeabilities, yet this third well pair possessed neither.

Bottom hole drill stem tests suggested the presence of a permeable zone somewhere between 480 and 540 m (the depth of the Medium Sandstone subdivision), with a 1.0E+03 md permeability. Core photographs illustrate interbedded and fractured sandstone within the zone of interest. A successful interval drill stem test between 492 and 504 m resulted in the interpretation of hydrostatic pressure conditions but permeability that is low compared to the two bottom hole tests. This indicates that this zone is likely part of a larger permeable unit between the two bottom hole tests. Core photographs reveal that the interval test had been performed on fractured siltstone overlying the sandstone package.

Table 5.4 - Comparison of PCS 0504 drill stem test results with PCS 08105 hydrophysical logging results. Yellow highlighting indicates zones that correlate between the two wells

DST depth (m)	kh (md*m)	PCS 0504 permeability (md)	HPL depth (m)	PCS 08105 HPL Ambient Condition (l/s)	PCS 08105 HPL Pumping Condition (l/s)	PCS 08105 permeability (md)
			40.2 to 40.9		2.5E-01	1.5E+04
			48.9 to 49.4		9.5E-02	4.1E+03
			55.3 to 57.0	7.3E-01	5.6E-01	8.1E+03
			90.9 to 91.7	<6.7E-03	9.5E-02	3.0E+03
			133.2 to 133.5	<6.7E-03	3.2E-02	2.1E+03
			148.4 to 149.9	<6.7E-03	1.2E+00	1.9E+04
		WHILE DRILLING	177.9 to178.8	<6.7E-03	3.2E-02	8.5E+02
		LOST CIRCULATION	188.2 to 188.7	<6.7E-03	6.1E-01	2.7E+04
		from 180 to 263m	227.9 to 229.3		3.2E-02	5.4E+02
			245.4 to 246.5		1.8E-01	4.2E+03
			261.3 to 261.9	Thieving zone -7.5E-01	8.2E-02	3.2E+03
						Intermittent flow. Permeability could not be calculated
492.0 to 504.0	7.5E+03	6.3E+02	521.1 to 526.7		3.3E-02	
		Report states that this zone is likely 12.6% of a larger permeable unit, based on difference of bottom hole tests of tops 480m and 540m.				
						Intermittent flow. Permeability could not be calculated
755.0 to 785.0	2.5E-01	6.0E-03	557.5 to 559.5	1.3E-02	3.3E-02	

Note: Two additional bottom hole tests were conducted in PCS 0504 and are not shown as they do not add value to the comparisons.
Pressure results of all DSTs in PCS 0504 are presented in Section 5.4.3.

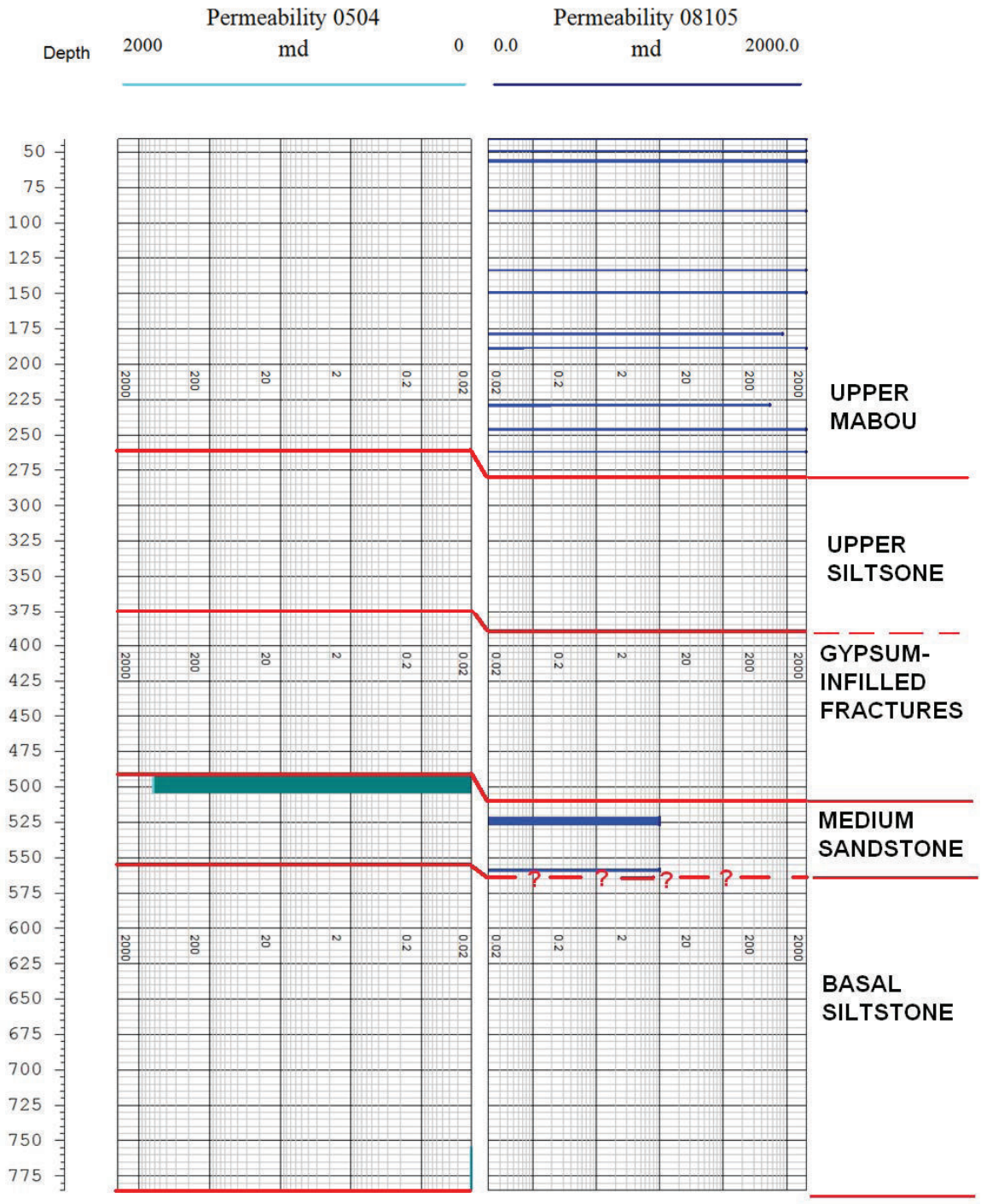

Figure 5.22 - Graphical representation of permeable horizons identified in PCS 0504 and PCS 08105

Figure 5.23 - PCS 0504 core 371.15 to 377.40 m (Photograph courtesy of PCS)

HPL results from PCS 08105 reported two flow zones within the Medium Sandstone subdivisions at depths of 521.1 to 526.7 m and 557.5 to 559.5 m. Permeabilities could not be calculated due to what RAS Inc. described as intermittent flow from the zones, which compromised their ability to compute hydraulic conductivities.

Hydraulic properties above the anhydrite caprock could not be verified by HPL logging because PCS 08105 was not drilled deep enough to intersect the base of the Mabou. The bottom hole test of PCS 0504 from 755 to 785 m recorded an extremely low permeability of 6.0 E-03 md (Baker Hughes, 2005b).

5.3.4 Well pair 0201 and 08107

The drill collars of well pair PCS 0201 and PCS 08107 are approximately 21 m apart from each other. Hydraulic properties for this well pair could not be compared because no hydraulic testing was conducted in PCS 0201. Data for PCS 08107 is presented here to determine if hydrophysical results in Table 5.5 and Figure 5.24 can be used to extend correlations to the south-western section of Picadilly.

Similar to results presented in the preceding sections, the dominant inflow zone under pumping conditions was the upper 200 meters in PCS 08107 (RAS, 2008b). However, no thieving zones were observed under ambient conditions in this upper stratigraphy in PCS 08107, which differs from the behaviour observed in other drill holes.

Previous well pairs reviewed suggest the next potentially mappable permeable zone with increasing depth would be the zone above the contact of gypsum-infilled fractures. Core from PCS 0201 shows gypsum-infilled fractures at a depth of approximately 316 m. The depth is relatively close to the base of several smaller permeable zones in PCS 08107, which terminate at a depth of 322.11 m, where gypsum has infilled the fractures. The data indicates that no large flow is present at the contact of gypsum-infilled fractures. This is consistent with the observed fact that core in PCS 0201 is relatively intact and is not vuggy, as seen in Figure 5.25. Lack of flow within the gypsum-infilled Upper Siltstone portion of PCS 08107 does suggest that a vertical flow barrier may be present within this part of the study area.

A permeable zone in the Medium Sandstone subdivision was present in PCS 08107. This zone was confirmed to be located in Medium Sandstone by PCS 0201 core photographs and geophysical logs of PCS 08107. The permeable zone was logged from 413.00 to 414.53 m, making it the second deepest permeable zone identified in this well.

The deepest measured permeable zone in PCS 08107 was located above the anhydrite caprock, from a depth of 595.24 to 597.59 m, with a permeability of 1.0 E+01 According to the lithological description of PCS 08107 interpreted from drill cuttings, this zone is isolated within siltstones ten meters above the claystone clasts that lie on the upper anhydrite.

Table 5.5 – PCS 08107 hydrophysical logging results

HPL depth (m)	PCS 08107 HPL Ambient Condition (l/s)	PCS 08107 HPL Pumping Condition (l/s)	PCS 08107 permeability (md)
76.2 to 77.0	9.3E-03	1.2E-01	4.8E+03
159.7 to 160.9	1.6E-01	2.2E+00	5.8E+04
161.5 to 136.1	<1.7E-04	<1.7E-03	3.5E+01
169.5 to 171.3	3.2E-03	1.7E-02	2.6E+02
195.1 to 196.0	<1.7E-04	<1.7E-03	5.9E+01
203.0 to 208.2	<1.7E-04	<1.7E-03	1.0E+01
253.0 to 256.6	<1.7E-04	<1.7E-03	1.5E+01
255.3 to 257.9	9.3E-03	4.8E-02	2.1E+03
259.1 to 259.8	<1.7E-04	<1.7E-03	8.5E+00
260.9 to 261.8	<1.7E-04	<1.7E-03	7.0E+00
275.6 to 276.0	0.0E+00	5.0E-04	3.0E+01
280.0 to 281.1	6.7E-04	3.3E-03	8.7E+01
284.5 to 285.5	8.3E-04	4.2E-03	1.2E+02
295.4 to 296.1	1.0E-03	5.0E-03	1.9E+02
313.5 to 314.3	5.0E-04	2.5E-03	8.7E+01
314.3to 322.1	8.3E-04	4.2E-03	1.5E+01
413.0 to 414.5	4.3E-03	2.3E-02	4.3E+02
595.2 to 597.6	1.7E-04	8.3E-04	1.0E+01

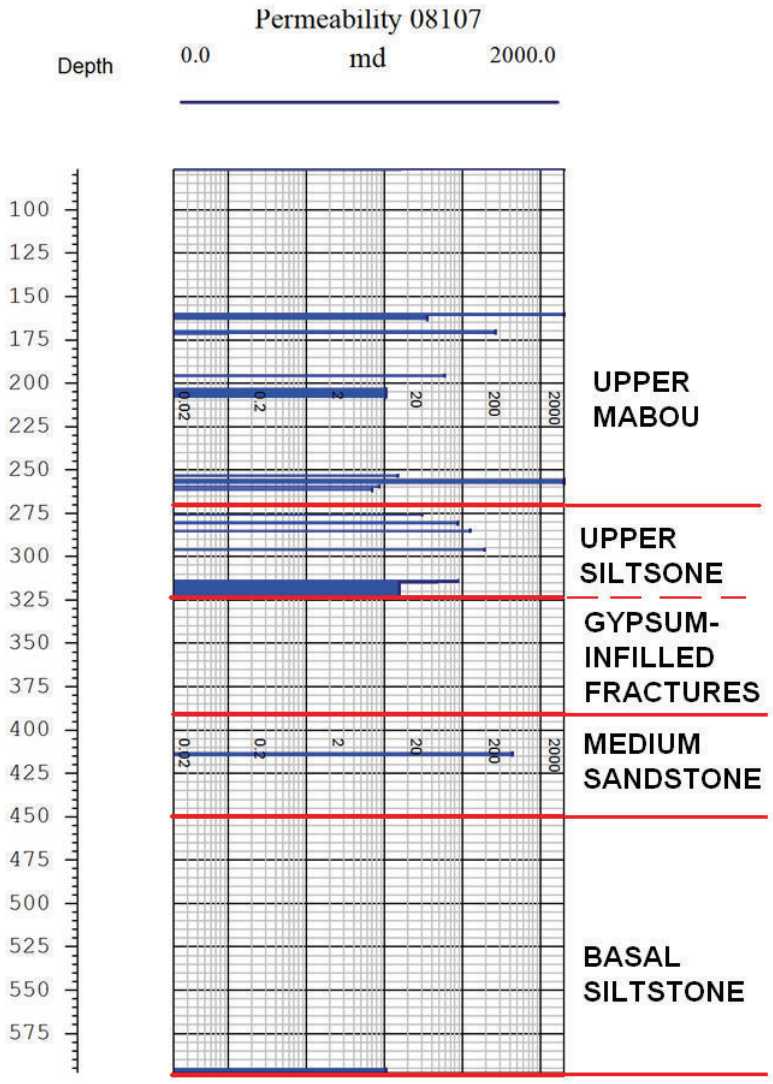

Figure 5.24 - Graphical representation of permeable horizons in PCS 08107

Figure 5.25- PCS 0201 Core 314.66 - 321.01 m (Photograph courtesy of PCS)

5.4 Comparison of porosity and permeability

The effective porosities presented in track 4 of Figures 4.18, 4.19, 4.20, 4.21 and 4.22 do not show strong correlation to the permeabilities interpreted from hydrophysical logging (presented in track 5 of these figures).

The author suggests that this lack of correlation between porosity and permeability is a consequence of the fact that permeability is predominantly controlled by secondary porosity in the rocks investigated in this research. Only the permeable horizons above the gypsum-infilled fractures consistently show a high porosity relative to the surrounding area; these elevated porosities being attributable to vuggy porosity. Specifically, the effective neutron-density porosities range from 9 to 15 % in this zone, where the hydrophysical logs show that a permeable horizon is present. The remainder of the permeable zones in the Mabou are believed to be attributable to fracture porosity. Fracture porosity typically does not exceed 1 to 2 % by volume (Doveton, 1999), hence the resulting increase in total porosity may be too small to be clearly evident.

5.5 Analysis of pore fluid chemistry

Water samples recovered during drill stem testing were tested for composition and isotopic signatures prior to this research project. The results were deemed inconclusive by PCS (personal communication, Terry Danyluk). The data were re-assessed in this project in light of their potential to shed light on the interconnectivity of permeable horizons; however they were confirmed to be of limited value due to the highly erratic correlations observed between salinity and electrical conductivity. As a result, an analysis of pore pressure distributions within the Mabou was pursued as an alternative means of assessing interconnectivity, as described in the following sections.

5.6 Analysis of pore pressure distributions

5.6.1 HPL and DST data

Although hydrophysical logs do not provide a direct measurement of pore pressures, they do provide evidence pertaining to under-pressured zones. The fact that some permeable zones acted as thief zones under ambient well bore conditions during hydrophysical logging suggests that these zones were under-pressured relative to the hydrostatic gradient of the well.

The fact that other permeable zones flowed at low rates under ambient wellbore conditions suggests that pore pressures within these zones were close to normally-pressured, relative to the freshwater hydrostatic gradient. Beyond these qualitative observations, HPL results were not used.

DSTs provide estimates of pore pressures; hence the DST results were used in this research to assess pore pressure distributions in the study area. Before using these results, however, a pressure transient analysis was conducted by the author on a selected DST as a quality control measure; i.e., to verify the permeability-thickness product and static (initial) pore pressure presented in the reports provided to PCS by the service companies that conducted the tests.

5.6.2 Verification of reported DST Results

The author conducted an independent pressure transient analysis of the data for the drill stem test from 337.5 to 349.5 m in well PCS 0601. The analysis was based on a version of the final build-up (shut-in) pressure graph that was manually digitized (Figure 5.26).

The first check for reliable permeability calculations is that the test was shut in for a sufficient duration that the pressure began to stabilize (i.e., the curve of a pressure versus time graph begins to "flatten off") at the end of the test. This test attribute will enable more accurate test interpretation, which is generally conducted using a Horner plot.

As described in Section 2.3.1.1, the functions of a Horner plot (Figure 5.27) are to enable an extrapolation of the late-time pressure measurements to a static (i.e., infinite time) formation pore pressure, and to determine the slope of the extrapolated pressure trend line over one log cycle of time. The less extrapolation required to obtain a static pore pressure, the higher the degree of confidence in the result.

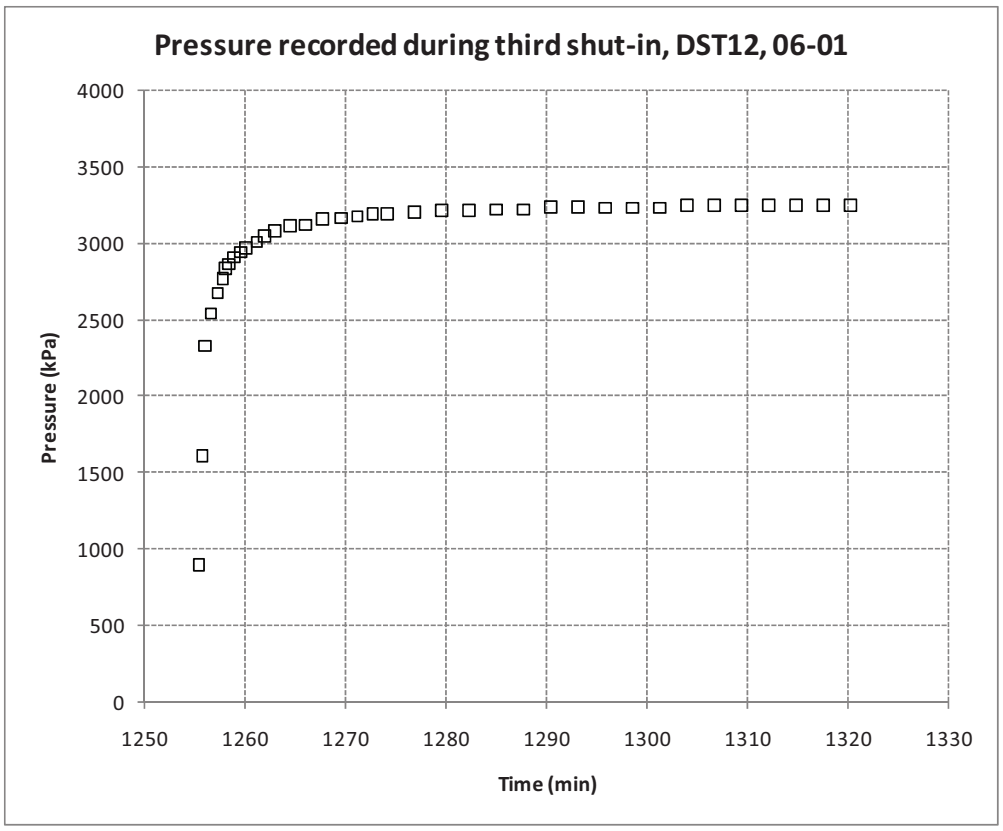

Figure 5.26 - PCS 0601, DST # 12, Final shut-in pressures

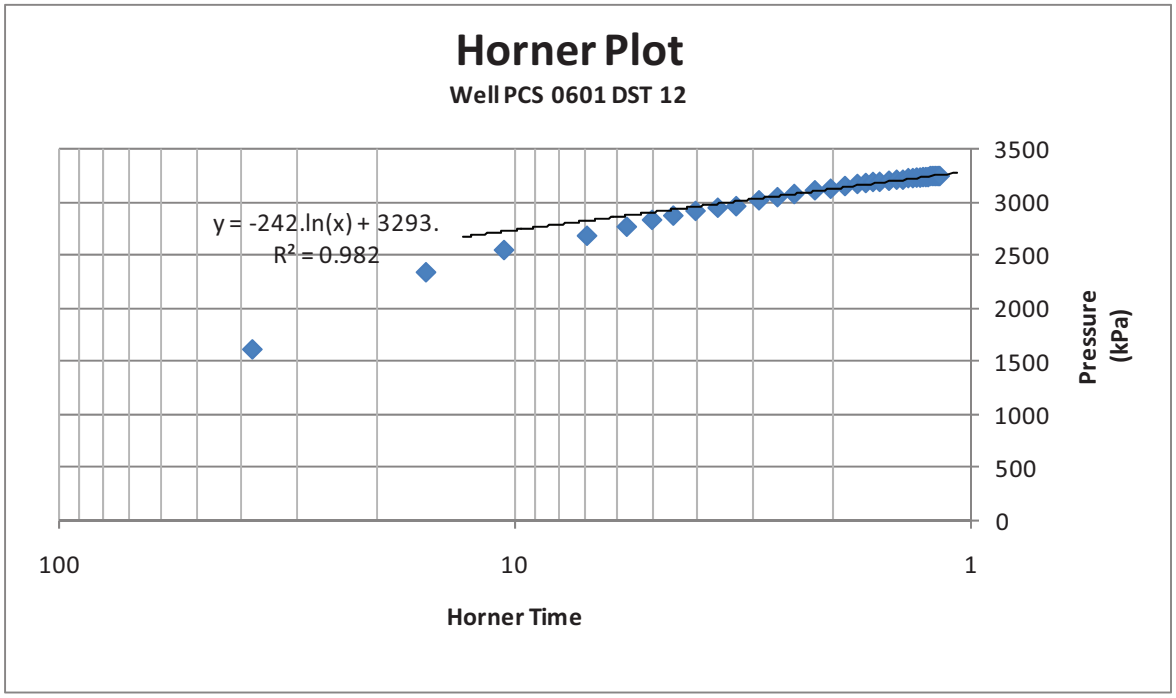

Figure 5.27 - PCS 0601, DST # 12, Horner Plot

For the test investigated here, the last pressure measured was approximately 3270 kPa, and the extrapolated static pore pressure interpreted by the author was 3293 kPa. This is identical to the static pore pressure (i.e., static "reservoir" pressure, as denoted on the service company graphs) presented to PCS in the DST report for PCS 0601. The low degree of extrapolation required in this case provides a high degree of confidence in the static pore pressures suggested by the test within this zone.

The slope (*m*) of the trend line interpreted by this author is 557 kPa per log cycle, determined as follows:

$$m = \frac{P_1 - P_{10}}{1\ cycle} \tag{5.1}$$

$$m = \frac{3293 - 2735}{1\ cycle}$$

The slope (*m*) of the Horner plot is one of three variables required for calculating the transmissivity of the tested formation, as follows:

$$T = \frac{kh}{\mu} = \frac{2149.4 Q \beta_0}{m} \tag{5.2}$$

Where:

T = Transmissivity (m^2/day)

Q = flow rate prior to shut-in (ambient or "standard" cubic meters per day)

β_0 = formation volume factor

m = slope From Horner plot trend line

From the DST reports for PCS 0601, a water formation volume factor of 0.997 Rm^3/ Sm^3 and a final flow rate of 43.8 Sm^3/D (0.507 l/s) were used for computer simulation of DST #12. Using Equation 5.2, the resulting transmissivity is 168 m^2/day (1.9E-03 m^2/s).

The permeability-thickness product (*kh*) is simply calculated by multiplying the transmissivity by the viscosity of the flowing phase, μ. The viscosity of water presented for DST #12 was 1.42 mPa·s, resulting in a permeability-thickness product of 239 md·m.

The transmissivity and permeability calculations conducted by the author were for the final flow and shut-in period; i.e., they were not calculated using flow rates and pressure responses from the two previous flow and shut-in periods. The flow rates for the first two flow periods were 50.8 and 50.3 Sm^3/D, which if substituted into the sample calculations that were based on final flow and shut-in periods transmissivity would yield 278 and 275 md·m, respectively. The transient pressure calculation of the final shut-in pressures yields almost double the permeability thickness when compared to the 127.1 md·m presented in the drill stem test report. The difference between the service company's and the author's permeabilities appears to be caused by the slope interpreted from the Horner plot. The total flowing time of all three flow periods was used to calculate Horner time in the sample calculations. Values closer to that presented in the Service Company's report are obtained when only the flow time of the final flow period is used, which is not standard practice. The pressure transient analysis on DST # 12 from well PCS 0601 suggests permeabilities presented in the DST report are conservative (i.e., low), and – more importantly (for the purpose of the analysis presented in this section) - validates the static formation pore pressure results presented for properly run drill stem tests.

5.6.3 Analysis of pressure gradients from DSTs

To assess the hydraulic connectivity of the Mabou Group within the study area (Figure 5.28), a systematic investigation of pore pressures and their variation with depth, from well-to-well and with respect to normal hydrostatic conditions, was undertaken. A pore pressure gradient depth plot was created (Figure 5.29); with pore pressures from drill stem test data plotted against test interval elevations relative to sea level. A freshwater hydrostatic gradient was initially plotted through the general trend of points as a basis of comparison to the pressures plotted from drill stem tests. Theoretically,

undisturbed pressures with hydraulic communication should plot along the same gradient line.

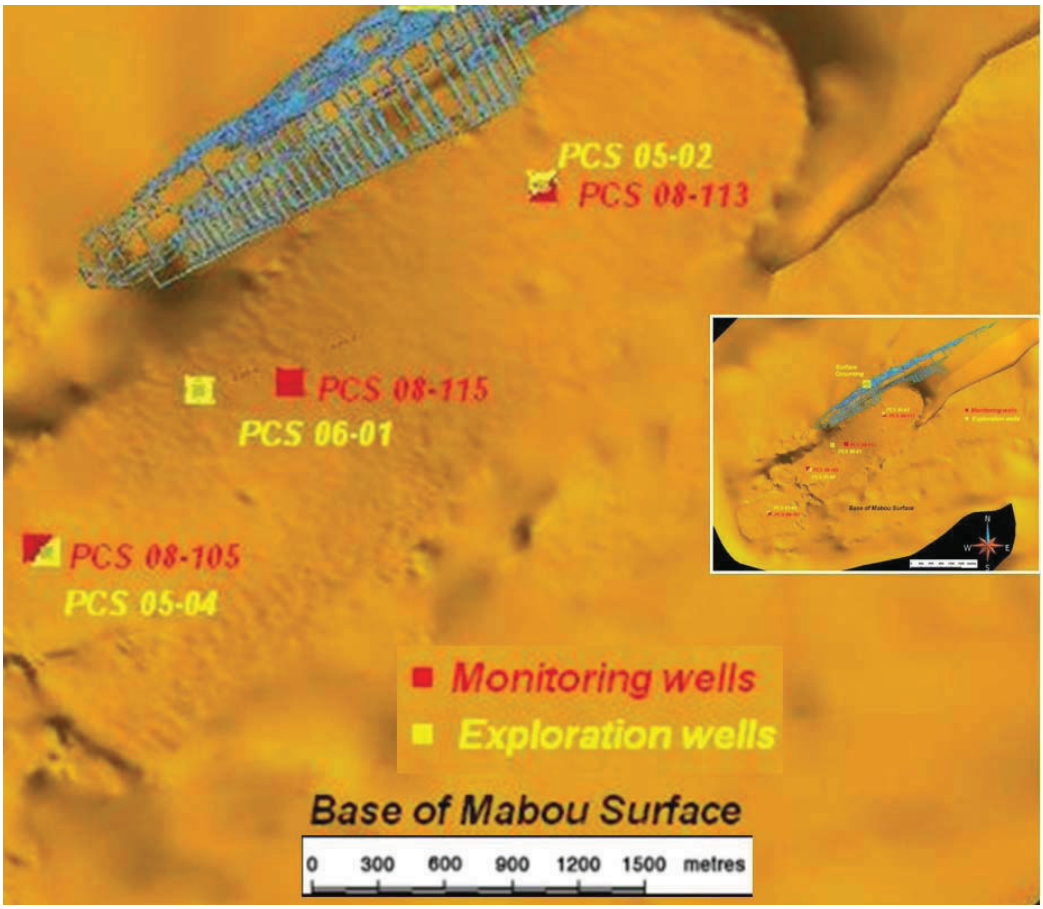

Figure 5.28 –Locations of exploration wells possessing drill stem test data (PCS 0502, 0504 and 0601)

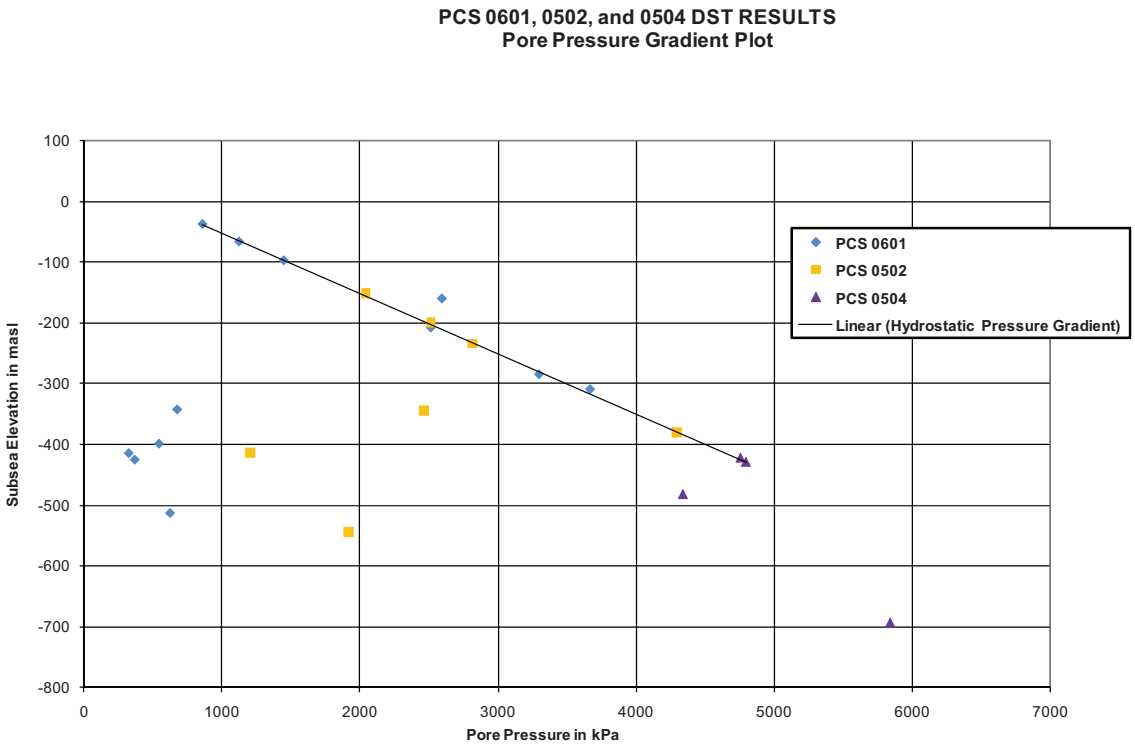

Figure 5.29- Plot of DST-interpreted pore pressure against depth plot

Not all of the data plotted along the hydrostatic gradient, which means that either multiple compartmentalised permeable zones were present or the data quality was poor. Two factors that are historically found to affect pore pressure–depth plots include: 1) the virgin pore pressure was not recorded during drill stem testing, as a nearby pumping well already influenced the virgin reservoir pressure; and 2) inaccurate extrapolation of the "reservoir" pressure using a Horner plot. Inaccurate extrapolation from a Horner plot occurs when the shut-in time is insufficient to allow the pressure to recover to a value that is close to the virgin pressure (i.e., the shut-in curve does not begin to "flatten"). In such a case, the difference between the final pressure measurement and the extrapolated value of the static pore pressure will be relatively large. As such, the difference between the last measured pressure and the extrapolated static pressure was used by the author as a data quality indicator. The results of this assessment are presented in tabular form in Table 5.6, and in graphical form in Figure 5.30. Static pressures ($(P_{av})_i$) that were obtained in cases where the difference (i.e., static pressure – last measured pressure) was

more than 15% of the static pressure are presented in red; these pressures were not used in subsequent analyses.

Hydraulic connectivity within the higher informal subdivisions of the Mabou is suggested by the pressure gradient plot. A regression of the high quality data present was performed on the points that appeared to follow a hydrostatic gradient and the results are shown in Figure 5.30 (green highlights). The regression suggests artesian conditions present in PCS 0502 and 0601, with ground elevations of 42.12 m and 42.25 m respectively, as these elevations are lower than the regression water level of 47.6 m. This observation is consistent with historical records of springs located just outside the study area which were used for the production of salt when the area was settled (personal communication, Brian Roulston).

Following the gradient line to depth, the Mabou Group demonstrates connectivity down to the gypsum infilling in PCS 0601 and the high flow zones within the Medium Sandstone in PCS 0502 and PCS 0504. Below such horizons the drill stem tests measure low flow rates, low permeability, and low pressures.

The low formation pressures recorded by drill stem testing could be caused by: the drill stem tests not being shut in long enough to enable stabilization in low permeability rocks; a naturally-occurring under-pressured zone in the Basal Siltstone subdivision; a natural process lowering the regional hydraulic pressure in the Basal Siltstone subdivision; or the dewatering of a moderately low permeable zone at the base of the Mabou Group (as interpreted from hydrophysical logs from two wells located several kilometres apart).

Table 5.6 - Verification of DST extrapolation pressures

PCS 06-01 Well

DST No.	3	4	8	9	10	11	12	13	14	15	16	17
Last pressure measure (kPa)	500	323	561	310	490	382	3270	2500	1460	1445	1125	860
$(P_{av})_i$, kPa	625.8	326.9	677.4	370.7	545.8	3662.6	3293.4	2510.6	2591.4	1448.0	1125.0	860.4
Extrapolation difference (%)	20.1	1.2	17.2	16.4	10.2	89.6	0.7	0.4	43.7	0.2	0.0	0.0
Pressure buildup flattened off	no	yes	no	no	no	no	yes	yes	no	yes	yes	yes
Depth, mKB	560.1	461.3	389.1	472.0	445.7	355.7	331.0	254.0	206.0	143.0	112.0	83.1
Sea level depth (masl)	-513.7	-414.9	-342.7	-425.6	-399.3	-309.3	-284.6	-207.6	-159.6	-96.6	-65.6	-36.7

KB (m)= 46.45

PCS 05-02 Well

DST No.	1	2	3	4	5	6	7
Last pressure measure (kPa)	1660	1130	4278	1205	2805	2025	2500
$(P_{av})_i$, kPa	1918.6	1207.9	4293.3	2463.1	2811.1	2041.0	2512.6
Extrapolation difference (%)	13.5	6.4	0.4	51.1	0.2	0.8	0.5
Pressure buildup flattened off	no	no	yes	no	yes	yes	yes
Depth, mKB	589.0	459.0	426.0	390.0	279.0	196.0	245.0
Sea level depth (masl)	-543.7	-413.7	-380.7	-344.7	-233.7	-150.7	-199.7

KB (m)= 45.26

PCS 05-04 Well

DST No.	1	2	3	6
Last pressure measure (kPa)	5323	2632	4754	4794
$(P_{av})_i$, kPa	5834.8	4340.2	4755.1	4794.1
Extrapolation difference (%)	8.8	39.4	0.0	0.0
Pressure buildup flattened off	no	no	yes	yes
Depth, mKB	751.0	540.0	480.0	487.0
Sea level depth (masl)	-693.6	-482.6	-422.6	-429.6

KB (m)= 57.45

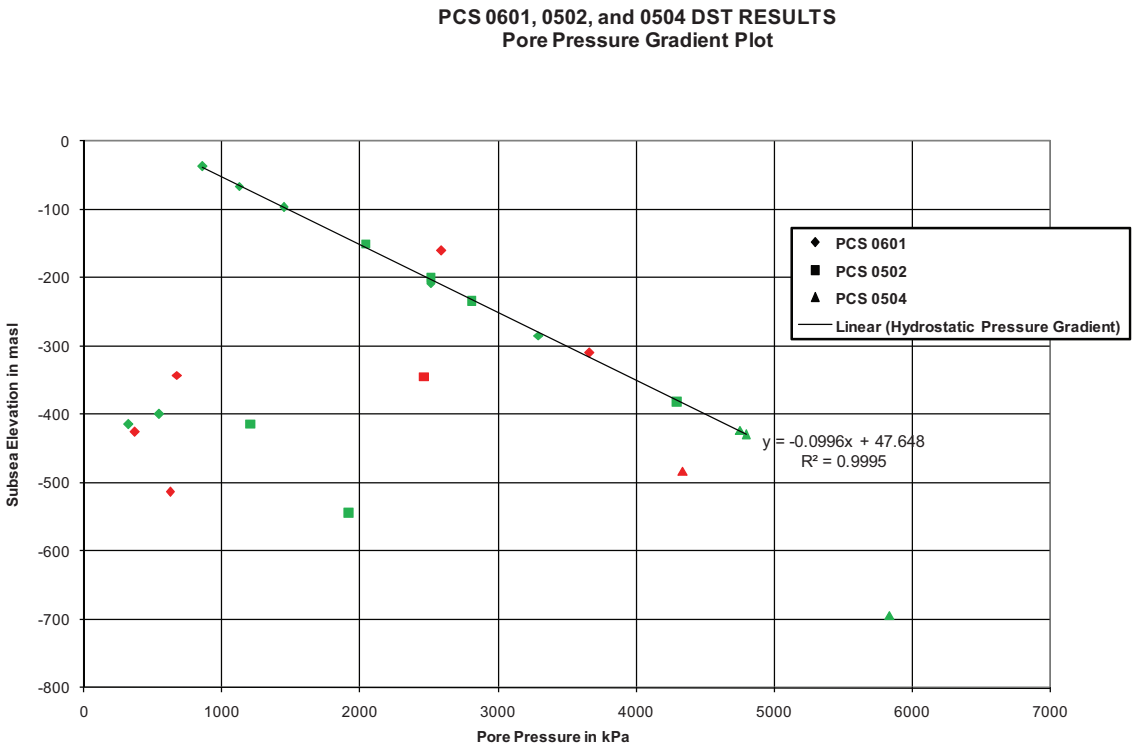

Figure 5.30- Plot of DST-interpreted pore pressure against depth (green symbols denote < 15% extrapolation from last measured pressure, red symbols denote >15% extrapolation)

The notion of a static undisturbed under-pressured aquifer existing naturally in the study area's Basal Siltstone subdivision is highly unlikely. Given that the under-pressured data points do not fall along a common gradient line, this suggests that each of the zones tested is either compartmentalized or a natural process is drawing formation water at rates greater than it can be recharged.

An alternative to a natural process drawing formation water at rates greater than it can be recharged is that this zone has been influenced by features or processes outside of the Picadilly study area, lowering the pressure within it.

An analysis to assess the potential connectivity of the lower Mabou to the inflow zone in the Penobsquis mine was undertaken in order to determine if this inflow might be responsible for the subhydrostatic zone at the base of the Mabou (i.e., above the potash deposit's anhydrite caprock). The inflow into the Penobsquis mine site was modelled as a flowing well, and a steady state draw-down calculation was conducted for an assumed

confined aquifer. The calculation assumed that 1) the inflow into the Penobsquis mine is occurring at the base of the Mabou Group, below the location labelled 'Surface grouting' in Figure 3.1, and is connected to the Picadilly side of the antiform; 2) a steady state flow rate has been reached; and 3) the pressure data from bottom hole drill stem tests of PCS 0502 and PCS 0504 are accurate and represent drawdown observation wells.

Based on the simple concept of drawdown occurring surrounding a pumping wellbore (Figure 5.31), the sub-hydrostatic water pressures (heads) measured by the DST's were assumed, in this scenario, to be part of a confined aquifer above the caprock and were caused by the inflow at Penobsquis. The closer the proximity to the inflow, the lower the pressure head is expected to be, as illustrated for PCS 0502 and PCS 0504 in Figure 5.32.

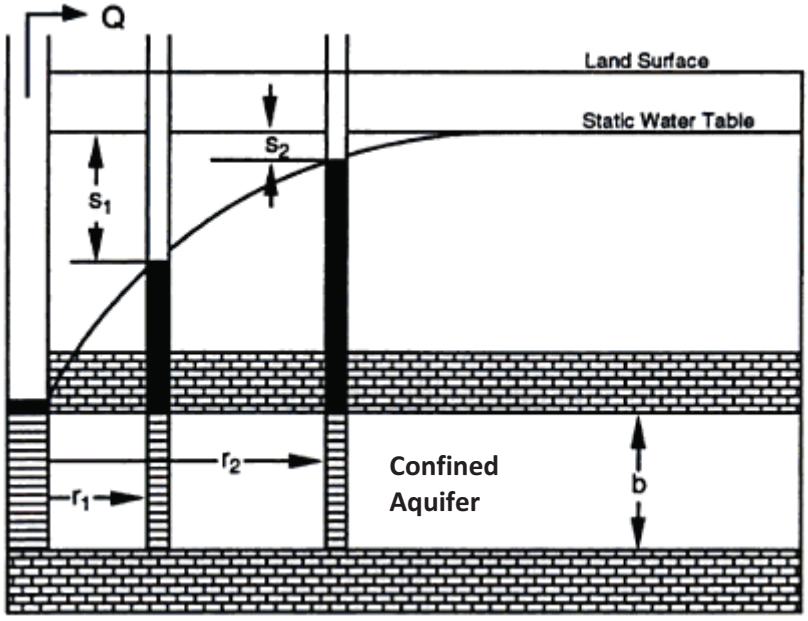

Figure 5.31 - Drawdown schematic for confined steady state aquifer (after Kasenow 2001)

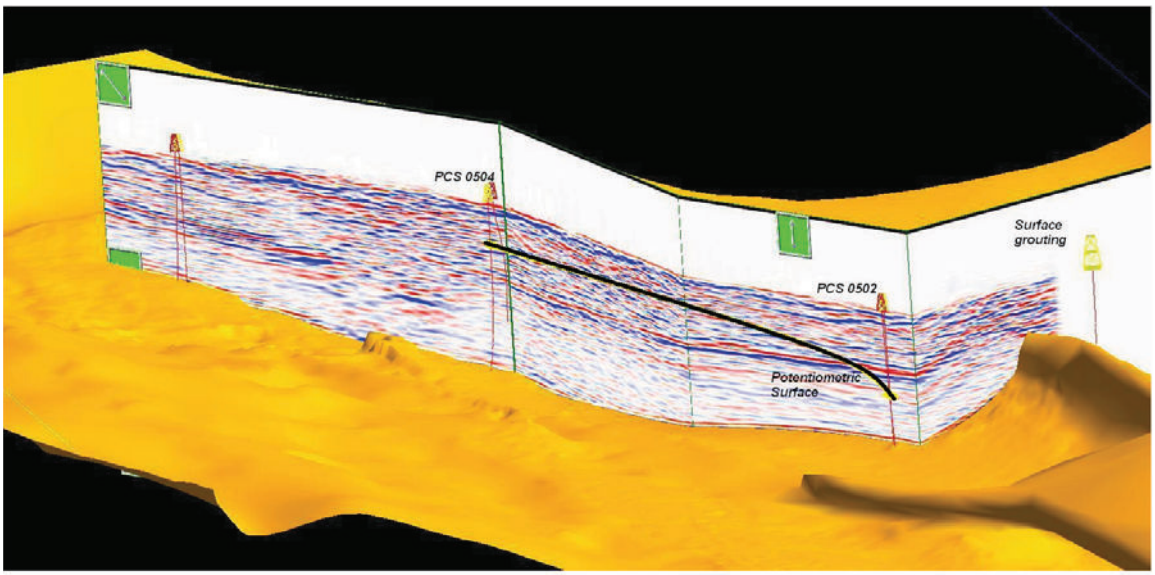

Figure 5.32 - Schematic representation of potentiometric surface (black line) from flow zone above the caprock (The orange-gold surface is the current PCS interpretation of the base of Mabou from seismic reflection profiles and surface geology)

The calculations presented here make use of the Theim solution for a confined steady state aquifer. To make use of the equations of the Theim solution, certain assumptions are required. These include:

1) The aquifer is homogeneous, isotropic, of equal thickness, and infinite in areal extent;
2) The production well penetrates and receives water from the entire aquifer thickness;
3) The transmissive property of the aquifer is constant at all times and at all locations in the aquifer;
4) The rate of discharge is constant and has occurred for a sufficient time to allow for a steady-state hydraulic system (i.e., no change in rate of drawdown); and
5) Flow to the well is horizontal, radial and laminar.

Clearly, none of these idealized conditions are truly met in this case. On the matter of homogeneity, at the scale of this problem (1000s of metres), it seems reasonable to suggest that the primary and secondary porosity systems may behave as an equivalent

porous medium. The connectivity between 0502 and 0504, implied by pressure data, suggests that this equivalent porous medium extends over a large area – though a measure of heterogeneity is implied by the lack of flow and pressure above the caprock in well PCS 0601. As such, an averaged permeability of the aquifer will be calculated for an equivalent homogenous aquifer. With over a decade of pumping water from the Penobsquis operation, it has been assumed for these calculations that sufficient time has passed to allow for a steady state hydraulic system with sub-horizontal and laminar flow to be occurring. To better assess the extent to which the study area conforms to these assumptions, more boreholes would be required to increase the spatial distribution of pressures at the base of the Mabou.

The Theim solution expresses transmissivity (T) and hydraulic conductivity (K) as follows (Peddler et al., 1992):

$$K = \frac{Q \ln \frac{r_2}{r_1}}{2\pi b(s_1 - s_2)} \qquad 5.3$$

$$T = \frac{Q \ln \frac{r_2}{r_1}}{2\pi (s_1 - s_2)} \qquad 5.4$$

Where:

T = Transmissivity (m^2/day)

Q = flow rate (m^3/day)

r_1= radial distance of first observation well from pumping well (m)

r_2 = radial distance of second observation well from pumping well (m)

s_1 = draw down of first observation well from original state (m)

s_2 = draw down of second observation well from original state (m)

b = aquifer thickness

The flow (Q) was assumed to be 1200 USGPM or 6540 cubic meters per day (75.6 l/s). The radial distances r_1 and r_2 were estimated for wells 0502 and 0504, respectively, assuming the inflow to be occurring at the base of the Mabou near the bottom of

historical grouting wells (Figure 5.32). The values used for r_1 and r_2 are 1000 m and 3500 m respectively. The drawdown for s_1 and s_2 were computed, correcting for collar elevations. The measured DST pressure of 1918 kPa above the caprock in PCS 0502 was calculated to represent an equivalent drawdown for s_1 of 391 m. The measured DST gauge pressure of 5834 kPa above the caprock in PCS 0504 was calculated to represent an equivalent drawdown for s_2 of 158.4 m.

Sample drawdown calculation for PCS 0504

5834 kPa = 583 m pressure head based on 10kPa/m for water

Pressure gauge depth = 751 m

Collar elevation = 57.6 m

Water elevation above caprock = 57.6 m – 751 m depth + 583m pressure

Water elevation = -110.4 masl

Drawdown = 48 masl – (-110.4 masl) = 158.4 m

The value obtained from the regression line of the formation pressure plot presented earlier in this section was applied to the Theim solution equations as a hydrostatic water table.

As shown in Table 5.7, with an original water table of approximately 48 masl, the transmissivity of the flow zone is 6.1 x 10^{-1} m^2/day and the associated permeability for a 10 meter thick aquifer would be roughly 75 md (which corresponds to a hydraulic conductivity of 7.2 x 10^{-5} cm/s).

Table 5.7 - Exploration DST drawdown results for a static water table of 48 m

Borehole	h (masl)	drawdown (m)	r (m)	T (m^2/day)	Perm (md)	K (cm/sec)
PCS 0502	-355	402.6	1000	6.1E-01	7.5E+01	7.2E-05
PCS 0504	-110.4	158.4	3500			

With limited data available on the water table, a second set of calculations was performed assuming a static water table of 36 masl to view the sensitivity of results to the water table input. Results presented in Table 5.8 indicate that a 12 meter variation in the water table changes the computed permeability by only 2 md. This demonstrates that the exact height of the water table prior to drawdown is not significant to the calculations.

Table 5.8 - Exploration DST drawdown results static water table 36 m

Borehole	h (masl)	drawdown (m)	r (m)	T (m^2/day)	Perm (md)	K (cm/sec)
PCS 0502	-355	391	1000	6.4E-01	7.7E+01	7.4E-05
PCS 0504	-110.4	146.4	3500			

The results suggest that with the under pressured recordings from DSTs, it is plausible that a confined flow at the base of the Mabou at Picadilly is within the cone of depression created by the Penobsquis inflow.

6 SUMMARY AND CONCLUSIONS

To facilitate the hydrogeologic characterization process, four informal lithological subdivisions were created within the Mabou Group, in the study area. From the base of the Mabou to surface, the informal subdivisions consist of: the Basal Siltstone subdivision; the Medium Sandstone subdivisions; the Upper Siltstone subdivision; and the Upper Mabou subdivision. The four subdivisions were used alongside the presence of gypsum-infilled fractures within the Upper Siltstone subdivision, down to the base of the Mabou Group for characterizing zones of hydrogeological interest.

Characterization led to the identification of four hydrogeologic zones of interest: the Upper Mabou; the vuggy porosity directly above gypsum-infilled fractures; the vugs and fractures within the Medium Sandstone subdivision; and the lower Mabou Siltstone at the base of the Mabou Group (within ~15m of base).

The Upper Mabou contains conglomerate sequences and is distinguished by the major inflows measured in hydrophysical logging (HPL) tests relative to the rest of the borehole under pumping conditions.

The vuggy zone above the gypsum-infilled fractures has a high potential for flow, but is of a heterogeneous nature based on drill stem tests, with indications that permeabilities range from approximately 11 md in PCS 0601, to 1843 md in PCS 0502. The high permeability of vuggy rocks from this zone was also demonstrated by the 590 md permeability measured on core in the laboratory.

The Medium Sandstone subdivision is associated with high permeability zones resulting from the presence of vugs and fracturing. It has been determined that the Medium Sandstone subdivision is well delineated from its sonic and density log responses in boreholes that were logged by Schlumberger.

In the east half of the study area, zones of low but measurable permeability in PCS 08113 and PCS 08115 were interpreted to be present between the vuggy porosity directly above

gypsum-infilled fractures and the Medium Sandstone subdivision using HPL logs. These zones of permeability may be considered as a connectivity point between the Medium Sandstone and the top half of the Upper Siltstone informal subdivision. Affirmation of hydraulic connectivity was presented in a pressure depth gradient plot where the Medium Sandstone pressures fell along the same gradient as the pore pressures further uphole.

The fourth significant hydrogeological zone is the base of the Mabou Group. The pressure transient responses and sub-hydrostatic pressures recorded by drill stem tests at the base of the Mabou Group indicate a zone of low but measurable permeability. Permeabilities measured in this zone by hydrophysical logging in PCS 08113 and 08107 indicate higher values than the surrounding rock. Drawdown calculations for a confined steady state aquifer model suggest plausible connectivity between the low permeability zone in the Basal Siltstone subdivision above the Picadilly caprock and the present inflow into the Penobsquis mine.

With the exception of the vuggy zone that is present above the gypsum-infilled fractures, permeable zones identified by the hydrophysical logs do not consistently correlate to increases in porosity determined from geophysical logs in the study area. The general lack of correlation may be due to fact that fractures often give rise to relatively small porosity increases (e.g., 1 to 2%), but substantial permeability increases if they are well connected. In the case of the vuggy porosity above the gypsum-infilled fractures, the effective neutron-density porosity curve showed porosities ranging from 9 to 15 % in zones where high permeabilities were measured.

Mapping the network of permeable zones was attempted by means of three-dimensional seismic reflection survey data using the limited number of wells in the area. Mapping zones of flow within the entire study area using the processed volume of seismic reflection data was found to be problematic as the seismic reflectors were too mottled in some areas. The only broadly mappable features using seismic data were the vuggy porosity zone above gypsum-infilled fractures in the eastern section of the study area, and the basal contact of the Mabou Group.

7 RECOMMENDATIONS AND FURTHER WORK

As drilling of further monitor wells is a costly option to improve the present characterization, it is recommended to consider reprocessing the original seismic dataset using newly developed technologies.

An option to improve the confidence in the subdivision of the Medium Sandstone unit by means of geophysical logs is to have one person re-log all the cored holes so that there is consistency in all the strip logs.

Further research is recommended and presently ongoing at the University of New Brunswick to perform detailed stratigraphic interpretation of the cores, thus improving on the informal subdivisions used in this thesis. As part of the stratigraphic analysis, thin sections of core containing gypsum nodules should be cut to determine if the center of any gypsum nodules consist of calcite or anhydrite. Such a scenario would support one of two theories of origin for the gypsum that has filled the fractures in the lower half of the Mabou. Such knowledge would then provide a basis for defining post-depositional processes in the area.

In order to confirm or refute the concept of a flow zone existing above the caprock in the Mabou, as well as whether it is connected to the Penobsquis inflow, it is recommended that additional wells be drilled to test the pressure and permeability at depth.

REFERENCES

Anderle, J.P., Crosby, K.S., and Waugh, D.C.E. Potash at Salt Springs, New Brunswick. Economic Geology, 1979 Vol 74 p. 389-396

Ashton, C.P., Bacon, B., Deplante, C., Sinclair, D.T., Redekop, G., 3D Seismic Survey Design, Oilfield Review, April 1994, p. 19-32.

Baker Hughes Inc., PCS 0502 Well DST Analysis Report New Brunswick. Internal document 2005a

Baker Hughes Inc., PCS 0504 Well DST Analysis Report New Brunswick. Internal document 2005b

Biondi, B.L., 3D Seismic Imaging. Investigations in Geophysics Series No. 14 Society of Exploration Geophysicists 2006

Boyd PetroSearch, Picadilly 2004 3D Acquisition report. Internal document. 2005

Chaudhry, A., Oil Well Testing handbook. Elsevier Science and Technology, Oxford 2004, p 387 - 414

Danyluk, T., Chief Geologist for the Technical Services Division at Potash Corporation of Saskatchewan. Personal communication, 2010

Deere, D.U., Technical description of rock cores, Rock Mechanics Engineering Geology Vol 1 1964 p. 16-22

Dictionary.com, "mean free path," in *Dictionary.com Unabridged*. Source location: Random House, Inc. http://dictionary.reference.com/browse/mean free path. Available: http://dictionary.reference.com. Accessed: January 23, 2011

DNR, Carboniferous Maritimes Basin, Department of Natural resources. http://www.gnb.ca/0078/minerals/GSB_Virtual_Carboniferous-e.aspx Accessed: January 24, 2011

Doveton, J., Basics of Oil and Gas log interpretation. Kansas Geological Survey. 1999

Fuzesy, A., Potash in Saskatchewan. Saskatchewan Energy And Mines Report 181, 1982

Gendzwill, D., Professor Emeritus, Department of Earth Sciences, University of Saskatchewan, Personal communication, 2011

Gibling, M.R., Clushaw, N., Rygel, M.C., Pascucci, V., The Maritimes basin of Atlantic Canada: Basin Creation and Destruction in the Collisional Zone of Pangea. Sedimentary Basins of the World, Vol 5. 2008 p. 211-245

Gomis-Yagues, V., Boluda-Botella, N., Ruiz-Bevia, F., Gypsum precipitation/dissolution as an explanation of the decrease of sulphate concentration during seawater intrusion. Journal of Hydrology Vol 228. 2000 p 48-55

Google, Map Data. http://www.google.ca/maps. 2010

Hackbarth, D. A., Application of the Drill-Stem Test to Hydrogeology. Journal of Groundwater Vol. 16. 1978 p 5-11

Kasenow K,. Applied Ground-water Hydrology and well Hydraulics 2nd edition. Water Resources Publications, LLC, 2001 Page 531-544

Keighley, D. Associate Professor, Department of Earth Sciences, University of New Brunswick, Personal communication, 2009

Kleyn, A.H., Seismic Reflection Interpretation. Applied Science Publishers Ltd. England 1983

Klinkenberg, L.J., The permeability of porous media to liquids and gases. Production Practice 1941 p 200-213

Magara, K., Compaction and Fluid Migration: practical petroleum geology. Elsevier Scientific Publishing Company. New York 1978 p. 18 -22

Munson, B., Young, D., Okiishi, T., Fundamentals of Fluid Mechanics 4th Edition. John Wiley & Sons, New York 2002 p. 829-831

Murray, R.C., Origin and diagenesis of Gypsum and Anhydrite. Journal of Sedimentary Research Vol 34 no 3 1964 p. 512-523

Paillet F.L., Kay R.T., Yeskis D., Pedler W.H., Integrating Well logs into a Multi-Scale Investigation of a Fractured Sedimentary Aquifer. The Log Analyst 1993 Vol. Jan-Feb p. 23-40

PCS, PCS 0201 Geological report. Internal document 2002a

PCS, PCS 0202 Geological report. Internal document 2002b

PCS, PCS 0502 Geological report. Internal document 2005a

PCS, PCS 0504 Geological report. Internal document 2005b

PCS, PCS 0601 Geological report. Internal document 2006

Pedler, W., Head, H., Williams, L., HydroPhysical logging: A New Wellbore Technology for Hydrogeologic and Contaminant Characterization of Aquifers. Proceedings of Sixth National Outdoor Action Conference, National Groundwater Association, May 1992

Prugger, F., The flooding of the Cominco potash mine and its rehabilitation. CIM bulletin, 1979 p 86-90

Prugger, F., Prugger, A., Water problems in Saskatchewan mining - what can be learnt from them? CIM bulletin, January 1991, pg 58-66

RAS, Report of Hydrophysical logging Well 08-105 Final Repor*t*, Internal document 2008a p 1-30

RAS, Report of Hydrophysical logging Well 08-107 Final Repor*t*, Internal document 2008b p 1-30

RAS, Report of Hydrophysical logging Well 08-113 Final Repor*t*, Internal document 2008c p 1-30

RAS, Report of Hydrophysical logging Well 08-115 Final Repor*t*, Internal document 2008d p 1-30

Reid, H., Modern Concepts in Drillstem Testing. Practical DST Interpretation Seminar, 2010

Roulston, B., Superintendent of Engineering, New Brunswick Division of Potash Corporation of Saskatchewan Inc., Personal Communication, 2010

Schlumberger, FMI Borehole geology, geomechanics and 3D reservoir modeling. Schlumberger brochure, 2002

Schlumberger, FMI processing and geological interpretation PCS 08-105 well, Internal document 2008a

Schlumberger, FMI processing and geological interpretation PCS 08-113 well, Internal document 2008b

Schlumberger, FMI processing and geological interpretation PCS 08-115 well, Internal document 2008c

Schlumberger, Fullbore Formation Micro-Image log for PCS 0601, Internal document 2006

Schlumberger, Log Interpretation Principles/Applications, Schlumberger Educational Services, 1991

St Peter, C., Maritimes Basin evolution: key geologic and seismic evidence from the Moncton Subbasin of New Brunswick. Atlantic Geology Vol 29. 1993 p. 233-270

St. Peter, C., Department of Natural Resources Geological Surveys Branch 2002

Szczepanik, Z., Chief Technician, Rock Mechanics Laboratory, University of Saskatchewan, Personal communication, 2010

Tiab, D., Donaldson, E., Petrophysics Theory and Practice of Measuring Reservoir Rock and Fluid Transport Properties. Gulf Publishing Company, Houston 1999

Tsang C., Hufschmied P., Hale F., Determination of Fracture Inflow Parameters with a Borehole Fluid Conductivity Logging Method. Water Resources Research 1990 Vol 26 No 4 p. 561-578

Wilson, P., White, J., Tectonic evolution of the Moncton Basin, New Brunswick, eastern Canada: new evidence from field and sub-surface data. Bulletin of Canadian Petroleum Geology Vol 54. 2006 p. 319-336

Wilson, P., White, J., Roulston, B. Structural geology of the Penobsquis salt structure: late Bashkirian inversion tectonics in the Moncton Basin, New Brunswick, Eastern Canada. Canadian Journal Earth Sciences. Vol 43. 2006 p. 405-419

Wightman,W.E., Jalinoos, F., Sirles, P., and Hanna, K. (2003). Application of Geophysical Methods to Highway Related Problems. Federal Highway Administration, Central Federal Lands Highway Division, Lakewood, CO, Publication No. FHWA-IF-04-021, September 2003

APPENDIX A - CONVERSION OF HYDRAULIC CONDUCTIVITY TO PERMEABILITY

To compare hydrophysical logging results to drill stem tests, the results required conversion of hydraulic conductivity (cm/s) values presented by RAS Inc. into permeabilities (md). Conversion of hydraulic conductivity into permeability was done using the following equation, which accounts for the density and viscosity of the fluid:

$$K = \frac{K_i(\rho g)}{\mu} \qquad A.1$$

Where:
K = hydraulic conductivity
K_i = Intrinsic permeability
ρ = Density
g = Gravity
μ = Dynamic viscosity

Conversions used physical properties of water at 20 degrees Celsius (Munson et al. 2002)

$$\mu = 0.01002 \frac{g}{s * cm}$$

$$\rho = 0.9980 \frac{g}{cm^3}$$

$$g = 980 \frac{cm}{s^2}$$

$$K_i = \frac{K\mu}{(\rho g)}$$

$$K_i = \frac{K * 0.01002 \frac{g}{s * cm}}{\left(0.9980 \frac{g}{cm^3} * 980 \frac{cm}{s^2}\right)}$$

$$K_i = \frac{K * 0.01002 \frac{g}{s * cm}}{\left(0.9980 \frac{g}{cm^3} * 980 \frac{cm}{s^2}\right)} \qquad [cm^2]$$

$$K_i = \frac{K * 0.01002 \frac{g}{s * cm}}{\left(0.9980 \frac{g}{cm^3} * 980 \frac{cm}{s^2}\right)} * \frac{1\ Darcy}{9.87x10^{-9} cm^2} * \frac{1000\ mDarcy}{1\ Darcy} \qquad [mD]$$

$$\boldsymbol{K_i = 1.04\ x\ 10^6\ * K\ (cm/s) \quad [mD]}$$

HPL depth (m)	PCS 08105 hydraulic conductivity (cm/s)	PCS 08105 permeability (mD)
40.2 to 40.9	1.48E-02	1.5E+04
48.9 to 49.4	3.99E-03	4.1E+03
55.3 to 57.0	7.80E-03	8.1E+03
90.9 to 91.7	2.88E-03	3.0E+03
133.2 to 133.5	2.00E-03	2.1E+03
148.4 to 149.9	1.80E-02	1.9E+04
177.9 to178.8	8.26E-04	8.5E+02
188.2 to 188.7	2.58E-02	2.7E+04
227.9 to 229.3	5.22E-04	5.4E+02
245.4 to 246.5	4.09E-03	4.2E+03
261.3 to 261.9	3.12E-03	3.2E+03
521.1 to 526.7	Intermittent flow hyd cond could not be calculated	Intermittent flow permeability could not be calculated
557.5 to 559.5	Intermittent flow hyd cond could not be calculated	Intermittent flow permeability could not be calculated

Figure A.1 Conversion from hydraulic conductivity to permeability PCS 08105

HPL depth (m)	PCS 08107 hydraulic conductivity (cm/s)	PCS 08107 permeability (mD)
76.2 to 77	4.7E-03	4.8E+03
159.72 to 160.93	5.6E-02	5.8E+04
161.54 to 136.07	3.4E-05	3.5E+01
169.47 to 171.3	2.5E-04	2.6E+02
195.07 to 195.99	5.7E-05	5.9E+01
203 to 208.18	1.0E-05	1.0E+01
252.98 to 256.64	1.4E-05	1.5E+01
255.25 to 257.92	2.0E-03	2.1E+03
259.08 to 259.78	8.2E-06	8.5E+00
260.91 to 261.76	6.8E-06	7.0E+00
275.57 to 275.97	2.9E-05	3.0E+01
279.96 to 281.06	8.5E-05	8.7E+01
284.47 to 285.45	1.2E-04	1.2E+02
295.38 to 296.14	1.8E-04	1.9E+02
313.46 to 314.28	8.5E-05	8.7E+01
314.28 to 322.11	1.5E-05	1.5E+01
413 to 414.53	4.2E-04	4.3E+02
595.24 to 597.59	9.9E-06	1.0E+01

Figure A.2 -Conversion from hydraulic conductivity to permeability PCS 08107

HPL depth (m)	PCS 08113 Hydraulic conductivity (cm/s)	PCS 08113 permeability (mD)
113.7 to 115.2	4.94E-03	5.1E+03
119.5 to 125	1.30E-02	1.3E+04
143 to 144.5	1.04E-03	1.1E+03
147.5 to 150	9.66E-03	1.0E+04
152.1 to 154.5	6.53E-04	6.7E+02
162.8 to 168.3	3.13E-04	3.2E+02
210.9 to 214.3	1.10E-04	1.1E+02
216.7 to 219.8	1.78E-04	1.8E+02
229.2 to 235.6	1.74E-05	1.8E+01
276.8 to 282.6	1.92E-05	2.0E+01
289.6 to 300.2	1.28E-04	1.3E+02
306.9 to 316.7	1.52E-04	1.6E+02
324.3 to 329.2	2.28E-05	2.4E+01
333.8 to 337.4	3.04E-05	3.1E+01
359.1 to 367.6	1.30E-05	1.3E+01
384.1 to 385.6	7.30E-05	7.5E+01
397.8 to 414.5	9.42E-05	9.7E+01
431.3 to 433.7	1.32E-04	1.4E+02
435.9 to 437.4	6.94E-05	7.2E+01
621.8 to 624.8	3.63E-05	3.8E+01

Figure A.3 – Conversion from hydraulic conductivity to permeability PCS 08113

HPL depth (m)	PCS 08115 hydraulic conductivity (cm/s)	PCS 08115 permeability (mD)
52.7 to 57.3	2.98E-04	3.1E+02
92.7 to 96.3	5.33E-04	5.5E+02
114.0 to 116.1	8.47E-04	8.8E+02
127.4 to 128.3	1.77E-04	1.8E+02
132.6 to 133.5	2.29E-04	2.4E+02
143.0 to 144.8	2.05E-04	2.1E+02
203.6 to 207.6	1.30E-04	1.3E+02
214.9 to 216.4	2.94E-05	3.0E+01
223.4 to 224.9	1.39E-05	1.4E+01
230.1 to 233.2	6.95E-06	7.2E+00
248.1 to 250.2	1.31E-04	1.4E+02
299.0 to 300.5	4.02E-05	4.2E+01
327.7 to 329.8	9.91E-06	1.0E+01
340.8 to 342.3	9.28E-06	9.6E+00
358.8 to 360.3	5.57E-05	5.8E+01
424.3 to 471.2	4.02E-07	4.2E-01

Figure A.4 - Conversion from hydraulic conductivity to permeability PCS 08115

APPENDIX B - LABORATORY PERMEABILITY MEASUREMENTS

The laboratory testing procedures for a Ruska gas Permeameter were followed to test gas permeability. The basic premise is to seal the outer surface of the core using an elastomer sleeve, apply (and maintain constant) a pressure drop across the sample, then measure the gas flow rate using a glass tube flow meter.

The data analysis procedures included applying a correction to the gas permeability results. The Klinkenberg correction was developed historically, when permeability results tested using air showed a higher permeability then when the permeability was tested using water. Investigations revealed that "the permeability to a gas is a function of the mean free path of the gas molecules" (Klinkenberg, 1941.). The mean free path is the "average distance that a particle travels between successive collisions with other particles" (Dictionary.com 2011).

Factors affecting the mean free path of gas are pressure, temperature, and the nature of the gas. To reduce the number of variables that affect the mean free path of gas, laboratory testing used nitrogen gas and maintained a constant temperature in the laboratory, leaving pressure as the only variable to affect the mean free path of the gas molecules. The mean free path was altered in the laboratory testing by forcing the nitrogen gas through each specimen at three different pressures: 0.25 atm, 0.5 atm and 1 atm above that of atmospheric.

Each increase in pressure theoretically reduced the mean free path of the gas molecules, theoretically decreasing the permeability. By plotting the permeabilities of each incremental increase in gas pressure against one over the pressure, a corrected permeability value was extracted by extrapolating the trend of one over the pressure zero. Theoretically the pressure at such a point would be extremely high and as such the gas permeability of a sample is expected to approach the permeability of liquids (Klinkenberg, 1941).

B.1 Discussion

The Klinkenberg correction worked less than ideally with the data from the testing program. Positive trend lines were found in each of the two tests on Sample 1 cut parallel to bedding; however, the trend line was based on two points and lacked a third point in each of the trends due to the permeability of the sample at 1 atm being too great for the testing equipment to measure at such a pressure. Corrected horizontal permeabilities of 589 md and 736 md were calculated from the trend lines presented in Figure B.1. The permeability increase with this sample was associated with separation of beds propagating along bedding planes during the first of two tests performed on the sample.

The correction trend line for the sandstone labeled Sample 4 exhibited a negative correction, a trend that was opposite to the theoretical expectation. The accuracy of the correction may be questionable in this case, given that the operating pressure range of the Ruska permeameter is limited. This may be endorsed by the fact that Klinkenberg (1941) used two apparatuses for his gas permeability experiments: one for pressure at or below 1 atm, and a second for pressures at or above 1 atm. Pressures as high as 20 atm were used to make permeability determinations in Klinkenberg's experiments (Klinkenberg, 1941). This represents pressures 20 times greater than the largest pressure used in the testing samples. As such, values presented in the thesis for each sample were either the corrected permeability (if a positive trend line was present in the data), or the permeability measured at the highest pressure tested.

B.2 Results

The corrected permeabilities presented in Table B.1 demonstrate anisotropic permeability within the interbedded siltstone. The interbedded siltstone produced horizontal permeabilities of 589 md and 736 md. The vertical permeability measured for the interbedded siltstone was 1 md. The small permeability was calculated based on results

from measurements taken at 1 atm pressure, reading off the lower end of smallest flow meter gauge and was borderline of being an acceptable flow reading. The corrected permeability was therefore labeled as being less than 1 md.

To confirm permeability in Sample 4, the average permeability of the highest pressure regime was considered to be the corrected permeability. The average permeability of the three tests performed at the highest pressure regime was 6 md.

Sample 5 did not provide any useable data as the permeability was greater than the capabilities of the testing equipment, the upper limit of which was calculated to be 2470 md. Visual inspection of the plug showed interconnectivity of vugs along the outside edge of the sample. The same interconnectivity was present in the core sample in which the plug was cut (Figure 5.6), suggesting that the interval of core has the ability to produce significant volumes of water.

The laboratory results of corrected permeability provide confirmation that on a centimeter scale, vugs in the formation provide sufficient interconnectivity to create measurable permeability.

Table B.1 - Uncorrected gas permeability results

Sample 1 - plug cut parallel to bedding planes (290.10-290.21)

Length (mm)	Length (m)	Diameter (m)	Area (m^2)	Weight (g)
26.26	0.02626	0.02516	0.000497177	28.32

Pressure (atm)	Pressure (Pa)	Flow meter range	Flow-meter reading (mm)	Temp °C	Viscosity (Pa s)	Q corrected (mL/s)	Q corrected (m^3/s)	Permeability (m^2)	k(darcies)	k(mD)	1/p
0.25	25331.25	Large	72	24	1.77E-05	30	3.00E-05	1.10E-12	1.10E+00	1.10E+03	3.95E-05
0.25	25331.25	Large	98	24	1.77E-05	42	4.20E-05	1.55E-12	1.55E+00	1.55E+03	3.95E-05
0.5	50662.5	Large	108	24	1.77E-05	46	4.60E-05	8.46E-13	8.46E-01	8.46E+02	1.97E-05
0.5	50662.5	Large	143	24	1.77E-05	62	6.20E-05	1.14E-12	1.14E+00	1.14E+03	1.97E-05
1	101325	Large	Above measureable limit								

Sample 1 - plug cut perpendicular to bedding planes (290.10-290.21)

Length (mm)	Length (m)	Diameter (m)	Area (m^2)	Weight (g)
30.06	0.03006	0.02517	0.000497572	34.17

Pressure (atm)	Pressure (Pa)	Flow meter range	Flow-meter reading (mm)	Temp °C	Viscosity (Pa s)	Q corrected (mL/s)	Q corrected (m^3/s)	Permeability (m^2)	k(darcies)	k(mD)	1/p
1	101325	Small	10	24	1.77E-05	0.125	1.25E-07	1.15E-15	1.15E-03	1.15E+00	9.87E-06
1	101325	Small	9	24	1.77E-05	0.12	1.20E-07	1.10E-15	1.10E-03	1.10E+00	9.87E-06

Sample 4 - sandstone with some vugs (432.43-432.47)

Length (mm)	Length (m)	Diameter (m)	Area (m^2)	Weight (g)
27.26	0.02726	0.02521	0.000499155	31.74

Pressure (atm)	Pressure (Pa)	Flow meter range	Flow-meter reading (mm)	Temp °C	Viscosity (Pa s)	Q corrected (mL/s)	Q corrected (m^3/s)	Permeability (m^2)	k(darcies)	k(mD)	1/p
0.25	25331.25	Small	21	23.5	1.76E-05	0.155	1.55E-07	5.89E-15	5.89E-03	5.89E+00	3.95E-05
0.25	25331.25	Small	20	23.5	1.76E-05	0.15	1.50E-07	5.70E-15	5.70E-03	5.70E+00	3.95E-05
0.25	25331.25	Small	22	23.5	1.76E-05	0.165	1.65E-07	6.27E-15	6.27E-03	6.27E+00	3.95E-05
0.5	50662.5	Small	45	23.5	1.76E-05	0.34	3.40E-07	6.46E-15	6.46E-03	6.46E+00	1.97E-05
0.5	50662.5	Small	46	23.5	1.76E-05	0.35	3.50E-07	6.65E-15	6.65E-03	6.65E+00	1.97E-05
0.5	50662.5	Small	46	23.5	1.76E-05	0.35	3.50E-07	6.65E-15	6.65E-03	6.65E+00	1.97E-05
1	101325	Small	70	23.5	1.76E-05	0.6	6.00E-07	5.70E-15	5.70E-03	5.70E+00	9.87E-06
1	101325	Small	75	23.5	1.76E-05	0.65	6.50E-07	6.18E-15	6.18E-03	6.18E+00	9.87E-06
1	101325	Small	76	23.5	1.76E-05	0.65	6.50E-07	6.18E-15	6.18E-03	6.18E+00	9.87E-06

Sample 5 - sandstone with lots of vugs (433.05-433.12)

Length (mm)	Length (m)	Diameter (m)	Area (m^2)	Weight (g)
29.4	0.0294	0.02517	0.000497572	29.2

Pressure (atm)	Pressure (Pa)	Flow meter range	Flow-meter reading (mm)	Temp °C	Viscosity (Pa s)	Q corrected (mL/s)	Q corrected (m^3/s)	Permeability (m^2)	k(darcies)	k(mD)	1/p
0.03	3039.75	Large	150	24	1.77E-05	Too large of flow for equipment to measure					3.29E-04
0.04	4053	Large	135	24	1.77E-05						2.47E-04

Maximum measureable permeabilities using the Ruska gas permeamter

Pressure (atm)	Pressure (Pa)	Flow meter range	Flow-meter reading (mm)	Temp °C	Viscosity (Pa s)	Q corrected (mL/s)	Q corrected (m^3/s)	Permeability (m^2)	k(darcies)	k(mD)	1/p
0.25	25331.25	Large	140	24	1.77E-05	60	6.00E-05	2.47E-12	2.47E+00	2.47E+03	3.95E-05
0.5	50662.5	Large	140	24	1.77E-05	60	6.00E-05	1.24E-12	1.24E+00	1.24E+03	1.97E-05
1	101325	Large	140	24	1.77E-05	60	6.00E-05	6.18E-13	6.18E-01	6.18E+02	9.87E-06

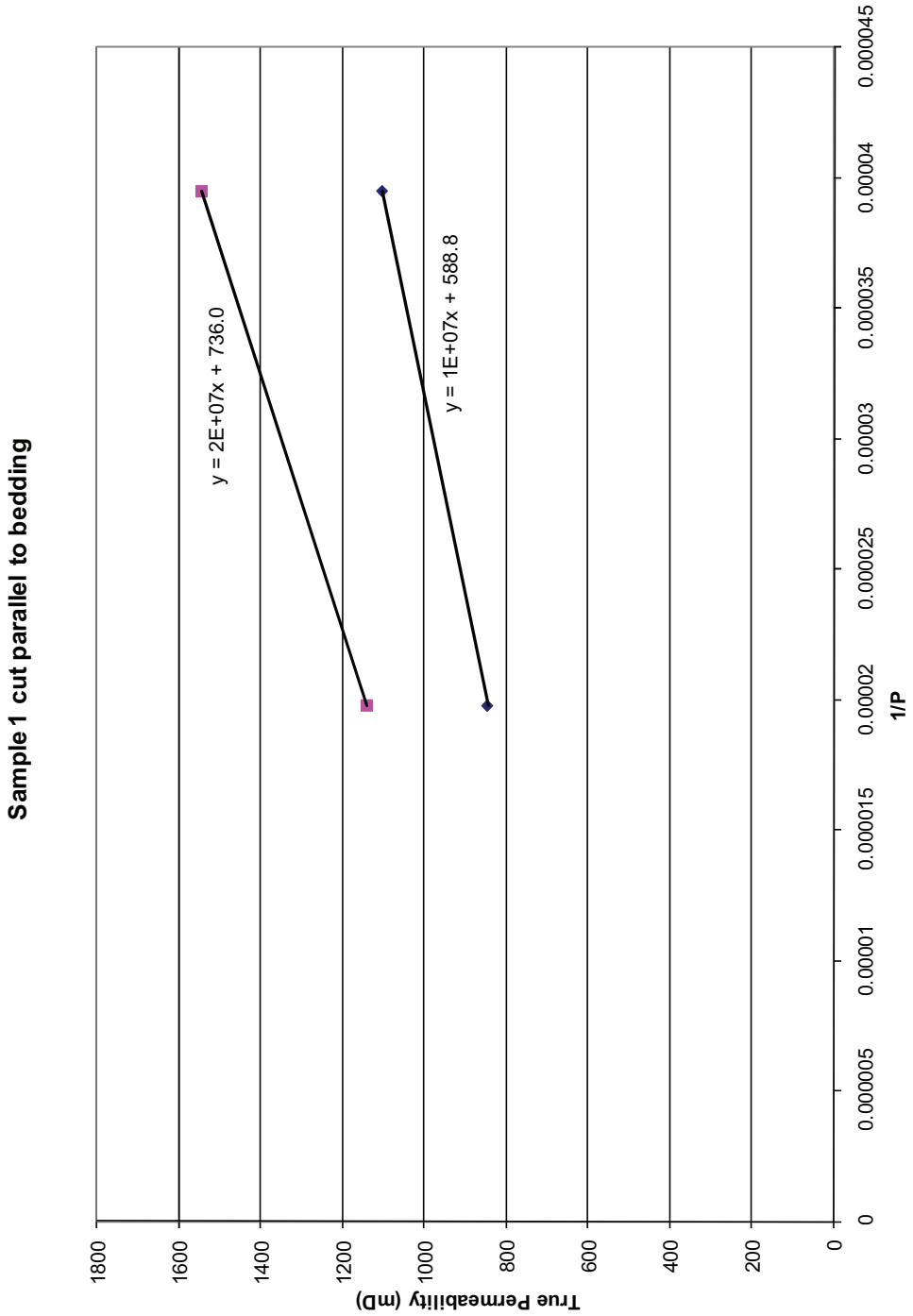

Figure B.1 - Gas permeability results for interbedded siltstone plug cut parallel to bedding

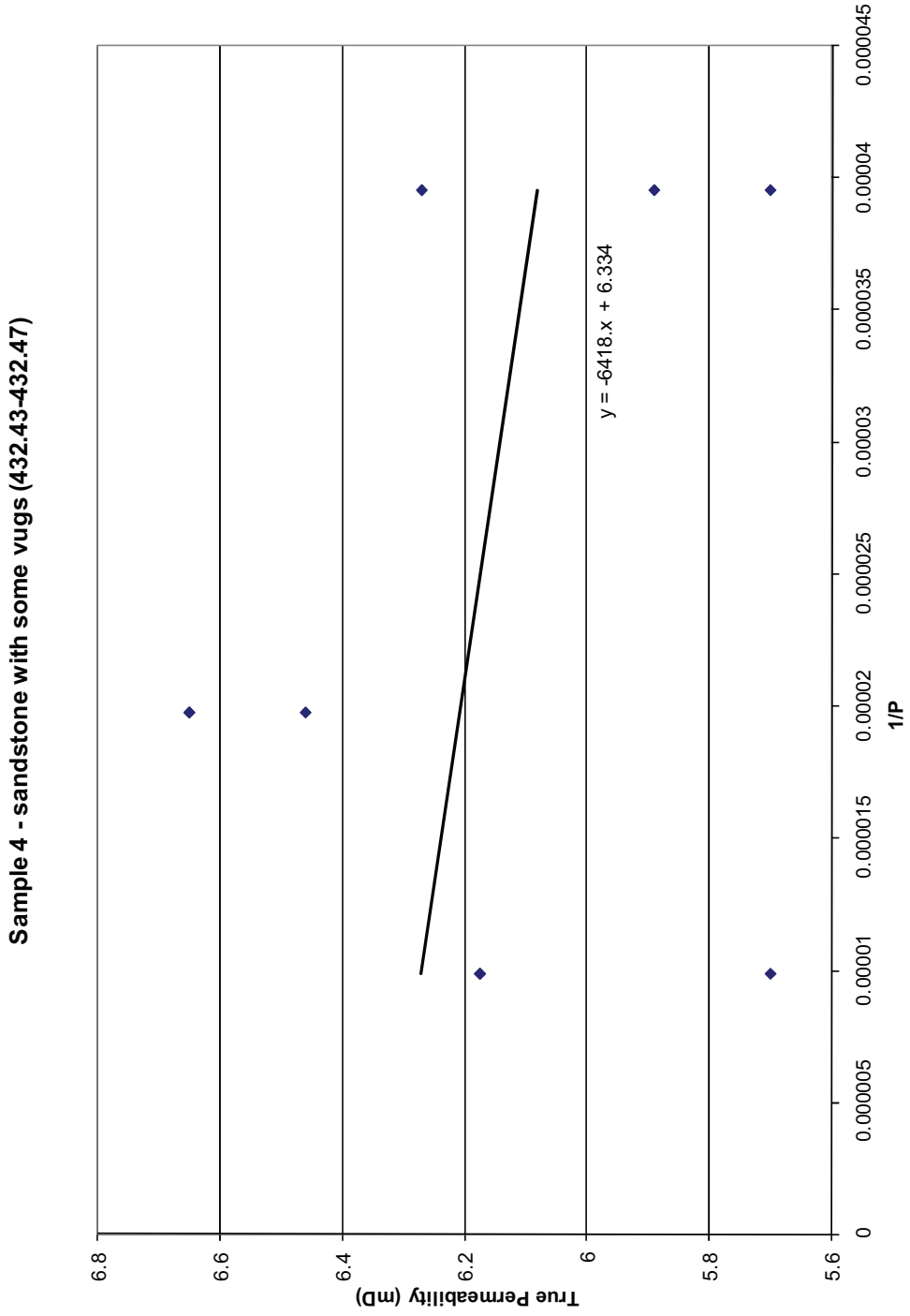

Figure B.2 – Gas permeability results for sandstone with some vugs. Results show a trendline with negative slope, which is contrary to the theory of Klinkenberg correction